Ageing of plastic pipes in urban drainage systems

Makris, K.

DOI
10.4233/uuid:06c11b2f-2df0-422f-802c-1b083e205323

Publication date
2022

Document Version
Final published version

Citation (APA)
Makris, K. (2022). *Ageing of plastic pipes in urban drainage systems*. [Dissertation (TU Delft), Delft University of Technology]. https://doi.org/10.4233/uuid:06c11b2f-2df0-422f-802c-1b083e205323

AGEING OF PLASTIC PIPES

IN URBAN DRAINAGE SYSTEMS

AGEING OF PLASTIC PIPES

IN URBAN DRAINAGE SYSTEMS

Proefschrift

ter verkrijging van de graad van doctor
aan de Technische Universiteit Delft,
op gezag van de Rector Magnificus Prof. dr. ir. T.H.J.J. van der Hagen,
voorzitter van het College voor Promoties,
in het openbaar te verdedigen op donderdag 8 december 2022 om 12:30 uur

door

Konstantinos MAKRIS

Master of Science in Civil Engineering, Delft University of Technology
Civil Engineering, University of Thessaly,
geboren te Larisa, Griekenland.

Dit proefschrift is goedgekeurd door de

promotor: prof. dr. ir. F.H.L.R Clemens
promotor: dr. ir. J.G. Langeveld
promotor: prof. dr. K.V. Horoshenkov

Samenstelling promotiecommissie:

Rector Magnificus,	voorzitter
Prof. dr. ir. F.H.L.R Clemens,	Technische Universiteit Delft
Dr. ir. J.G. Langeveld,	Technische Universiteit Delft
Prof. dr. K.V. Horoshenkov,	The University of Sheffield
Onafhankelijke leden:	
Prof. dr. B.W. Drinkwater,	University of Bristol
Dr. M.J. Lepot,	INSA-Lyon
Prof. dr. ir. A.S.J. Suiker,	Technische Universiteit Eindhoven
Prof. dr. ir. L.C. Rietveld,	Technische Universiteit Delft
Prof. dr. Z. Kapelan,	Technische Universiteit Delft, reservelid

Printed by: Proefschrift All In One (AIO)

Cover design by: Guus Gijben

ISBN 978-94-93315-13-6

An electronic version of this dissertation is available at
http://repository.tudelft.nl/.

CONTENTS

LIST OF TABLES

LIST OF FIGURES

SUMMARY

Sewer systems are extensive and capital-intensive structures which are liable throughout their operational life to several defects concerning their structural stability, flow regime, and leak tightness. Sewer managers are responsible for the inspection and maintenance of sewer systems in order to ensure a cost-effective and environmentally safe operation. However, asset management strategies are mainly based on prior visual inspections which limit the knowledge of the structural status to the inner-side of the pipes while physical and (bio)chemical mechanisms that affect their longevity are ignored. Identification and comprehensive understanding of these mechanisms is a key issue for better decision making and more affordable investments. Further, depending on the construction material, different degradation mechanisms exist. Sewer pipes are mainly constructed from concrete or plastic materials, such as Polyvinyl Chloride (PVC), Polyethylene (PE), Polypropylene (PP), and Glass-fiber Reinforced Polyester (GRP or FRP). Since the performance of concrete sewer pipes has been extensively studied in the literature, the main objective of this thesis concerns the ageing of plastic sewer pipes. Main focus is given to PVC pipes, as PVC has become one of the dominant construction materials for sewer systems in the past four decades.

The main factors that affect a PVC pipe's lifetime originate from the production, installation and/or operation stage. Review of relevant case studies indicates that PVC is a durable material for urban water infrastructure, while it shows high chemical resistance against substances that are found in sewers. Therefore, material degradation, if any, occurs slowly. Additionally, the elastomeric joints that are used to connect different pipe segments remain operational (without leakages) even when they are subjected to excessive values of bending or deflection. These findings encourage several researchers to suggest a lifetime of PVC sewer systems that exceeds 100 years. However, inspection data of four Dutch municipalities (Almere, Amstelveen, Breda, Haarlem) revealed that severe defects have already surfaced and degradation evolves at an unexpected fast rate. A main reason for this gap between literature and practice is the fact that comprehensive material testing of PVC sewer pipes is rarely found in literature, although it proves to be essential in order to trustfully assess the level of degradation and its origins.

In order to explore the noted gap between scientific literature and observations in practice, extensive testing was conducted on eight excavated PVC sewer pipes (16-43 years old) with known defects and one brand-new for reference purposes. The pipes were selected based on the year of installation, the existing defect and the feasibility of excavation. The structural or operational defects of the excavated pipes concerned cracks, breaks, deformations, and root intrusion. The conducted tests and analyses on pipe material included the following: determination of density and intrinsic viscosity, differential scanning calorimetry, thermo-gravimetric analysis, Fourier transform infrared spectroscopy, dispersive X-ray fluorescence, scanning electron microscopy, and

tensile and flexural testing. The target of these analyses was to identify signs of material crystallization, characterize the molecular structure, determine the thermal characteristics (e.g. glass and decomposition temperature), detect any changes in carbonyl and hydroxyl functional groups, identify the elemental composition (stabilizers, fillers, pigments), study the material microstructure, and determine the mechanical properties of the material (i.e. ultimate tensile and flexural strength, elongation at break, and the elastic modulus). The test results indicated that physical ageing was extensively detected while other degradation mechanisms had minimal or no effect on the investigated pipes. Nevertheless, mechanical testing on exhumed 3-layer pipes (with a core) showed that the incorporation of layered wall constructions is potentially a critical factor for the structural status of the pipe. Further, visual examination during excavation revealed various failure causes, including uncontrolled handling of the pipes during construction or due to digging activities in the direct vicinity of the pipes.

The transition from a ductile towards a more brittle material behaviour due to physical ageing is crucial for the mechanical performance of pipes. Aged plastic pipes could face issues concerning their stability during certain activities (e.g. placement of new household connections). Hence, it is necessary to obtain information on the process of ageing of the pipe material, which results in an increase of its storage modulus. In this thesis, low-frequency vibro-acoustics was the selected non-destructive method to explore ageing of plastic pipes. Moving to lower sonic frequencies is beneficial as it allows for higher sensitivity to ageing and it limits the number of propagating modes to the axisymmetric ones, simplifying the overall analysis. Initially, the theoretical part of the method was developed by solving the equations of motion while assuming that the coupled system was harmonically oscillated. This led to a solution of the storage modulus of the pipe material based on acoustical data. Three types of axisymmetric waves were found to propagate in a water-filled pipe at low frequencies: the longitudinal, torsional, and water-borne wave. If the pipe is coupled with soil, only the water-borne wave is able to propagate. As a result, there is a precondition that the tested pipe is filled with water.

Subsequently, the vibro-acoustic method was put into practice by testing two water-filled PE pipes, one surrounded by air and another by sand. The excitation was achieved via an impact hammer and the propagating signal was recorded with the aid of hydrophones. Signal analysis led to the estimation of the axial wavenumber of the propagating water-borne wave. This value was used to evaluate the storage modulus of the pipe material given measurements or assumptions for the properties of the pipe shell (density, Poisson's ratio, loss factor, wall thickness, internal radius), water (density, sound wave velocity) and, if any, soil (density, compressional and shear wave velocity). An uncertainty analysis showed which parameters have to be more accurately known in order to lower the overall uncertainty of the estimated storage modulus and increase the ability to distinguish the alterations in terms of ageing. Irrespectively of the medium surrounding the pipe (air or soil), the distance between the points of the recording signals should be as long as possible. It is also essential to ensure the accurate knowledge of the pipe's geometry, i.e. the wall thickness and internal radius. Finally, when the pipe is surrounded by soil, there is a limited dependence of the overall uncertainty of the pipe's storage modulus on the parameters of the soil, although a good approximation of the soil's density and shear wave velocity is desired.

SAMENVATTING

Rioolsystemen vormen een kapitaalintensieve infrastructuur en tijdens de gebruiksfase veroudering ondergaan, dit leidt onder meer tot lekkage, constructieve instabiliteit en een verlies aan hydraulische capaciteit. Rioolbeheerders voeren inspecties en onderhoud uit om zo de infrastructuur doelmatig te beheren. Kennis van de constructieve sterkte en stabiliteit van deze systemen is een belangrijk element bij het formuleren van succesvolle assetmanagementstrategieën, met als doel een verbeterde besluitvorming en beter verantwoorde investeringen. Dergelijke strategieën zijn voornamelijk gebaseerd op voorafgaande visuele inspecties die alleen informatie geven over de binnenzijde van de buis, terwijl schade als gevolg van bv. fysieke en (bio)chemische mechanismen die hun levensduur beïnvloeden worden genegeerd. Het identificeren en begrijpen van deze mechanismen is echter cruciaal voor een betere besluitvorming. Afhankelijk van het constructiemateriaal bestaan er verschillende faalmechanismen. Rioolbuizen zijn voornamelijk gemaakt van beton of kunststof, zoals polyvinylchloride (PVC), polyethyleen (PE), polypropyleen (PP) en glasvezelversterkt polyester (GVK of FRP). Aangezien de veroudering van betonnen rioolbuizen uitgebreid is bestudeerd in de literatuur, is het hoofdonderwerp van dit proefschrift de veroudering van kunststof rioolbuizen. De nadruk ligt op PVC-buizen, omdat PVC een van de meest gebruikte bouwmaterialen voor rioleringssystemen is.

De factoren die de levensduur van een PVC-buis beïnvloeden, zijn afkomstig uit de productie-, installatie- en/of exploitatiefase. Beoordeling van casestudies geeft aan dat PVC een duurzaam materiaal is voor leidingsystemen, terwijl het een hoge chemische resistentie vertoont tegen stoffen die in riolen worden aangetroffen. Daarom vindt materiaaldegradatie, indien aanwezig, langzaam plaats. Bovendien blijven de elastomere verbindingen intact (dat wil zeggen dat lekkage door de buiswand niet of nauwelijks optreedt), zelfs wanneer ze onderhevig zijn aan overmatige deformatie. Deze bevindingen hebben geleid tot algemeen aangenomen theoretische levensduur van meer dan 100 jaar. Uit inspectiegegevens van vier Nederlandse gemeenten (Almere, Amstelveen, Breda, Haarlem) blijkt echter dat er weldegelijk defecten zijn waardoor degradatie onverwacht snel optreedt. Een belangrijke reden voor deze discrepantie tussen literatuur en praktijk is dat uitgebreide materiaaltests van PVC-rioolbuizen zelden worden uitgevoerd en gerapporteerd, hoewel dit essentieel blijkt om de mate van degradatie en de oorsprong ervan betrouwbaar te beoordelen.

Om de opgemerkte discrepantie tussen de wetenschappelijke literatuur en waarnemingen/ervaringen in de praktijk te onderzoeken, zijn uitgebreide tests uitgevoerd op acht opgegraven PVC-rioolbuizen (16-43 jaar oud) met bekende defecten en één nieuwe buis die werd gebruikt als referentie. De leidingen zijn geselecteerd op basis van het jaar van aanleg, het bestaande defect en de praktische uitvoerbaarheid van de extractie uit de grond. De structurele of operationele defecten van de opgegraven buizen omvatten

scheuren, breuken, vervormingen en wortelingroei. De uitgevoerde tests en analyses op leidingmateriaal omvatten de bepaling van dichtheid en intrinsieke viscositeit, differentiële scanningcalorimetrie, thermo-gravimetrische analyse, Fourier-transform infraroodspectroscopie, dispersieve röntgenfluorescentie, scanning-elektronenmicroscopie en trek- en buigtesten. Het doel van deze analyses was het identificeren van indicaties voor materiaalkristallisatie, het karakteriseren van de moleculaire structuur, het bepalen van de thermische eigenschappen (bijv. glas- en ontledingstemperatuur), het detecteren van eventuele veranderingen in carbonyl- en hydroxylfunctionele groepen, het identificeren van de elementaire compositie (stabilisatoren, vulstoffen, pigmenten), het bestuderen van de materiaalmicrostructuur en het bepalen van de mechanische eigenschappen van het materiaal (de trek- en buigsterkte, de rek bij breuk en de elasticiteitsmodulus). De testresultaten lieten zien dat fysieke veroudering op grote schaal optreedt terwijl andere degradatiemechanismen een minimaal of geen effect hadden op de onderzochte buizen. Mechanische tests op opgegraven drielaagse buizen (met een kern van gerecycled of geschuimd PVC) hebben aangetoond dat het aanbrengen van gelaagde buiswandconstructies potentieel een kritische factor is voor de constructieve eigenschappen van de buis. Verder bracht visueel onderzoek tijdens het opgraven van de buizen diverse faaloorzaken aan het licht, waaronder het ongecontroleerd hanteren van de buizen tijdens de aanleg of door graafwerkzaamheden in de directe omgeving van de buizen.

De overgang van een ductiel naar een brozer materiaalgedrag als gevolg van fysieke veroudering is cruciaal voor de mechanische prestaties van buizen. Verouderde kunststof buizen kunnen tijdens bepaalde werkzaamheden (bijv. de inspectie van buizen of bij het realiseren van nieuwe huisaansluitingen) problemen krijgen met hun stabiliteit. Daarom is het noodzakelijk om informatie te verkrijgen over het verouderingsproces van het buismateriaal, wat bleek te resulteren in een verhoging van de opslagmodulus. De gebruikte methode in dit proefschrift was laagfrequente vibro-akoestiek om de veroudering van kunststof buizen te onderzoeken. Het gebruik van lagere geluidsfrequenties is gunstig omdat het een hogere gevoeligheid voor veroudering mogelijk maakt en omdat het aantal voortplantingsmodi wordt beperkt tot de axisymmetrische modi, waardoor de algehele analyse wordt vereenvoudigd. Aanvankelijk werd het theoretische deel van de methode ontwikkeld door de bewegingsvergelijkingen op te lossen met de aanname dat het gekoppelde systeem in een harmonische trillingstoestand was. Dit leidde tot een oplossing voor de opslagmodulus van het buismateriaal op basis van akoestische data. Er werden drie soorten axisymmetrische golven gevonden die zich bij lage frequenties voortplanten in een met water gevulde pijp: de longitudinale golf, de torsiegolf en de watergedragen golf. Als de buis in de grond ligt, kan alleen de watergedragen golf zich voortplanten. Vanwege dit effect is er een voorwaarde dat de geteste buis volledig gevuld is met water.

Vervolgens werd de vibro-akoestische methode in het laboratorium getest door op twee met water gevulde PE-buizen, de ene omgeven door lucht en de andere door zand. De excitatie werd bereikt via een slaghamer en het voortplantingssignaal werd opgenomen met hydrofoons. Signaalanalyse leidde tot de schatting van het axiale golfgetal van de voortplantende watergedragen golf. De waarde van het golfgetal werd gebruikt om de opslagmodulus van het buismateriaal te bepalen, gegeven metingen of aannames voor de eigenschappen van de buis (dichtheid, Poisson-factor, verliesfactor, wanddikte,

interne straal), het water (dichtheid, geluidsgolfsnelheid) en, indien aanwezig, de grond (dichtheid, compressie- en schuifgolfsnelheid). Een onzekerheidsanalyse laat zien welke parameters nauwkeuriger bekend moeten zijn om de onzekerheid van de geschatte opslagmodulus te verlagen en de mogelijkheid om de veranderingen als gevolg van veroudering te onderscheiden te vergroten. Ongeacht het medium dat de buis omringt (lucht of grond), moet de afstand tussen de meetpunten van de opnamesignalen zo groot mogelijk zijn. Het is ook essentieel om te zorgen voor nauwkeurige kennis van de geometrie van de buis, d.w.z. de wanddikte en interne straal. Ten slotte wordt opgemerkt dat de kennis van de bodemeigenschappen wel relevant is, maar niet de grootste bijdrage levert aan de onzekerheid.

1

INTRODUCTION

1.1. SEWER ASSET MANAGEMENT

The management of sewer systems concerns the inspection, cleaning and (proactive or reactive) recovery of all the elements that constitute the main sewer system. *Sewer asset management* is a term that has become popular the past years as it associates the structural and operational status of the "invisible" sewer systems with the "visible" financial, societal and environmental effects. The outcome of this relation is demonstrated in practice. For instance, in 2015 the Dutch municipalities invested 650 million euros on renovation, improvement or replacement of 960 km sewer pipes. 99% of this amount originated from local taxes of residents and companies, resulting in an average amount of 92 euros per inhabitant (Kunst, 2016). The environmental impact is reflected in a different case in Australia, where the failure of a sewer main led to an estimated amount of more than 40 m^3 of sewage being discharged within several months to the environment (Gould et al., 2013).

Therefore, failure and/or maintenance of such capital-intensive and extensive infrastructure have inevitably multifaceted consequences, imposing to sewer managers the establishment of asset management strategies which include a constant trade-off between cost bearability and undisrupted, environmentally safe service. Closed-circuit television (CCTV) inspection data is one of the main information sources for these strategies (Van Riel, 2017). Subsequently, decisions are taken whether replacement, rehabilitation or a near future inspection should take place. However, CCTV offers limited information, as it depicts only an inner-side snapshot of the pipes with no meaningful quantification of the physical and (bio)chemical mechanisms that affect the structural and operational integrity (Tscheikner-Gratl et al., 2019). In addition, the available data are highly disputed due to the involved high uncertainty which stems from the subjectivity

Parts of this chapter have been published in: Makris, K. F., Langeveld, J., & Clemens, F. H. (2020). A review on the durability of PVC sewer pipes: Research vs. practice. Structure and Infrastructure Engineering, 16(6), 880–817. doi:10.1080/15732479.201973442

included in defect recognition and/or description, and in the interpretation of inspection reports (Dirksen, 2013).

Further, the average annual rate of inspected sewers is around 10% of the total length (Van Riel, 2017), depriving the opportunity for up to date knowledge on the condition state of the largest part of the network and the timely capture of processes that occur in smaller timescales (e.g. third-party impacts). Nonetheless, inspection programs for the whole system are usually established based on this limited data along with the operator experience, customer complaints or specific system characteristics (material, age, operational conditions), leading often to inefficient schedules (Tscheikner-Gratl et al., 2019). Lately, municipalities have also become more cautious whether a pipe has to be replaced or not, in an effort to save capital (Kunst, 2016). Shifting to a less proactive approach, however, could result in unpredicted high costs and working loads, besides the release of untreated sewage to the environment until a potential failure is noted and fixed.

1.2. THE DUTCH URBAN DRAINAGE NETWORK

Approximately 99.5% of the Dutch households are connected to sewer systems, forming a sewer system of circa 153,000 km total length, from which 97,300 km are gravity sewers and around 36,600 km are pressurized pipes. The remaining systems concern rainwater gathering and drainage tubes controlling the groundwater table. It is also estimated that around 50,000 km of extra conduits serve as connections between the main sewer system and households or gully pots (Kunst, 2016). The wastewater of roughly 27.3% of the Dutch households is discharged via separate sewer systems (Oosterom et al., 2013). The need for a further shift towards separate systems could be justified by the offered merits, including reduction of public health hazards, recycling of run-off water, stable and less diluted load on the wastewater treatment plant and minimization of discharged wastewater on receiving water bodies. Nonetheless, a known issue of separate systems is the existence of illicit connections (Lepot et al., 2017).

Figure 1.1 depicts the percentage use of different materials for sewer pipes, indicating that both concrete and plastic pipes are selected for urban drainage purposes. Although concrete is the dominant material, the use of plastic pipes is also considerable while it becomes more extensive over the years. Further, observation of inspection databases from three Dutch municipalities, namely Almere, Breda and Haarlem, indicates that PVC is the most popular plastic material (Figure 1.2), especially for construction of gravity sewers (48.6% in Almere, 35.5% in Breda and 12.5% in Haarlem). Category "Other" in Figure 1.2 includes mainly other types of plastic materials (e.g. polyethylene). In Almere, the youngest city in The Netherlands largely built after 1970, the existence of two different sub-systems is profound: a storm sewer system constructed mainly of concrete pipes and a wastewater sewer system constructed mainly of PVC. In Breda and Haarlem there is a variation of installed plastic pipes in terms of construction materials and types of application (stormwater, wastewater and combined system). Concrete sewer pipes, which occupy the largest portion of sewer systems, have been extensively studied in terms of structural and hydraulic conditions (Stanić, 2016). On the other hand, literature is de-

prived of a comprehensive study on plastic sewer pipes. In this thesis, initial focus is mainly given to PVC pipes given their broader use.

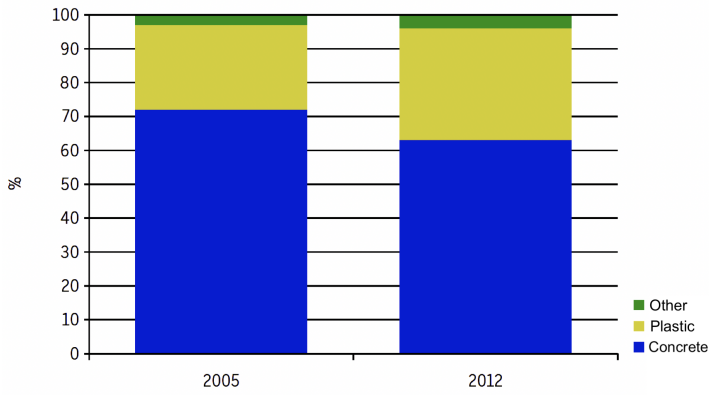

Figure 1.1: Overview of materials used for sewer pipes in The Netherlands in 2005 and 2012. Graph retrieved from Rioned (2013).

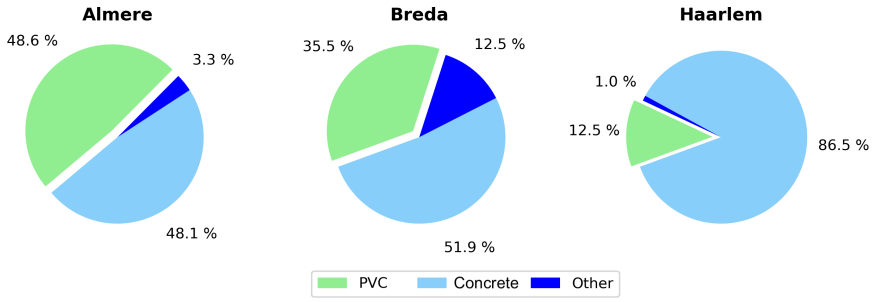

Figure 1.2: Sewer pipe materials used in three Dutch municipalities (Almere, Breda and Haarlem).

1.3. FACTORS AND MECHANISMS AFFECTING PVC PIPES LIFETIME

From the initial stages of production until the last stages of operational lifetime, several factors exist which could potentially influence the physical, chemical and, hence, mechanical properties of PVC pipes. An overview of these factors and the observed mechanisms is provided in the following sections.

1.3.1. PRODUCTION

Suspension polymerization is the most applied process for PVC particles production (80%), while emulsion and mass polymerization provide 12 and 8% of the world production respectively (Fischer et al., 2014). Although the specific details of the PVC par-

ticles size slightly differ in literature (Faulkner, 1975; Benjamin, 1980; Butters, 1982), the microstructure follows the same pattern. This can be described in three stages (Butters, 1982): the stage III-PVC particle ($\sim 100-150\,\mu m$), the stage II-primary particle ($\sim 0.1-2\,\mu m$), and the stage I particle ($\sim 10\,nm$). The conversion of the material to a homogeneous product requires that the boundaries of the primary particles disappear and a new continuous entanglement network is developed (Visser, 2009). This procedure is known as the gelation process and its quality is expressed by the gelation level. There are several methods to obtain information about the gelation level (Terselius et al., 1981; Gilbert et al., 1981; van der Heuvel, 1982; Marshall et al., 1982; Johansson et al., 1986; Kim et al., 1987; Choi et al., 1992; Fillot et al., 2006; Gramann et al., 2010; Castillo, 2016; Real et al., 2018).

A general accepted opinion suggests optimum gelation levels of 60-85% (Benjamin, 1980; Breen, 2006). A temperature $> 250\,^{\circ}C$ is needed for this purpose (Guerrero et al., 1981), much higher than the degradation temperature of PVC which is $\sim 205\,^{\circ}C$ (Wypych, 2015). Hence, thermal energy is complemented with mechanical energy (high shear stresses) by the use of twin rotating screws, so as to accelerate this process without extensive exposure of the material to too high temperatures (Visser, 2009). Subsequently, the molten material is introduced in a die so that the final pipe is shaped and cooled. This manufacturing technique is called extrusion and is extensively used to form pipes. Fittings, such as joints, are formed by the injection moulding technique. In the injection moulding process, the melted plastic is injected in a mould, which gives the desired form to the fitting, and after cooling the product is ejected.

During the production process, several additives and fillers may be incorporated in the polymers structure in order to enhance its chemical and physical properties, respectively. Plasticizers and stabilizers are the main additives as they affect the behaviour and degradation rate of the material through its lifecycle. Plasticizers are utilized in order to replace some monomers of the polymer chain, offering a higher degree of mobility and, hence, more flexibility. For sewer applications unplasticised rigid PVC pipes are used. Stabilizers are added for increased resistance to e.g: UV rays, chemical attack, and other relevant external factors (Cardarelli, 2008). For PVC pipes in Europe, lead has been used until the early 2000s, when it was replaced by calcium-based stabilizers in most countries (Anders, 2014).

Every step within the production of PVC pipes and fittings can have an effect on the long-term performance of the final product. The levels of water and oxygen during polymerization could influence the formation and quality of the produced PVC particles (Butters, 1982). The gelation process, already affected by the degree of polymerization (Fujiyama et al., 2004), plays a major role in the mechanical properties (Mandell et al., 1982; van der Heuvel, 1982; Truss, 1985; Moghri et al., 2003). These properties are determined by the morphology of the material (Benzamin, 1980; Kuriyama et al., 1998) and by the polymer's orientation and molecular mobility (Fillot et al., 2007). Additionally, impurities and voids in the polymer structure, frequently referred to as inherent defects, are introduced during production, resulting in crack initiators, while their presence seems to be inevitable (Johansson et al., 1987). The wear observed at the pipe extruders (Gladchenko et al., 1997) might also contribute to the occurrence of inherent defects.

Table 1.1: Observed values for circumferential residual stresses in PVC pipes.

	Residual Stresses (MPa)		
DN	**Tensile**	**Compressive**	**Reference**
-	1.5-4.8	-	Breen (2006)
315	2.6	-	Meerman (2008)
125	2.2	-	
110	1.7	-	
125	1.1	-	
125	1.3	-	
125	2.3	-	
200	0.9	-	
32	-	5.6-9.4	Scholten et al. (2016)
110	-	3.9-6.6	

Residual stresses are also introduced during production, as a result of different cooling rates between the inner and outer pipe surface (Siegmann et al., 1981), and constitute another parameter that affects the mechanical properties of the produced pipe (Siegmann et al., 1982). Relevant research on residual stresses in PVC pipes (Breen 2006; Meerman 2008; Scholten et al., 2016) has revealed that their magnitude is in a range of 0.9-4.8 MPa for tensile and 3.9-9.4 MPa for compressive stresses (Table 1.1). In principle, a faster cooling rate or a thicker pipe wall thickness will lead to higher levels of residual stresses (Janson, 2003; Scholten et al., 2016). However, irrespectively of their magnitude, residual stresses affect the crack propagation as they change the stress profile through the pipe (Chaoui et al., 1987; Burn, 1992), increase the brittle-ductile temperature (Scholten et al., 2016), and, consequently, they seem to have a tremendous effect on the lifetime of pressurized plastic pipes (Hutař et al., 2013; Poduška et al., 2016).

In literature, the residual stresses in plastic pipes have been estimated by solely slitting pipe rings approaches and measuring the change in perimetry (Janson 2003; Breen, 2006; Meerman, 2008), or slitting is combined with layer removal methodologies (Williams et al., 1981; Doshi, 1989; Poduška et al., 2014, 2016) in order to acquire a more accurate distribution of the residual stresses through the pipe thickness. Tensile residual stresses presented in Table 1.1 are estimated with Eq. 1.1 (Breen, 2006):

$$\sigma = \frac{l_o \cdot d}{4 \cdot \pi \cdot R^2} \cdot E \tag{1.1}$$

where l_o is the overlap length (m), d is the pipe wall thickness (m), R is the mean radius of the pipe wall (m) and E is the modulus of elasticity (Pa).

Compressive residual stresses presented in Table 1.1 are estimated with Eq. 1.2 (Janson, 2003):

$$\sigma = \frac{\alpha}{\pi \cdot D - \alpha} \cdot \frac{d}{D} \cdot E_c \tag{1.2}$$

where α is the reduction of the pipe perimetry (m), d is the pipe wall thickness (m), D is

the mean pipe diameter (m) and E_c is the creep or relaxation modulus of the pipe (Pa).

1.3.2. INSTALLATION

The conventional installation procedure involves the digging of an open trench, lying of the pipe, and soil covering and compaction. However, during transport and installation of plastic pipes, scratches and dents can be inflicted on the pipe surface. These plastic deformations can later act as stress risers, and can eventually lead to failure under certain service conditions. Improper soil compaction is also the cause of pipe ovalization, resulting in high tensile stresses at the 12 and 6 o' clock positions of the inner surface and at the 3 and 9 o' clock positions of the outer surface. In pressurized systems, homogeneous soil embedding can exert external pressure on the pipe, counteracting the internal pressure and, hence, reducing the probability of crack formation (Hutař et al., 2011).

Additionally, poor quality of soil embedding could amplify the effects of the low bending stiffness found in plastic pipes, resulting in improper and challenging to measure longitudinal slopes in gravity systems, and in pre-buckling conditions (Stein, 2001). Another factor that can affect the material degradation is determined by the conditions of storage prior to installation. Photochemical degradation caused by UV rays has been proven to be harmful for the mechanical properties of PVC pipes (Hussain et al., 1995; Anton-Prinet et al., 1999).

1.3.3. OPERATION

During operation, four main ageing mechanisms have been identified: physical ageing, mechanical degradation, chemical degradation and environmental stress cracking. Physical ageing in polymers is a phenomenon which imposes changes on a material's property as a function of time, at a constant temperature and independently of other external factors (Hutchinson, 1995). Amorphous (or glassy) polymers, such as PVC, experience physical ageing due to the fact that they are cooled to a temperature below their glass transition temperature (Tg), and, hence, are not in a thermodynamic equilibrium state. In this non-equilibrium state, the glassy polymer has excessive thermodynamic properties (volume, enthalpy) and there is a continuous effort to reach the equilibrium state (Hutchinson, 1995). Physical ageing can be traced by reduction in volume and enthalpy, but also by changes in the mechanical properties (Rabinovitch et al., 1992). The polymer becomes stiffer and more brittle, while its creep and stress relaxation rates decrease (Struik, 1977; Laiarinandrasana et al., 2011). In principle, physical ageing is an inevitable, although reversible (Hutchinson 1995), process in polymers which is accelerated at higher temperatures (Visser et al., 2011).

Mechanical degradation is the result of stresses which are exerted on the pipe (or joint) and their level surpasses the material's fracture threshold. It appears in the form of fissures (crazes, cracks) or breaks. Stresses originate from internal pressure, deflections due to soil cover, and the production process (residual stresses). Additional stresses can be imposed by axial bending due to improper soil bedding and compaction. The quality of pipe extrusion can be a decisive factor for the longevity of the pipe, as crack initiation

is observed in built-in voids and impurities. Subsequently, the propagation of the crack is governed by the magnitude and direction of the applied stresses. This failure mechanism is known as Slow Crack Growth (SCG). In case of external impacts (e.g. hit by an excavator), mechanical degradation could surface as rapid crack propagation (RCP). Apart from processing quality, temperature is also a critical factor concerning the mechanical properties of the material. Lower temperatures result in more brittle failures, while the amount of energy that can be absorbed by PVC pipes before fracture seems to reduce dramatically (McGarry et al., 1985; Visser et al., 2011; Scholten et al., 2016).

Chemical degradation involves the occurrence of chemical reactions between the polymer pipe and the environment, leading to breakage of the polymer covalent bonds. The covalent bonds build up the main back bone of a polymer chain, hence their breakage results in chain scission and molecular weight reduction. Dehydrochlorination (HCl abstraction) is often the cause that commences chemical degradation in PVC (Breen, 2006), due to the creation of sequential conjugated polyenes (Arnold, 2003), which is also the source of the discolorization appearance. The impact on the mechanical properties has been characterized with the term “stress corrosion cracking”, and is realized in 4 stages (Choi et al., 2005): initiation of microcracks, slow crack growth, clustering of cracks, and clusters growth.

Environmental stress cracking (ESC) is a failure mechanism very similar to slow crack growth in terms of shape. It is a physical process driven by the applied stress but accelerated by the presence of an active environment (Bishop et al., 2000), as diffusion is the factor that enhances the susceptibility to fractures due to the creation of plasticized (softer) layers and surface energy reduction (Arnold, 2003). Breen (1993, 1994, 1995) has explored crazing and crack growth mechanisms concerning PVC pipes in vapour and liquid environments, concluding that above a certain level of environment concentration and stress intensity, the material’s load bearing capacity can decrease. In general, a wide range of glassy polymers (including PVC) has been investigated regarding their ESC resistance under various types of environments (Robeson, 2013), indicating that issues of ESC may appear in certain combinations of “material-environment”.

1.4. LIFETIME PREDICTION METHODS AND THEIR LIMITATIONS

This section includes the reported lifetime prediction methods for plastic pipes. Some methods can be used to describe specific degradation or failure mechanisms, while others can be used in a more general way. The limitations of the presented methods are also discussed here.

1.4.1. HYDROSTATIC TESTING AND STANDARD EXTRAPOLATION METHOD

A conventional way of rating a thermoplastic pipe is by determining the resistance to constant internal pressure, as described in ISO 1167-1 (2006). The experiments are implemented under several internal pressures and temperatures, and under certain environmental conditions (i.e., water in water, water in air, water in liquid). The time to failure is recorded and the results are depicted as a double logarithmic σ_{hoop} vs $t_{failure}$

1

curve. An incident of failure is considered when there is leak or break. The type of failure can be ductile (Region I), quasi brittle (Region II) or brittle (Region III).

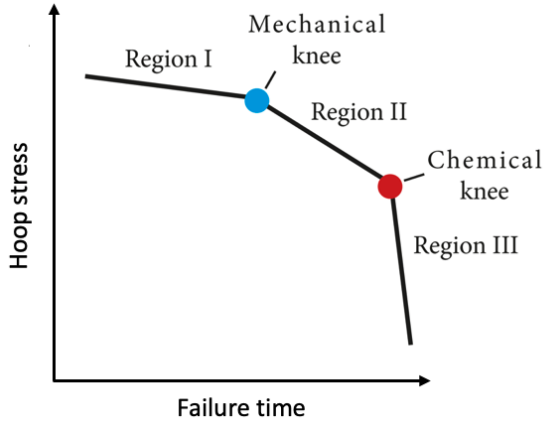

Figure 1.3: The types of failures observed in thermoplastic pipes subjected to various levels of hoop stress.

Figure 1.3 presents how the level of applied stress leads to one of the three types of failure as a function of time. In case of high stress values (Region I), a yield deformation in the failure zone is vivid with fracture appearing within relatively short testing times. For intermediate stress levels (Region II), the failure is generated in longer testing times and is characterized by slow crack growth with local plastic deformation only at the crack front. In even longer testing durations (Region III), there is no apparent yield deformation and the occurrence of fractures is nearly independent of the stress level. The points of transition from region I to II and from II to III are frequently referred to as the "mechanical knee" and the "chemical knee", respectively.

Higher testing temperatures tend to move the curves to lower failure times, allowing for shortest testing periods. This is obvious in Figure 1.4, in which the maximum level of hoop stress as a function of time and temperature is presented for unplasticized PVC pipes. Extrapolation to service temperatures can then be performed according to the standard extrapolation method (SEM) published in ISO 9080 (2012). SEM requires extensive hydrostatic testing at 2 or more testing temperatures (>30 samples per temperature) and the application of certain statistical methods to the experimental datasets.

One apparent limitation of performing hydrostatic pressure tests is the necessary duration of the experiments. The relevant standardized guidelines (ISO 1167, ISO 9080) indicate that the applied internal pressures should be at such levels that at least four specimens would fail after 7000 hours (292 days) and at least one after 9000 hours (375 days). This fact could justify that this kind of method has been used only by a few researchers and usually partially, in order to avoid the extensive testing required by SEM. A case of full implementation of this method has been published by Krishnaswamy (2005), who tested 8 different kinds of HDPE pipe resins. Other reported limitations originate from the thermal ageing involved in this method. Sorption and diffusion of oxygen or other

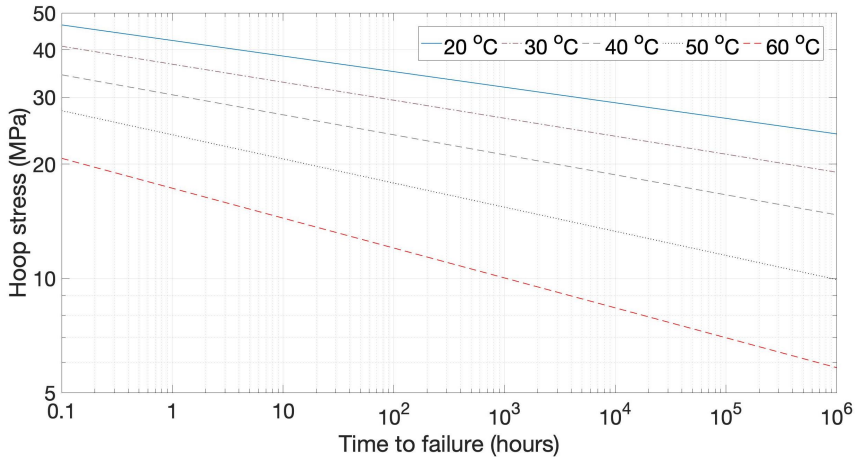

Figure 1.4: The types of failures observed in thermoplastic pipes subjected to various levels of hoop stress. Data is retrieved from Kunststoffrohrverband (1997).

chemicals in the polymer matrix are temperature dependent micro-mechanisms which contribute to the failure process (Lang et al., 1997). However, SEM lacks in incorporating the variability of different temperature dependent rates introduced by different physical and chemical processes.

1.4.2. LINEAR ELASTIC FRACTURE MECHANICS (REGION II)

Numerous researchers have focused on simulating slow crack growth (region II in Figure 1.3) which originates from inherent flaws and is propagated by the applied stresses. The applied stresses are expressed via the stress intensity factor K_I, which considers the internal pressure, the pipe and crack geometrical characteristics, and the type of loading (Maiti, 2015). K_I corresponds to the mode I type of loading which indicates tension of the pipe in a direction perpendicular to the plane of the crack. The time of crack initiation can be expressed via (Lang et al., 1997):

$$t_{in} = B\, K_I^{-n} \tag{1.3}$$

where B and n are constants which depend on the tested material.

As it is observed in Figure 1.5, when the crack growth rate da/dt is plotted against the stress intensity factor K_I in a double logarithmic scale, Eq. 1.4 can be established for a specific range of da/dt in order to describe slow crack growth. Prior to this phase, crack growth rate decreases rapidly as the threshold value K_{Ith} is approached, while at the end it increases rapidly as the material's fracture toughness K_{IC} is approached:

$$\frac{da}{dt} = A\, K_I^m \tag{1.4}$$

where A and m are constants which depend on the tested material.

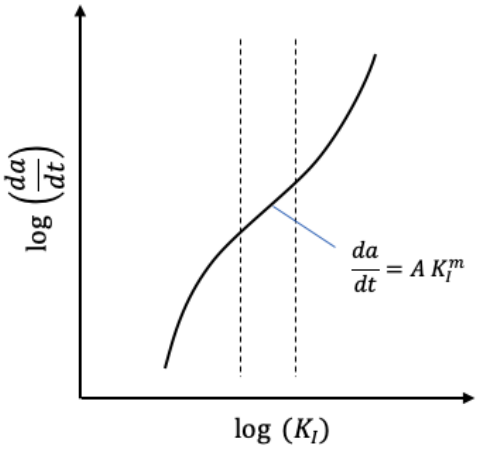

Figure 1.5: Creep crack growth rate as a function of stress intensity factor K_I.

The lifetime prediction can be accomplished by estimating the crack initiation time according to Eq. 1.3 and integrating Eq. 1.4 for the stable crack growth period:

$$t_f = t_{in} + t_{SCG} = B\, K_I^{-n} + \int_{a_o}^{a_f} \frac{da}{A\,(K_I)^m} \tag{1.5}$$

where a_o is the assumed initial flaw size and a_f is the critical crack size which is usually assumed to be the pipe wall thickness. Most of the authors, however, tend to neglect the initiation time t_{in} as separate experiments are needed for the determination of B and n, and it is considered negligible compared to the magnitude of t_{SCG}.

This lifetime prediction model has been the basis for extensive research on PE pipes (Pinter et al., 2007; Frank et al., 2009, 2012; Zhao et al., 2013; Kratochvilla et al., 2014; Wee et al., 2016; Deveci et al., 2017), PVC pipes (Balika et al., 2002; Gould et al., 2013) and elastomers (Arbeiter et al., 2015). The type of specimens used in such experiments are usually the cracked round bars (CRB) or circular notched specimens (CNS). Other types of experiments include specimens for the Pennsylvania notched test (Brown, 2007; Robledo et al., 2013; Nezbedová et al., 2013) and the strain hardening test (Robledo et al., 2013; Deveci et al., 2017).

The Linear Elastic Fracture Mechanics (LEFM) method is based on short-term (mainly fatigue) tests and focuses on describing the fracture mechanisms (i.e. slow crack growth) at the crack tip. This fact implies that other types of degradation, such as chemical, which may occur in a plastic pipe should be restricted in the area of the crack tip. Otherwise, slow crack growth is no longer the critical factor for the pipe's failure, and the application of the LEFM method in its conventional form seems to be invalid. Another limitation in applying the LEFM method is the requirement for input of the precise geometry (size and shape) of the initial defect. Analysis of the uncertainties that are introduced in modeling slow crack growth by means of LEFM for PVC (Davis et al., 2007) and HDPE (Khelif

et al., 2007) emphasized the significance of inherent defect sizes in the reliability of the model's outcome. Other researchers (Burn, 1991; Lu et al., 2003) have also commented on the sensitivity of the estimated lifetime prediction to the initial flaw geometry.

1.4.3. ARRHENIUS EQUATION (REGION III)

Application of the Arrhenius equation is considered feasible under the assumption that the degradation rate of the material follows a first order kinetics. It is a method highly connected with the chemical aspects involved in the degradation process indicating the depletion of the introduced stabilizers and the onset of thermo-oxidative degradation (region III in Figure 1.3). These aspects are usually expressed via the reduction of the oxidation induction time (OIT) or the build-up of hydroperoxides (ROOH). The concept behind this method is also higher testing temperatures and shorter testing periods. Subsequently, the Arrhenius model is used for extrapolation of the rate of degradation reaction (k) to other (service) temperatures, allowing for lifetime prediction. The Arrhenius model is defined as:

$$\ln k = -\frac{E_a}{R}\,\frac{1}{T} + \ln C \tag{1.6}$$

where k is the degradation reaction rate (s^{-1}), E_a is the activation energy of the reaction (J mol^{-1}), R is the gas constant (8.31 J K^{-1} mol^{-1}), T is the testing temperature (K) and C is a constant.

The assumed linearity involved in the Arrhenius model seems, nonetheless, to be valid only for a range of testing temperatures (Celina et al., 2005). For instance, relevant research on PP (Celina et al., 2005) has shown that at circa 80 °C the degradation rate of PP seems to lose its Arrhenius linearity. This fact indicates that caution should be also exercised for the use of the extrapolation factors k_e which are included in ISO 9080 and concern lifetime prediction in case of region III failure based on the Arrhenius linearity. Generally, thermo-oxidative degradation based on accelerated ageing experiments is a more complicated mechanism that depends on the physics involved in the process (e.g., diffusion), and the behaviour of the present stabilizers and other additives (Celina, 2013).

1.4.4. QUALITY NUMBER

The quality number method was applied for plastic pipes solely by Whittle and Tennakoon (2005). It considers the properties that affect the durability of the system and their respective weighting factors in a cumulative form. Lifetime prediction is made by applying Eq. 1.7 on several pipes of different age and creating a simple linear regression with the pipe age as the independent variable. Subsequently, extrapolation is feasible to longer ages until a threshold quality number is reached, below which a pipe is considered to be unsafe for further operation. The age which corresponds at the threshold is considered as the predicted lifetime:

$$Q = \sum_{i=1}^{n} W_i\,\frac{M_i}{R_i} \tag{1.7}$$

where Q is the total quality number, W_i is the weighting factor of a property, M_i is the measured value of a property, and R_i the reference value of a property.

It is reasonable to state that the results obtained by this method are certainly open to dispute. This is due to the fact that the outcome is dependent on the arbitrary choice of the weighting factors and the threshold quality number, rising the levels of uncertainty. Additional caution should be also exercised when applying this method as it implies a connection between the age and the integrity of the pipe, irrespectively of the quality of production. However, older pipes which are more well processed than newer pipes could provide higher values of Q, leading to a regression model with positive slope. This fact would result in the poorly founded conclusion that failure will never occur.

1.5. THESIS OBJECTIVE AND OUTLINE

Production, installation and operation include numerous factors which can affect the lifetime of a plastic (e.g. PVC) pipe. These factors appear to interact with each other under certain conditions resulting in different failure mechanisms. Four lifetime prediction models have been utilized in literature to describe some of these failure mechanisms and conclude on the residual lifetime of plastic pipes (Balika et al., 2002; Celina et al., 2005; Krishnaswamy, 2005; Whittle and Tennakoon, 2005; Gould et al., 2013). However, given their limitations, the predicted lifetimes are certainly open to dispute, as no model encompassing all possible failure mechanisms has been proposed yet. The development of such a model would yield inaccurate results due to the overall heterogeneity (pipe material, soil conditions, installation quality) and the lack of required data for calibration and validation. Therefore, this thesis is not dedicated to the development of models for direct estimation of a pipe's residual lifetime assessment.

This thesis deals with **ageing of plastic sewer pipes** and it is structured based on a consequential order outside of a strict framework of predefined research questions. Therefore, the next step was sensibly dictated by the previous one, originally starting from a holistic review on the available literature. Due to the massive use of PVC as construction material of plastic urban drainage pipes, initial focus is directed exclusively to PVC pipes. However, the main conclusions are based on properties shared also by other kinds of plastics used for sewers. This is also depicted on the general applicability of the eventually proposed technique for quantification of ageing in plastic pipes. The overall objective of this thesis is to provide appropriate knowledge and tools concerning the assessment of plastic pipes, in order to facilitate the establishment of future sewer asset management strategies.

The 2nd chapter includes a critical assessment of the theoretical durability of plastic sewer pipes found in several case studies and the actual performance as it is depicted in inspection data. The 3rd chapter explores this discrepancy via examination of inspection images, and observation of the excavation site and extensive laboratory testing of eight PVC sewer pipes. The rest of the thesis concerns the development of a vibro-acoustic method in order to track ageing in plastic pipes. Accordingly, Chapter 4 presents the theoretical background of the proposed method, including the derivation of an analytical solution for acoustic wave propagation in the pipe and development of a relevant

finite element model. Subsequently, Chapter 5 includes the experimental application of the developed technique, while the capability of detecting ageing in real world conditions is discussed. The last part of this thesis, Chapter 6, summarizes all the main findings of this research, while it provides points of attention and recommendations for researchers and sewer asset managers.

2

A COMPARATIVE STUDY ON THE DURABILITY OF PVC PIPES

2.1. INTRODUCTION

Plastics are used for a wide range of commercial and industrial piping applications. The most known are Polyvinyl Chloride (PVC), Polyethylene (PE), Polypropylene (PP), Acrylonitrile Butadiene Styrene (ABS), Polybutylene (PB) and Glass-fibre Reinforced Polyester (GRP or FRP). Concerning systems for drinking water supply, gas distribution and sewage disposal, PVC, PE and PP are the most popular polymer materials (PlasticsEurope, 2017). Especially for gravity wastewater pipes, PVC has been extensively used in the past decades and has become one of the dominant construction materials. Cost-efficiency, ease of installation, range of available diameters (40-630 mm) and its reputed chemical resistance favor its wide acceptance by decision makers in urban drainage (Davidovski, 2016). However, since there are PVC sewer pipes in operation for at least four decades, concern over their longevity has been lately raised. It is still unknown whether the expectations of long-lasting PVC pipes (Folkman, 2014) will prove realistic or new asset management strategies should be established in the near future. A necessary condition for achieving this, is comprehensive understanding of the mechanisms that affect a PVC pipe's lifetime, their combined effects, and eventually their results, which are the defects found in practice.

The objective of this chapter is to present case studies of tested PVC sewer pipes found in the literature and compare the derived conclusions on PVC durability with findings in inspection data. Emphasis is given on studies that investigate the properties that define the structural integrity and overall performance of a sewer system. The inspection data concerns four different municipalities in The Netherlands: Almere, Am-

Parts of this chapter have been published in: Makris, K. F., Langeveld, J., & Clemens, F. H. (2020). A review on the durability of PVC sewer pipes: Research vs. practice. Structure and Infrastructure Engineering, 16(6), 880–817. doi:10.1080/15732479.201973442

stelveen, Breda and Haarlem. The main discrepancies between literature and inspection data are discussed, as a step towards bridging results from scientific research and observations from practice.

2.2. PVC PIPES IN LITERATURE

2.2.1. MATERIAL PROPERTIES

A moderate amount of research is published concerning PVC sewer pipes, which are either new or used for several years, and have been utilized in different areas. Table 2.1 provides an overview of specifications of the tested excavated pipes. An early study (Bauer, 1990) was conducted on a 15 years old PVC sewer pipe in Texas based on the requirements imposed by ASTM D3034. The pipe had a nominal diameter (DN) of 254 mm and standard dimension ratio (SDR) of 35. SDR denotes the ratio between the external diameter and wall thickness of the pipe. Measurements of the tensile properties showed a mean tensile strength of 52.36 MPa and mean modulus of 2839 MPa in the circumferential direction, and 55.4 and 3059 MPa respectively in the longitudinal direction. The pipe's ability to withstand vertical loads (e.g. soil) was measured via the average pipe stiffness and it was reported to be 433 kPa according to ASTM D2412. A series of other tests following the respective American standards took place, including extrusion and installation quality, dimensions measurement, impact resistance, and flattening resistance. According to the study, the results revealed that all the measured properties comply with ASTM D3034 and no observable degradation had occurred over the quoted time period.

Similar studies in Europe (Alferink et al., 1995; Meerman, 2008) include the investigation of several PVC sewer pipes of different standard dimension ratio and ages (Table 2.1). A lot of emphasis has been given to deflection measurements and production or installation practices. However, there is no extensive exploration of mechanical properties and their potential deterioration. The only case concerns two PVC pipes from Norway (Notteroy) and Sweden (Torshalla), whose properties have been compared with a brand-new pipe. The results (Table 2.2) indicate that the properties of pipes have been compromised. The pipe tested from Norway, which is of the same diameter but of lower pipe wall thickness (higher SDR value) compared to the reference pipe, indicate only a slight decrease of 16.8% in strain at break while the yield stress remains intact. Concerning the pipe from Sweden, the results revealed a 7.8% decrease in yield stress and 80.6% decrease in strain at break, a fact which may be explained by the low degree of gelation. A contributing factor to the decrease in the strain at break is also physical ageing, although an increase in yield stresses was expected. In this study, the degree of gelation was expressed as a percentage of attack of methylene on PVC. Based on the provided values for all pipes, it is obvious that the majority of the pipes seem to be of poor production quality, i.e. low degree of gelation.

In the Netherlands the case of seven excavated PVC sewer pipes has been reported (Meerman, 2008). The level of degradation of these pipes was evaluated based on visual and microscopic inspection, geometrical analysis, and surface roughness measurements (Table 2.3). Comprehensive testing on the pipe's properties did not take place,

Table 2.1: Overview of tested PVC sewer pipes in literature.

Reference	Location	Age (years)	DN	SDR	Testing method/tested property
Bauer (1990)	Texas	15	254	35	Acetone immersion, dimensions, flattening, impact resistance, joint tightness, pipe stiffness, tensile properties, workmanship
Alferink et al. (1995)	France	12	315	41	Dimensions, pipe stiffness
		25	200	51	Dimensions, Fourier transform infrared spectroscopy
		23	315	51	(FTIR), joints tightness, methylene chloride test
		25	400	41	(MCT), pipe stiffness, X-ray fluorescent (XRF)
	Denmark	23	160	41	
		30	200	34	
		28	200	41	
	Norway	22	250	51	Dimensions, Fourier transform infrared spectroscopy
	Sweden	24	200	41	(FTIR), joints tightness, methylene chloride test (MCT), pipe stiffness, tensile properties, X-ray fluorescent (XRF)
Whittle and Tennakoon (2005)	Australia	25	150	38	Differential scanning calorimetry (DSC), impact resistance, pipe stiffness, joints tightness, specific gravity, tensile properties
			150		
		16	150		
			150		
		11	225		
			225		
		20	150		
Meerman (2008)	The Netherlands	35	315	34	Dimensions, microscopic inspection, residual stresses, surface roughness, visual assessment
		Up to 25	110		
			125		
			125		
			125		
			125		
			200	51	
Gould et al. (2013)	Australia	34	200	~20 (PN12)	Attenuated total reflectance Fourier transform infrared spectroscopy (ATR-FTIR), scanning electron microscope (SEM) with energy dispersive X-ray spectrometer (EDS)
Folkman (2014)	USA	20	610	18	Acetone immersion, dimensions, hydrostatic integrity

Table 2.2: Material properties of 10 PVC sewer pipes in France, Denmark and Norway (Alferink et al., 1995).

Place	DN	SDR	Age (years)	Percentage of attack (%)	Yield stress (MPa)	Strain at break (%)
Gerzat	200	51	25	No attack	-	-
Montpellier	315	51	23	25 - 30	-	-
St. Agathe	400	41	25	100 – 100	-	-
Courchevel	315	41	12	-	-	-
Odense	160	41	23	75 – 100	-	-
Nykobing	200	34	30	65 – 100	-	-
Nykobing	200	41	28	25 - 90	-	-
Notteroy	250	51	22	35 – 100	50	142
Torshalla	200	41	24	50 - 100	46.1	33
Reference	250	41	New	No attack	50	170

and suggestion of at least 100 years lifetime was based on a previous report on PVC water pipes (Breen, 2006). It has to be realized that in drinking water pipes the environment is totally different from urban drainage systems, and the failure mechanisms of chemical degradation or environmental stress cracking are neglected.

The results of a more comprehensive, in terms of mechanical properties, study (Whittle et al., 2005) of seven PVC sewer pipes that had served for up to 25 years in Australia

Table 2.3: Material properties of 7 PVC sewer pipes in the Netherlands (Meerman, 2008).

DN	Age (years)	Circularity (Dmax/Dmin)	Microscopic/Visual Assessment		Roughness(μm)
			Inner	Outer	
315	35	1.02	Scratches, wear, crazes	Discoloration, scratches	-
125	Up to 25	1.01	Scratches, wear, crazes, discoloration	Slight discoloration, scratches	1.0
110		1.03	Wear, discoloration	Scratches	0.9
125		1.02	Moderate wear	Scratches	0.4
125		1.01	Wear, discoloration	Strong discoloration, scratches	0.4
125		1.05	Crazes	Moderate discoloration, scratches	0.3
200		1.02	Scratches, wear	Scratches	0.6

are presented in Table 2.4. These properties were also combined with the production process conditions. In this case study, the degree of gelation is expressed as the gelation level, determined by means of differential scanning calorimetry. As it is indicated by the results, there is no actual connection between the age, gelation level and mechanical properties of the tested pipes. In fact, the pipe with the lowest gelation level (35%) corresponds to the highest magnitudes of stress (39.3 MPa) and elongation (117.2%) at break. At the same time, pipes with optimum gelation levels (76-88%) correspond to the lowest magnitudes of yield stress and tensile strength. A valid argument provided by the researchers of this study is that higher concentrations of fillers, expressed as an increase in specific gravity (i.e. from 1.465 for DN 150 to 1.522 for DN 225), could have led to this discrepancy. Finally, application of the quality number method (Eq. 1.7) yields proposed lifetimes of 98 to 288 years based on a worst case and best-case scenario respectively.

Table 2.4: Material properties of 7 PVC sewer pipes (SDR 38) in Australia (Whittle and Tennakoon, 2005).

DN	Age (years)	Gelation Level (%)	Processing Temperature (°C)	Ring stiffness (N/m/m)	Yield stress (MPa)	Stress at break (MPa)	Elongation at break (%)	Impact result*
150	25	43	172	6.047	42.2	37.8	18.3	Brittle (4)
150	25	59	173	5.905	43.2	37.9	28.9	Brittle (1) / No fracture (1)
150	16	46	173	7.309	43.9	38.9	84.5	Brittle (1) / No fracture (3)
150	16	35	173	6.834	43.0	39.3	117.2	Brittle (3)
225	11	88	182	7.785	39.1	34.9	56.5	Brittle (2) / No fracture (4)
225	11	76	181	8.759	39.4	34.9	79.4	Brittle (6) / No fracture (4)
150	20	73	175	10.350	41.7	36.3	63.8	Brittle (2) / No fracture (10)

* the number of tested specimens is in parenthesis

Pipe stiffness is considered as the main design property in gravity sewer pipes. This fact has led some research approaches to focus on mechanisms and properties of plastic sewers which are considered to be connected with pipe stiffness, such as deflection and stress relaxation. The deflection of a flexible pipe is a function of several parameters. Pipe material and geometrical characteristics, the bedding and backfilling material, the compaction degree, the burial depth and existence of geogrid reinforcement could change the levels of deflections significantly (Välimaa, 1982; Rajkumar et al., 2008; Hsieh et al., 2010; Mohamedzein et al., 2016; Dawood, 2018).

The results of deflection measuring programmes regarding PVC sewer pipes in several countries are presented in Table 2.5. In Europe, deformations of up to 14% were observed (Välimaa, 1982; Walton et al., 1989; Alferink et al., 1995). The magnitudes of these values are in accordance with the values observed in the USA (Moser et al., 1990).

Table 2.5: Measured deflection levels of PVC sewer pipes in literature.

Area	DN/SDR	Soil	Surrounding material	Age (years)	Deflection(%) Mean	Deflection(%) Maximum	Reference
Dartford (England)	457/41	Chalk	Pea gravel	2	1	3	Walton and
				17	1	3	Elzink (1988)
	406/41	Chalk	Pea gravel	2	1	2	
				17	1	2	
	273/41	Chalk	Silty sand	2	2	4	
				17	2	5	
Dragör (Denmark)	400/34	Sand with fine clay part	Sand surround	0.5	2	5	
				13	3	5	
	400/41	Sand with fine clay part	Sand surround	0.5	2	7	
				13	4	7	
Lelystad (The Netherlands)	250/41	Fat clay	Sand surround	2	3	5	
				14	3	5	
	250/41	Fat clay	Sand surround	2	3	6	
				14	3	6	
Buckie (Scotland)	244/44	Loam with gravel	Coarse sand	6	3	5	
				20	3	5	
	244/44	Loam with gravel	Coarse sand	6	3	7	
				20	3	7	
	244/44	Loam with gravel	Coarse sand	6	4	9	
				20	4	10	
	323/44	Loam with gravel	Coarse sand	6	3	7	
				20	3	7	
	244/44	Loam with gravel	Coarse sand	6	7	13	
				20	7	14	
USA	254/NA	Gravel pit	Silty fine sand	0.01	3.6	-	Moser et al. (1990)
				0.1	4	-	
				1.1	6	-	
				11.4	6.1	-	
	254/NA	Gravel pit	Silty fine sand	0.01	3.2	-	
				0.1	3.5	-	
				1.1	5.5	-	
				11.4	5.6	-	
	254/NA	Gravel pit	Silty fine sand	0.01	2.8	-	
				0.1	3.3	-	
				1.1	5.2	-	
				11.4	5.2	-	
	254/NA	Gravel pit	Silty fine sand	0.01	2.1	-	
				0.1	2.9	-	
				1.1	4.2	-	
				11.4	4.3	-	
Kauniainen (Finland)	315/34	Silt-Siltmoraine	Gravel	0.01	-	1.1	Välimaa (1982)
				9.5	-	2.7	
	315/34	Silt-Siltmoraine	Gravel	0.01	-	1	
				9.5	-	3.2	
	315/51	Siltmoraine	Sand	0.01	-	2	
				9.5	-	2.9	
	315/51	Siltmoraine	Siltmoraine	0.01	-	3.3	
				9.5	-	4.2	
	315/51	Rock	Sandy silt	0.01	-	1.4	
				9.5	-	6.2	
Gerzat (France)	200/51	Sand		25	2.5	-	Alferink et al. (1995)
Montpellier (France)	315/51	Rock		23	7.5	20.5	
St. Agathe (France)	400/41	Sand		25	5.5	11.5	
Courchevel (France)	315/41	Sand		12	7.5	20	
Odense (Denmark)	160/41	Sand		23	13	17.5	
Nykobing (Denmark)	200/34	Sand		30	2.5	6	
	200/41	Sand		28	4	7	
Notteroy (Norway)	250/51	Clay		22	10	16	
Torshalla (Sweden)	200/41	Sand		24	8	12.5	

Observation of the temporal alterations of these values with respect to time since installation, justifies that 90-95% of total deflection is realized within the first two years (Joekes et al., 1985). This period is also considered sufficient to account for soil consolidation due to groundwater fluctuations (Moser et al., 1990). Other research (Alferink et al., 1995) has also highlighted the importance of installation quality. Moderate installation yields magnitudes of mean deflection up to 5.5%, while poor installation results in mean deflections of up to 13% and maximum deflections up to 20.5%.

The impact of pipe stiffness (expressed as SDR) on the performance of an operating pipe was explored by Välimaa (1982) via an elaborated field test of six PVC pipes with variations in pipe stiffness, soil cover and compaction method (Table 2.6). By the end of the testing period (i.e. 7.5 years), at which the deflection levels are considered to be stable, soil cover appears to be the most dominant factor. At 1.2 m depth, the pipe of lower stiffness with better soil compaction was less deflected than the pipe of higher stiffness. At 0.6 m depth pipe stiffness played a more significant role than the compaction method. Hence, pipe stiffness seems to be more important in low depths, while in high soil covers the compaction method becomes more significant.

Table 2.6: Approximate deflection values of PVC sewer pipes 7.5 years after installation as a function of SDR, compaction quality and soil cover (Välimaa, 1982).

SDR	Soil cover (m)	Compaction	Deflection (%)
51	0.6	light vibration	3.1
	0.9	treading	2.1
	1.2	heavy vibration	0.3
34	0.6	treading	2.6
	0.9	heavy vibration	1.6
	1.2	light vibration	0.9

Stress relaxation in PVC sewer pipes has been extensively studied by Struik (1977) and Janson (1988, 1995, 2003). It is proved that under constant deflection, stress decreases implying that the elastic modulus decreases. Viscoelasticity causes a stress relaxation state which indicates that if failure does not occur during the initial loading, it is very unlike that failure in the long-term will occur, as the applied stress will continuously decline. However, this decrease in the modulus should not be translated as a decline in the strength of the pipe, since the short-term value of the elastic modulus remains intact, or even enhanced as a result of physical ageing (Janson 1995, 2003). This has generated a confusion among researchers as to whether the long-term (Koski, 1982; Janson 1988; Hsieh et al., 2010) or short-term (Moser et al., 1990; Janson, 1995, 2003) value of elastic modulus should be used to describe pipe stiffness. Janson (1995) argues that whether the short-term or long-term stiffness should be considered depends on the type of soil and the impact it has on the behaviour of the pipe. Therefore, for sandy soils the use of short-term stiffness is appropriate, while for plastic soils the long-term stiffness is. Concerning this dispute, Moser et al. (1990) presented the results of the pipe stiffness of PVC pipes samples that had been constantly strained for 13 years under testing conditions. The pipe stiffness was determined after 1 hour of the initial imposed deflection (5% and

25%), and was compared to the pipe stiffness measured after 13 years by imposing an additional deflection of 5%. The pipes proved to be capable of withstanding additional deflections, which is in accordance with the final findings of Janson (2003). Finally, the influence of fillers and notches on pipe stiffness has been also investigated (Moser et al., 1990), but hardly any significant differences appeared compared to the un-notched or unfilled segments.

The vast majority of research in the literature concerns plastic sewer pipes that operate under gravity in which the applied stresses are limited to the effect of pipe-soil interactions. In contrast, there is a scarcity on research regarding pressurized plastic sewer systems. Only two such case studies have been reported (Gould et al., 2013; Folkman, 2014). Therefore, cases of conducted research on pressurized PVC pipes for other applications, which could apply for sewer systems, are also addressed hereafter. At this point, it has to be stressed that the operation of sewer pressurized systems is not governed by a steady internal pressure (creep) as in gas and water systems, but by a cyclic pressure pattern (fatigue). Nonetheless, the failure mechanism of slow crack growth remains the same in both cases (Hu et al., 2003).

Investigation (Folkman, 2014) of a 20 years old pressurized PVC sewer pipe took place in the USA. The pipe successfully passed the tests of hydrostatic integrity and acetone immersion. A more detailed study has been published concerning a failed 34 years old rising main sewer PVC pipe in Australia (Gould et al., 2013). In order to assess the failure cause, a series of methods based on micro-scale examination (SEM) and fractography (FT-IR and EDS) have been applied. The conclusion was that an inherent inclusion created during the manufacturing process served as a stress riser and resulted in crack initiation and eventual failure. In particular, EDS during SEM indicated that iron (Fe) elements were found in the revealed inclusions, implying a low-quality manufacturing process. However, no material degradation due to the contact with sewage was detected, although the crack seems to have initiated in the area of the pipe where discolorization is most profound.

Besides inherent defects, notches caused during installation could also affect the performance of the pipe. Towards this direction, Burn (1991) explored the effect of notches on PVC pipes which are subjected to cyclic pressure. The experiments included PVC pipes of certain specifications (DN110, class 20, AS 2977) tested at a cyclic pressure of 1.2 $\pm$ 0.3 MPa at a frequency of 0.5 Hz. The results revealed that notch depths above a certain level could reduce the lifetime of a pipe drastically. For the given pipe, a notch 1.2 mm increases the failure probability when subjected to 1.7 million cycles (resembling 100 years lifetime for Australian operating conditions). Finally, the response of thermoplastic pipes (including PVC) under two cases of combined loading has been investigated (Alferink et al., 2004): i) internal pressure and deflection, and ii) internal pressure and axial bending. The results revealed that external loads in fact enhance the performance of the pressurized pipe and the bending stresses relax in time. However, failures due to excessive axial bending have been recorded (Broutman et al., 1990) concerning two PVC (SDR 26) water pipes.

2.2.2. CHEMICAL RESISTANCE

The materials used for the production of thermoplastic pipes, which are destined for fluid conveyance applications, are generally considered as chemically resistant. Especially PVC is thought to be the most resistant material against both chemical degradation and abrasion, a fact which explains its massive use in sewer systems. An important issue for both drinking and wastewater plastic pipes is the existence of certain disinfectants in drinking water. Their influence on PVC pipes was studied extensively by Fumire (2008). Static tensile and dehydrochlorination (DHC) tests, combined by molecular weight measurements and SEM examinations, took place before and after exposure to some common water disinfectants, i.e. sodium hypochlorine-dichlorine ($NaClO$-Cl_2) and chlorine dioxide (ClO_2). Even concentrations of 8 ppm of such disinfectants at 40 °C did not manage to impose significant changes on the material. Indeed, according to other studies (Kowalska et al., 2014; Kowalska et al., 2016), the added chlorine atoms that derive from chlorinated water are considered as a possible reason for a slight increase in the mechanical properties of PVC.

Similar studies have been published for the performance of polyethylene pipes against chlorine-based solutions (Hassinen et al., 2004; Castagnetti et al., 2011; Yu et al., 2011; Ghabeche et al., 2015). In these cases, the amorphous part of polyethylene proved to be very sensitive especially to chlorine dioxide and hydrochloric acid, followed by rapid depletion of antioxidants and an increase in crystallinity. The outcome of the mentioned studies indicates the overall superiority of PVC over PE concerning chemical resistance to frequently utilized disinfectants. This trend comes partially in contrast with the findings of the comparative research conducted by Kowalska et al. (2016), as chemical changes at the material surface seem to be more profound in PVC than HDPE pipes, albeit the mechanical properties are not affected in both materials.

Earlier relevant research on PVC also confirmed its chemical resistance. Bishop (1990) introduced a test method for estimating the pipe stiffness of PVC samples, while subjected to constant deflections of 5-10%, and 5% concentration of sulfuric acid (H_2SO_4) or sodium hydroxide (NaOH). After testing periods of more than one year, the results revealed negligible effects on the pipe stiffness. The resistance of PVC against sulfuric acid was also verified in another study (Hawkins et al., 1994), in which calcium carbonate ($CaCO_3$) filled PVC sewer pipes were investigated by means of SEM and wavelength dispersive X-ray (WDS) analysis. The pipe samples were exposed to H_2SO_4 (20%) for testing periods up to 6 months. The PVC matrix proved to be very resistant, as $CaCO_3$ reacted with H_2SO_4 only at the surface of the material.

Finally, a comparative research on the chemical resistance of PVC, PE and PP to sulfuric acid and sodium sulphate (Na_2SO_4) at 25 and 40 °C has been published (Lasfar et al., 2014). The research included measurements of the tensile strength and elongation at break for several durations of immersion. According to the results (Table 2.7), tensile strength was enhanced while the elongation at break was reduced, implying an increase in crystallinity and diffusion of the environment in the material, but no chemical degradation.

Table 2.7: Tensile strength and elongation at break of PVC specimens aged in H_2SO_4 (Lasfar et al., 2014).

Immersion time (h)	Tensile strength at 25 °C (MPa)	Elongation at break at 25°C (%)	Immersion time (days)	Tensile strength at 40°C (MPa)	Elongation at break at 40 °C (%)
0	42.58	126.2	0	42.58	126.2
35	49.4	120.3	504	49.97	33.93
56	48.03	115.85	1200	51.9	30.1
92	49.6	108.73	1704	52.47	22.5
127	52.27	83.33	2040	54.17	18.5
182	56.9	74.81	2208	48.8	18.1

2.2.3. ELASTOMERIC JOINTS

There are several types of thermoplastic pipes jointing, including mechanical and welding techniques (Stokes, 1989; Headford, 1998). The most common types of joints in sewer systems are the push-fit, i.e. bell and spigot, and double socket joints. Developments of the conventional push-fit joints can be found, such as the Rieber joint (Magnusson, 1982; Rahman et al., 2006).

Some researchers have focused exclusively on the performance of the joints in plastic pipe systems. Meijering et al. (2004) studied double socket joints that had been for up to 30 years in service of PVC gas distribution systems. The assessment of the condition of the joints was made based on leak tightness testing under deflection, compression set estimation and determination of basic mechanical properties. Leakage was observed only for pipe critical deflections over 36%, while in one case the critical deflection reached the level of 81% (Table 2.8). The compression set was measured in an approximate range between 15 and 50%.

Table 2.8: Critical deflection values that caused leakage under testing (Meijering et al., 2004)

Pipe	Diameter (mm)	Age	Sealing material	Critical deflection (%)
PVC SDR41	110	30	SBR	44
		-	SBR	81
		17	NBR	74
		22	NBR	36
		23	NBR	50
		23	NBR	64

Arsenio (2013) also concluded that only extreme bending angles (above 10°) or complete pull-off of the pipe could lead to leakage at the joints regarding drinking water systems. In terms of leak tightness in elastomeric joints, the failure modes that can be observed in push-fit joints are listed and described in detail in (Arsenio et al., 2009). Namely, these are joint bending, vertical displacement, horizontal displacement, pipe bending, axial displacement, torsion by slight rotation/vibration, and pipe ovalization. The standardized methods and conditions used to test the leak tightness of joints in gravity flow applications are presented in NEN 1277:2003, and are discussed and assessed by

García et al. (2016). Furthermore, Bauer (1990) and Meerman (2008) commented on the excessively good quality of the elastomeric seals of excavated PVC sewer pipes, albeit their conclusions were drawn only by visual inspection. In the mentioned studies, the effects of potential microbiological attack on the sealing material have not been investigated.

Other researchers have focused on the performance of elastomeric joints towards root intrusion considering the interfacial pressure as a critical factor. Whittle et al. (2005) investigated the interfacial pressure of 7 PVC sewer pipes and they concluded that only two comply with the requirements provided by the relative Australian Standards (AS 1260-1984) and Hunt (1979), which recommend that the interfacial pressure should be higher than 0.55 MPa for 7mm of continuous width. Similarly, Sadler et al. (2001) tested 22 joints (slip-coupling and lip-seal) used in PVC sewer pipes. After 29 months of accelerated root intrusion testing, it was concluded that for interfacial pressures of 0.04-0.20 MPa, root intrusion is likely to occur, but the values of interfacial pressures suggested by AS 1260-1984 are very restrictive and could lead to ring removal and installation difficulties. The detailed experimental set up is described in (Lu et al., 2000), which includes preliminary tests regarding elastomeric joints of PVC, Vitrified Clay (VC) and Fiber Reinforced Concrete (FRC) pipes. The superiority of PVC compared to VC and FRC was finally reported by Whittle (2003), who claimed that the surface roughness and porosity of the latter materials were the main cause of root intrusion through the sealing joints. Scharwächter (2001) also assessed the magnitude of sealing forces that must be applied for achieving long-term tight joints in non-pressure systems. By applying method 4 of WG13 (TC 155/CEN), it was concluded that a long-term (considering the relaxation of the elastomer) sealing force of 3-4 N/mm (compression set 25-30%) seems to be sufficient.

The performance of bell and spigot joints of PVC with respect to the burial depth, bedding conditions and loading position, has also been studied (García et al., 2013). The results revealed that several issues may arise such as vertical deformations, changes in pipe diameter, rotation and shear forces, but the leak tightness of the joints under the imposed conditions was not assessed. Balkaya et al. (2009) investigated the interaction between a Rieber-type PVC gasket and the pipe with the means of finite elements modeling (FEM). The results from the analyses revealed that the friction coefficient affects the stiffness of the joint and that increased gasket modulus leads to increased insertion force and bending moment. In a later publication (Balkaya et al., 2012), the same model was studied in order to test the bell and spigot jointed PVC water pipes that lie on non-uniform bedding, which was simulated by voids of different sizes. The conclusions derived by FEM included higher deformations in the case of improper bedding under the joint and lower deformations in the case of stiffer soils around the pipes.

2.3. PVC PIPES IN PRACTICE

Examination of the inspection data from the Dutch municipalities of Almere, Breda and Haarlem reveals the presence of a range of defects, affecting the structural stability, flow regime and leak tightness of the system. Figure 2.1 presents the occurrence rate of such

defects in PVC pipes (number of defects normalized per kilometer), classified according to NEN 3399. The defects are grouped without considering the level of severity in order to compensate for the uncertainty involved in CCTV inspections (Dirksen et al., 2013). Detailed exploration of the available datasets proved that there is not a clear pattern that could link the use of a PVC pipe, a specific range of diameters or other characteristics of the system to increased levels or exclusive types of defects. This fact might be attributed to the limited available data (506.3 km of PVC pipes in Almere, 269.1 km in Breda and 39.6 km in Haarlem), especially since there is a minimal variation in the dataset of Almere.

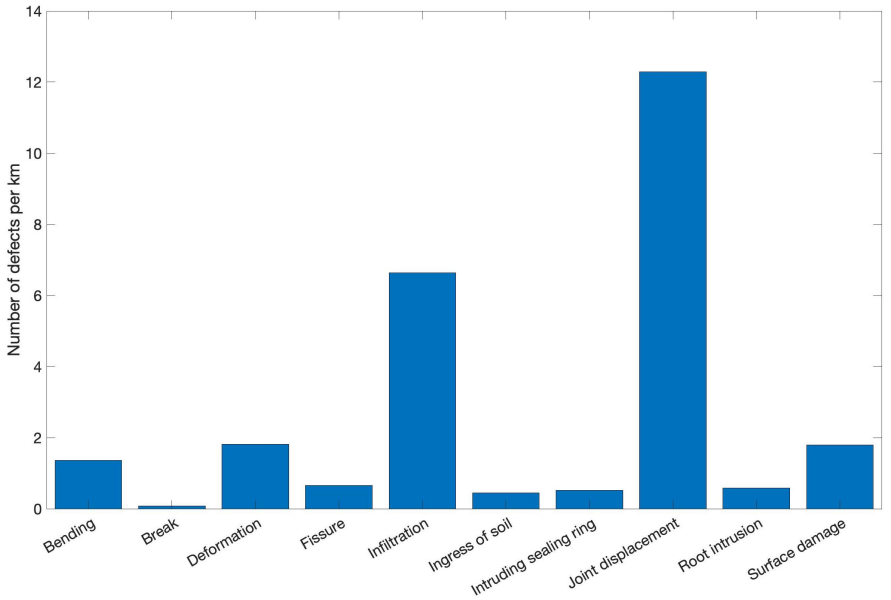

Figure 2.1: Defect rates (number of defects per kilometer) estimated based on CCTV inspections for PVC sewer pipes from three Dutch municipalities: Almere, Breda and Haarlem

Another approach was implemented for the PVC pipes (2.4 km) in the municipality of Amstelveen. In an effort to verify whether the degradation of PVC systems is depicted, inspection data of pipes that have been inspected twice was explored. This analysis (Figure 2.2) reveals an increase in the occurrence rate of the initially found defects, followed by the appearance of new ones (breaks, fissures, root intrusion). These changes are noticed within a timespan of 7-8 years.

2.4. CRITICAL ASPECTS

2.4.1. EVALUATION OF THE LITERATURE

Although some researchers focused on operating PVC pipes in sewers, research was restricted to measuring only deflection levels (Walton et al., 1988; Moser et al., 1990) or

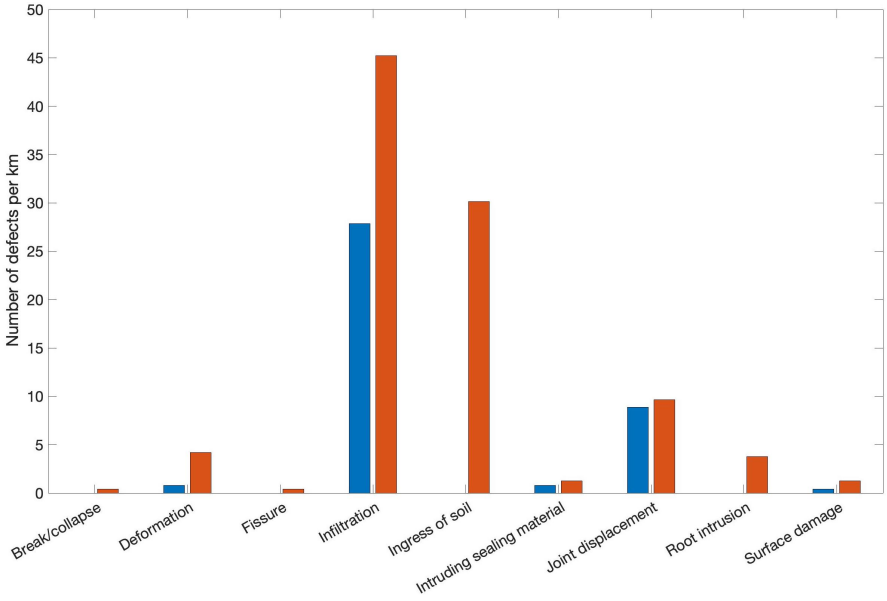

Figure 2.2: The number of defects per kilometre observed in CCTV and Panoramo® inspections of the same PVC sewer pipes in the municipality of Amstelveen in 2003 (blue) and in 2010/2011 (red).

conducting visual based assessments (Meerman, 2008). Bauer (1990) made a more comprehensive assessment of an operating pipe, but testing included merely one pipe which had served for 15 years only. Additionally, despite some visual assessments of the joints used in sewer pipes (Bauer, 1990; Meerman, 2008), there is hardly any relevant research reported on the effect of the sewer environment on the elastomeric material properties and performance. There are indications, however, that the hostile environment that prevails in sewer systems (acids, FOG, etc.) have an impact on certain sealing materials, such as natural rubber and styrene-butadiene rubber (Plastics Industry Pipe Association, 2009).

The need for comprehensive testing is implied by this literature review. For instance, while a connection between extrusion quality and tensile properties could be partially established in one study (Alferink et al., 1995), this was unfeasible in another case (Whittle et al., 2005). In fact, in the latter study a physical property (i.e. specific gravity) was utilized to explain the differences in the mechanical (tensile) properties. Comparing and combining results from different researchers in order to draw conclusions is challenging, due to among others a lack of uniformity in materials and methods applied. The conditions and methods of specimen preparation and testing are based on different standardized (ISO, ASTM, AS/NZ) or non-standardized methods. Additionally, the production quality of new pipes used as reference specimens has changed over the years, making the direct comparison with aged pipes just indicative. Finally, comparing individual properties with respect to the requirements of norms for safe operation of PVC sewer pipes does not provide any indication concerning material degradation, as the

exact initial conditions are still unknown.

A property that is used extensively in design and classification of gravity sewer pipes is pipe stiffness. Research (Välimaa, 1982) has proved that under high soil covers (as for sewer pipes), pipe stiffness is not the most crucial parameter. However, it is expected to become significant for house connections which are usually placed under soil covers <0.8m. Besides that, in the explored literature a confusion between ring (or nominal) stiffness and pipe stiffness has been noticed. The respective formulas as included in ISO 9969 (Eq. 2.1) and ASTM D2412 (Eq. 2.2) are provided for clarification. The ring stiffness is defined as:

$$S = (0.0186 + 0.025\ \frac{y}{d})\ \frac{F}{L\ y} \tag{2.1}$$

where y is the measured pipe deflection (m), d is the average inside diameter, F is the applied force (kN) and L is the length of the test piece (m). Sometimes the ring stiffness is denoted as SN. The pipe stiffness is defined as:

$$PS = \frac{F}{y} \tag{2.2}$$

where F is the applied force (N/m) and y is the pipe deflection (m).

In terms of elastic modulus, ring and pipe stiffness are expressed as (Moser and Folkman, 2008):

$$SN = \frac{E\ I}{D^3} \tag{2.3}$$

$$PS = \frac{6.7\ E\ I}{r^3} = 53.6\ \frac{E\ I}{D^3} \tag{2.4}$$

where E is the modulus of elasticity of the pipe material (Pa), I is the moment of inertia of pipe wall per unit length (m^4/m) and D is the mean pipe diameter (m).

An additional remark concerning pipe stiffness is on its attributed unit. Using kPa or psi for this property has no physical meaning and confusion among engineers may be caused. As indicated in Eqs. 2.1 and 2.2, pipe stiffness is a measure of the resistance of a pipe expressed as a ratio between the applied linear loading in the longitudinal direction (kN/m) and the vertical deflection in the radial direction (m). Therefore, the unit should be strictly notated as $kN/m_{linear}/m_{deflection}$ or $lbf/in_{linear}/in_{deflection}$ instead of kPa (=kN/m^2=loading/area) or psi (lbf/in^2) respectively.

2.4.2. INCONSISTENCY BETWEEN SCIENTIFIC LITERATURE AND PRACTICE

Kuliczkowska et al. (2016) presented a range of early defects found on newly installed PVC sewer pipes during CCTV inspections. These defects included dents due to installation or soil compaction, excessive deflections, buckling and improper longitudinal slopes. Inspection data from Almere, Breda and Haarlem indicate that additional

defects may emerge: surface damage, fissure, displaced/destroyed sealing ring, root intrusion and break/collapse. Given the limitations that exist in CCTV inspections due to subjectivity of the inspector and only inner pipe inspection (Dirksen et al., 2013; Van Riel, 2017), defects not reported may also occur as CCTV inspections likely result in an optimistic estimate of the pipe's condition.

Although linking the observed defects in CCTV to the actual physical state of a pipe is arduous (Van Riel, 2017), it is quite obvious that there is a certain gap between scientific research and what is observed in practice. Several studies (Whittle et al., 2005; Meerman, 2008; Folkman, 2014) suggest that PVC sewer pipes are expected to exceed a 100 years lifetime, while inspection data suggests that severe defects (cracks and fissures) already exist. The most emphasized discrepancy is observed regarding the performance of elastomeric joints. Literature (Meijering, 2004; Arsenio, 2013) indicates that leakage is possible only under extreme cases (deflection > 36%, bending angle > 10°, complete pull-out) and root intrusion is impossible given that installation is proper (Sadler et al., 2001). However, this comes in contrast to the presented failure rates (Figures 2.1 and 2.2), as well as results of CCTV inspections published concerning Sweden (Stål, 1998; Ridgers et al., 2006; Östberg et al., 2012) and Denmark (Randrup, 2000). Applied installation techniques (proper laying and jointing) could be considered as an indisputable contributing factor (Stephens et al., 1982), nonetheless it is unknown whether or not it is the only or most significant one.

2.5. CONCLUSIONS

Several case studies are presented in literature, focusing on the mechanical durability and chemical resistance of PVC pipes, as well as the mechanisms which affect the leak-tightness of elastomeric joints. Research on material degradation reveals that the properties of PVC sewer pipes in operation have not altered significantly or at all, while a lifetime that exceeds 100 years is usually suggested. Only one case of failure is recorded, concerning a sewer main, and the failure was attributed to poor extrusion quality. Nonetheless, there is no published research on the effect of sewage on the elastomeric seals of PVC systems.

Inspection data from 4 Dutch municipalities highlights that PVC sewer pipes have already developed all types of known defects, while degradation evolves with time at a relatively fast rate. Especially defects associated with the elastomeric joints have a considerably high occurrence rate. Analysis of a larger inspection dataset would allow the detection of a possible connection between defects (types, rates) and elements of the system (diameter, type of drainage pipe, soil cover etc.).

There is a certain discrepancy between literature and observations in practice on the issue of lifetime expectancy of PVC sewer pipes. This emphasizes the need for further material properties assessment of operating PVC sewer pipes and elastomeric joints. Additionally, only comprehensive testing of physical, mechanical and chemical properties could yield safe conclusions regarding the level of degradation and its origins. In literature, efforts to determine just individual properties have proved to be inadequate leading to inconsistencies and unanswered questions.

3

EXPERIMENTAL CHARACTERIZATION OF PVC PIPES

3.1. INTRODUCTION

Numerous studies have been conducted concerning the structural integrity and chemical resistance of PVC pipes. As discussed in Chapter 2, research on excavated PVC sewer pipes suggests that there are no signs of impoverished physical and mechanical properties (Bauer, 1990; Alferink et al., 1995; Whittle et al., 2005; Folkman, 2014). Furthermore, testing of a series of chemicals usually found in sewers on PVC pipes has led to the conclusion that no significant chemical alterations in PVC composition are observable (Bishop, 1990; Hawkins et al., 1994; Fumire 2008; Lasfar et al., 2014). Concerning the elastomeric joints, only extreme values of bending and deflection, or the complete pull-off could result in leakages (Meijering et al., 2004; Arsénio, 2013). Based on these findings several researchers (Whittle et al., 2005; Meerman, 2008; Folkman, 2014) have expressed their expectation for an exceptional operational lifetime of at least 100 years. Nonetheless, CCTV inspection data unambiguously indicate that all kinds of known defects already occur and they even evolve at a relatively fast pace.

This chapter aims at exploring the discrepancy between scientific research and observations in practice by discussing the durability of eight PVC sewer pipes (that have been in operation) with known defects. These pipes were excavated and subjected to a range of tests and analyses. The results of such comprehensive testing offer the opportunity to conclude on potential degradation and the overall performance of the examined pipes, while indicating prerequisites for establishing future sewer asset management strategies.

Parts of this chapter have been published in: Makris, K. F., Langeveld, J., & Clemens, F. H. (2021). Extensive testing on PVC sewer pipes towards identifying the factors that affect their operational lifetime. Structure and Infrastructure Engineering. doi:10.1080/15732479.2021.1907601

3.2. MATERIALS AND METHODS

3.2.1. PIPE SAMPLES

Eight operating PVC pipes, incorporated in municipal wastewater systems, were excavated in cooperation with the municipalities of Almere and Breda. The pipes were selected based on the year of installation, existing defect(s) and feasibility of excavation. The length of the excavated pipes was approximately one meter of unaffected material in addition to the length that included the developed defect. A brand-new, recently manufactured PVC pipe was also included in the study for reference purposes. The main characteristics of the tested pipes are presented in Table 3.1.

Table 3.1: Characteristics of sewer PVC pipes used for analyses

Sample	Installation area	Installation year	Excavation year	DN	Embedded core	Soil	Surface	Mean soil cover (m)	Defect (EN 13508-2)
A-1	Almere (NL)	1976	2019	250	-	Clay	Paved path	1.55	Crack at the connection (BAF)
A-2		1977		250	-		Paved street	2.32	Deformed at crown (BAF)
A-3		1978		250	Void		Paved path	1.52	Pointy break at side (BAF)
A-4		1980		250	Void		Paved street	1.51	Crack at bottom (BAB)
B-1	Breda (NL)	1977	2018	250	-	Sand	Paved street	1.55	Root intrusion (BBA)
B-2		1979		250	-		Paved street	1.30	Break (BAC)
B-3		1995		200	Recycled		Paved street	1.58	Complicated crack (BAB)
B-4		2002		160	Foamed		Soil	1.16	Root intrusion (BBA)
R (new pipe)	-	-	-	250	-	-	-	-	-

Pipes A-3 and A-4 are perforated across the longitudinal axis forming a void core, while pipes B-3 and B-4 are 3-layer pipes having a recycled PVC and a foamed core, respectively. The remaining pipes are produced with a single PVC layer. Figure 3.1 presents the inspection images of the pipes which suffered from a structural defect. Concerning pipes B-1 and B-4, the detected defect was root penetration which occurred via elastomeric connections, the integrity of which is not assessed in the current work. Therefore, these pipes had no visually detected defects, except for scratches which were present on all excavated pipes and were inflicted most likely during installation and/or excavation, although appropriate care was taken regarding the latter.

3.2.2. ANALYSES

Several tests were conducted in order to identify the main physical, chemical and, relatedly, mechanical properties of the samples. Additionally, information about the pipe production process was obtained by certain analyses, in an effort to explore the possible correlation between the production method, choice of materials and the properties of the pipes.

DETERMINATION OF PHYSICAL PROPERTIES

Quantification of physical properties included the estimation of density and intrinsic viscosity of the examined samples. The density of the pipes was estimated by immersing samples in distilled water (ISO 1183-1, Method A). The masses of the dry sample and the displaced water were measured (Mettler Toledo PG2002-S balance), as well as the water

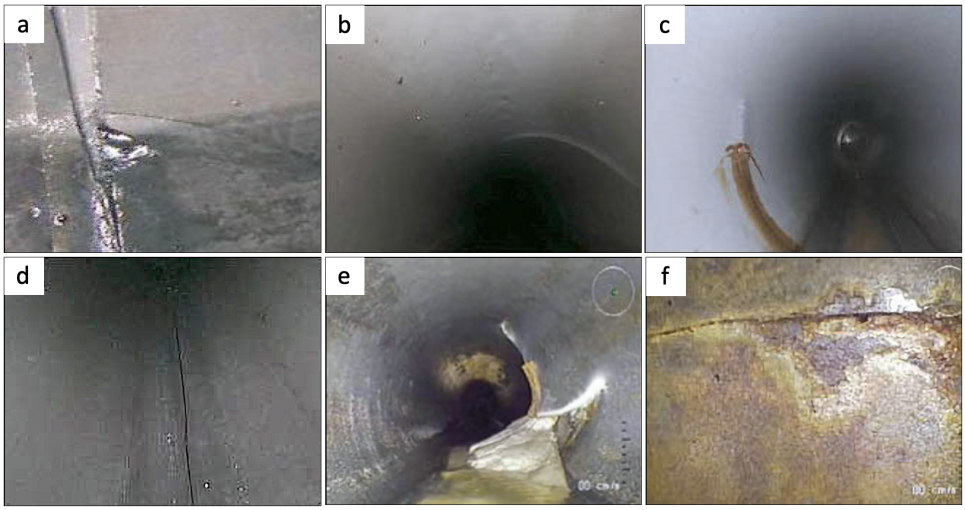

Figure 3.1: CCTV or Panoramo® footage of excavated pipes: a) Pipe A-1 (DN 250, 43 years old) with crack at the connection. b) Pipe A-2 (DN 250, 42 years old) with deformed top. c) Pipe A-3 (DN 250, 41 years old) with pointy break at the side. d) Pipe A-4 (DN 250, 39 years old) with crack at the bottom. e) Pipe B-2 (DN 250, 39 years old) with break. f) Pipe B-3 (DN 200, 23 years old) with complicated crack.

temperature (Testo 104-IR thermometer). Subsequently, the volume of each sample was estimated, resulting in the determination of density.

The chain lengths of polydisperse polymers (like PVC) were assessed via their intrinsic viscosity, which represents the resistance against internal flow. Intrinsic viscosity was estimated by following a series of steps based on the use of a rheometer (Anton-Paar MCR 302). The rheometer was equipped with a concentric cylinder (40.018 mm effective bob length, 26.663 mm bob diameter) and a measuring cup (diameter: 28.920 mm). The investigated solutions were prepared by dissolving PVC samples of various weights (ranging from 100 to 250 mg) in 50 mL cyclohexanone (vapor pressure 3.4 mmHg at 20 °C, assay ≥ 99.5%) at 80 ± 5°C, in Erlenmeyer flasks equipped with stoppers (ASTM D2857). A Mettler Toledo xs205 balance and a Thermo Fisher 4500 pipette were utilized for measuring the weight of the samples and volume of the solver, respectively. Subsequently, the polymer solutions were rested at ambient temperature for at least 45 minutes. After filtering (0.45 µm Whatman discs) in order to remove the inorganic elements, each solution was introduced in the rheometer, resting at the temperature chamber for 30 minutes at 20 °C. Finally, the viscosity was measured at shear rates ranging from 1-250 s^{-1} at 1 s^{-1} steps, allowing 10 seconds at each shear rate to stabilize (pre-shearing). The described testing protocol was established after numerous trials, striving towards a consistent measuring technique with lower measuring uncertainties.

The intrinsic viscosity at each shear rate was acquired via multi-concentration measurements by extrapolating the inherent viscosity (Eq. 3.1) to zero concentration (Kraemer, 1938). Finally, the zero-shear intrinsic viscosity has to be estimated by extrapolating to the theoretical zero-shear point. The inherent viscosity (η_{inh}) is defined as:

$$\eta_{inh} = \frac{1}{c} \ln \frac{\eta}{\eta_o} \tag{3.1}$$

where η is the solution's viscosity (Pa s), η_o is the solver's viscosity (Pa s) and c is the polymer solution concentration (g/mL).

THERMAL ANALYSES

Differential Scanning Calorimetry (DSC) is a thermal analysis which detects the fluctuations in the required heat flow, so that the temperature of the tested samples increases at a specific rate. DSC reveals the major thermal transitions, i.e. the glass transition temperature (T_g) and the processing temperature (T_c). A DSC device (Perkin Elmer 8500) supplied the samples with heat from ambient temperature to 250 °C at a 10 °C/min rate under a nitrogen gas atmosphere flowing at 20.0 mL/min (similar to ISO 18373-1). For this analysis, four samples (10 mg approximately) per pipe were tested, being sealed in Perkin Elmer standard aluminum sample pans and covers.

An additionally utilized thermal technique is Thermo-Gravimetric Analysis (TGA), in which the weight is measured as a function of the temperature of the specimen, which is increased at a specific rate (ISO 11358-1). This analysis shows the onset and rate of thermal degradation, as well as the residual content of inorganic elements (stabilizers, fillers or impurities). For this purpose, one sample (10 mg approximately) per pipe was tested in a TGA instrument (Perkin Elmer 4000), at a temperature range from ambient to 600 °C at 10 °C/min rate under a nitrogen gas atmosphere (20.0 mL/min).

SPECTROMETRIC AND MICROSCOPIC MEASUREMENTS

In order to directly detect chemical degradation of the pipe material, a Perkin Elmer Spectrum 100 device supplied with an ATR (Attenuated Total Reflection) crystal was used within an IR wavenumber range of 4000 to 550 cm^{-1}. With the aid of infrared spectroscopy, the molecular motions which are not attributed exclusively to the composition of PVC can be tracked, indicating potential chemical alterations. Moreover, X-Ray Fluorescence (XRF) analysis was utilized in order to detect the existence and concentrations of inorganic elements which are present within the composition of the examined pipe samples. The measurements were conducted with a Panalytical Axios Max WD-XRF spectrometer and data evaluation was implemented with the aid of SuperQ5.0i/Omnian software.

Finally, a Scanning Electron Microscope (SEM, JEOL JSM-7500F) configured with secondary and backscattered electron detectors was used. The microstructure was observed by SEM, providing information for identifying the likely failure cause(s) (e.g. cavities) of the specimens subjected to tensile tests. Energy Dispersive X-ray Spectroscopy (EDS) during SEM has been applied to detected inherent defects, obtaining information about the elemental composition of failure areas and the processing quality.

TENSILE AND FLEXURAL TESTING

The results of mechanical testing incorporate any type of present degradation, as well as production quality and installation quality. Furthermore, while for other conducted

analyses the material properties were traced with very small samples or surface analyses, the tensile and flexural testing specimens were milled from the whole pipe thickness. Therefore, the complete structural composition of the pipes was considered. Flexural tests were conducted with a Zwick Universal Testing Machine of 20 kN load cells combined with a four-point bending set-up on five specimens per pipe which were milled along the longitudinal direction at the crown of each pipe. Depending on the thickness of each pipe, the displacement rate varied from 11 to 15 mm/min in order to achieve 5 mm/mm maximum strain in the outer fibres of the specimens (ASTM 6272-17).

Although flexural tests activate similar mechanisms found at unpressurized pipes within soil (in particular deflection), tensile testing is mainly found in the literature (Bauer, 1990; Alferink et al., 1995; Whittle et al., 2005), as it is discussed later-on in this chapter. Therefore, uniaxial tensile tests were complementarily performed only on the pipes which were firstly excavated (B-1, B-2, B-3 and B-4) and the reference pipe (R). Tensile testing was conducted with a Zwick Universal Testing Machine (20 kN load cells) at 5 mm/min displacement rate on 10 specimens per tested pipe. The specimens were milled from various circumferential positions along the longitudinal direction based on ISO 6259-2 (Type 1). The ultimate tensile strength, elastic modulus and elongation at break were determined in order to track the degree of physical ageing and assess the effect of potentially compromised physical or chemical properties. The elastic modulus was estimated from the slope of the derived stress-strain curves in the elastic region. Respective parameters (flexural strength and modulus) were obtained from the derived flexural stress-deformation curves.

3.3. RESULTS

The values of density and intrinsic viscosity of the tested samples are summarized in Table 3.2. The majority of the pipes demonstrate similar values, close to the reference pipe R. A lower intrinsic viscosity value is distinguished only regarding pipe B-4. Further, the process followed in order to estimate the intrinsic viscosity is illustrated in Figures 3.2 and 3.3. The relationship between inherent viscosities and solution concentrations is fitted using linear regression (Figure 3.2). Linear extrapolation to zero concentration provides the intrinsic viscosity for each tested shear rate. This procedure was repeated for the considered shear rates, whose selection has been derived by the conducted uncertainty analysis for rheometric measurements with Anton-Paar 302 (Appendix A). Additionally, the shear-dependent intrinsic viscosities can be also described by a linear fit (Figure 3.3), which allows the extrapolation to the zero-shear rate and the estimation of the respective intrinsic viscosity.

The glass transition temperature (T_g) is obtained by the DSC curve as shown in Figure 3.4 (left). All pipe samples demonstrate a glass transition temperature within the range of 81.6 – 83.7 °C with onset temperature values of the rubbery state within 79.2 – 81.4 °C. The point between the two endotherms (ΔH_a & ΔH_b) reveals the production process temperature (T_c). ΔH_a and ΔH_b signify the melting of secondary and primary crystallites respectively. Processing temperature varied between 169.3 – 179.9 °C for pipes manufactured before 1980, whereas newer PVC pipes (after 1995) were processed at a

temperature range of 185.7 – 192.4 °C.

Table 3.2: Main physical properties of examined PVC pipes.

Pipe	Density (g/cm^3)	Intrinsic Viscosity (mL/g)
A-1	1.42 ± 0.00	128.26 ± 3.87
A-2	1.41 ± 0.00	128.47 ± 1.93
A-3	1.41 ± 0.01	128.94 ± 1.99
A-4	1.41 ± 0.01	128. 17 ± 1.76
B-1	1.41 ± 0.01	124.49 ± 1.48
B-2	1.41 ± 0.01	128.78 ± 1.46
B-3	1.41 ± 0.01	*
B-4	1.49 ± 0.01	85.21 ± 0.92
R	1.41 ± 0.01	120.74 ± 1.13

* Pipe not tested due to equipment failure

The curves derived by TGA (Figure 3.4, right) indicate two characteristic decomposition temperature points (Primary (T_{onset}) and Secondary (T_{SD}) Decomposition Temperature). T_{onset} denotes commencement of dehydrochlorination and volatile components loss, and T_{SD} reveals the starting point of scission of the main polymer chains backbone. The plateau formed at the end of the analysis represents the amount of inorganic elements in the PVC matrix, which required additional thermal energy to decompose.

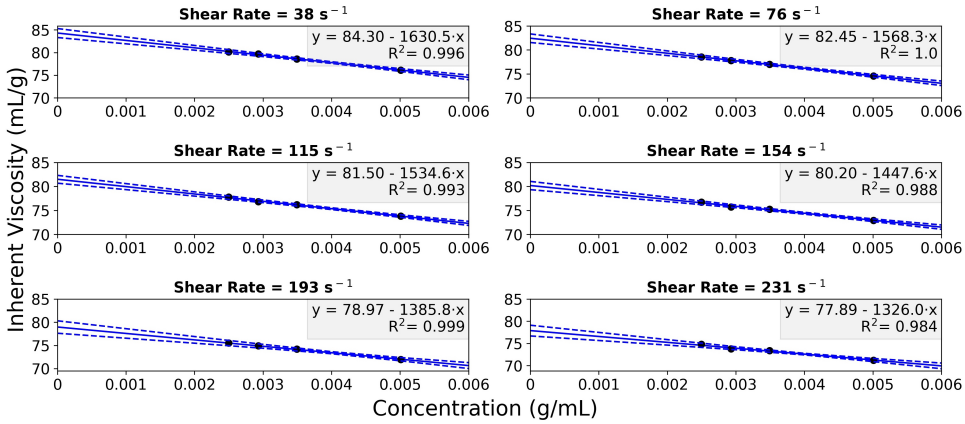

Figure 3.2: Inherent viscosity with respect to solution concentrations of pipe B-4 for shear rates of lowest uncertainties. The blue dashed lines denote the 95% confidence intervals obtained via Monte Carlo simulations. Parameters "x" and "y" in the given function correspond to concentration and inherent viscosity, respectively. The value of the intrinsic viscosity for each shear rate is obtained by extrapolation of the linear regression fit to zero concentration (e.g. 84.30 mL/g for shear rate 38 s^{-1}).

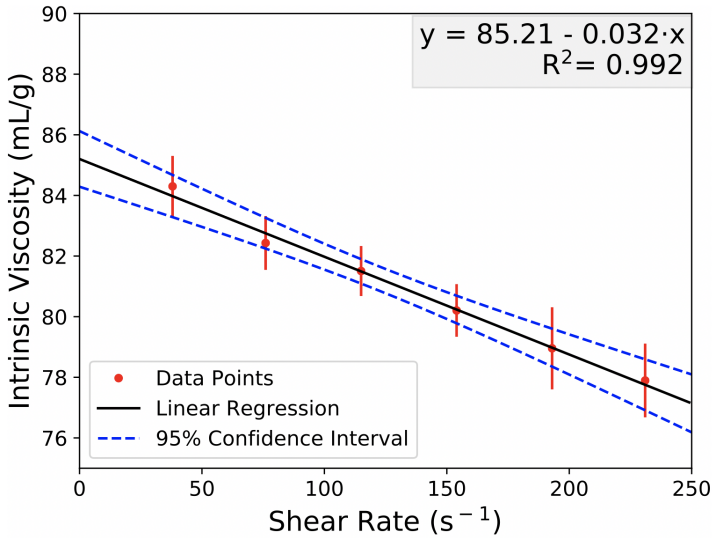

Figure 3.3: Intrinsic viscosity with respect to shear rates of lowest uncertainties for pipe B-4. The blue dashed lines denote the 95% confidence intervals obtained via Monte Carlo simulations. Parameters "x" and "y" in the given function correspond to concentration and intrinsic viscosity, respectively. The values of the intrinsic viscosity are obtained from Figure 3.2. The zero-shear intrinsic viscosity is estimated via extrapolation of the linear regression fit to zero shear rate (i.e. 85.21 mL/g).

The characterization of the thermal stability of the investigated samples was finalized by detecting the points of Maximum Rate of Decomposition Temperature ($MRDT$) on the weight curve (inflection points in the respective first derivative). All pipe samples show values of T_{onset}, T_{SD} and $MRDT$ in close proximity, while the concentration of resid-

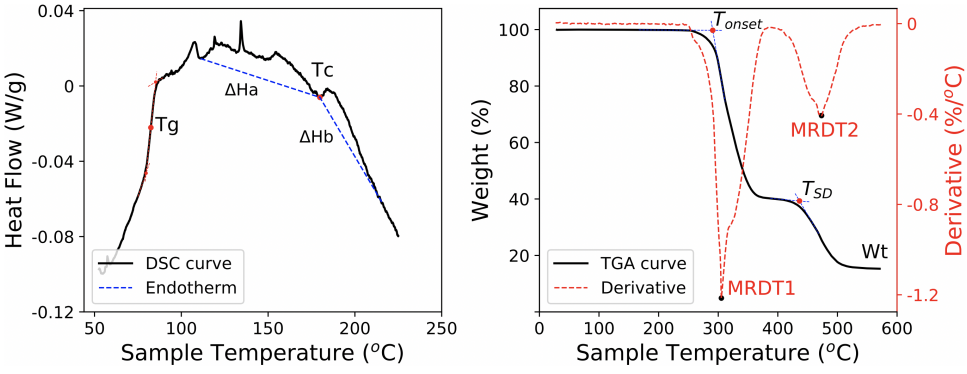

Figure 3.4: Left: Curve obtained via Differential Scanning Calorimetry on pipe B-2 including indication of the glass transition (T_g), processing temperature (T_c) and endotherms ΔH_a and ΔH_b. Right: Curve obtained via Thermo-Gravimetric Analysis on Pipe B-2 and the respective derivative (dashed line) including indication of temperature of thermal degradation onset (T_{onset}), maximum degradation rates ($MRDT1$ & $MRDT2$), and residual inorganic elements (Wt).

ual content of non-volatile inorganic elements differs (15.3-26.6%). The results obtained from the thermal analyses for all tested pipes are presented in Table 3.3.

Table 3.3: Parameter values obtained from Differential Scanning Calorimetry and Thermo-Gravimetric Analysis for the examined pipes.

	DSC			TGA				
Sample	**T_{onset} (°C)**	**T_g (°C)**	**T_c (°C)**	**T_{onset} (°C)**	**MRDT1 (°C)**	**T_{SD} (°C)**	**MRDT2 (°C)**	**W_t (%) at 600 °C**
A-1	80.0	82.4	174.1	288.8	296.4	451.9	476.3	21.1
A-2	79.8	83.1	169.3	290.2	301.8	448.3	474.7	18.4
A-3	79.6	82.0	174.7	288.4	303.4	443.2	478.1	17.9
A-4	79.2	81.6	175.1	287.3	296.4	450.1	479.9	19.5
B-1	79.4	82.5	179.8	290.8	305.4	436.5	472.3	15.3
B-2	81.4	83.4	179.9	290.4	299.7	438.2	481.3	16.8
B-3	80.8	83.2	185.7	292.0	303.2	435.0	474.6	17.2
B-4	81.2	83.7	192.4	291.4	304.4	439.7	476.7	26.4
R	80.6	83.1	185.7	286.7	301.2	442.6	479.4	19.6

Elemental analysis via XRF (Table 3.4) revealed 15 different inorganic elements, the majority of which were present in all pipe samples in various concentrations. Three main types of inorganic elements were justifiably present, as they contribute to the production process of PVC pipes in the form of stabilizers, fillers and pigments. For piping applications, lead (Pb) based stabilizers were used until early 2000's in Europe (Anders, 2014), predominantly tribasic lead sulphate ($3PbO{\cdot}PbSO_4{\cdot}H_2O$), dibasic lead stearate [$2PbO{\cdot}Pb(OOC\text{-}C_{17}H_{35})_2$] and normal lead stearate [$Pb(OOC\text{-}C_{17}H_{35})_2$] (Wilkes et al., 2005). The transition from Pb to Zn based stabilizers due to high toxicity of Pb was tracked among the old and reference pipes. Common mineral fillers are calcium carbonate ($CaCO_3$), kaolin ($Al_2O_{32}SiO_{22}H_2O$), talc [$Mg_3SiO_{10}(OH)_2$], mica [$K_2Fe(Al_2Si_6O_{20})(OH_4)$], wollastonite ($CaSiO_3$), barite ($BaSO_4$) and calcium sulphate ($CaSO_{22}H_2O$). Pigments ($TiO_2$) are introduced in order to enhance color weatherability. Other present inorganic elements originate from introduced clay minerals, namely Al, Fe, Mg, Ba, K, Ca, and Sr (Wilkes et al., 2005).

Table 3.4: Elemental composition (Wt % $\cdot 10^{-3}$) of the examined pipes derived from XRF analysis.

Sample	**Al**	**Ba**	**Bi**	**Ca**	**Fe**	**K**	**Mg**	**P**	**Pb**	**S**	**Si**	**Sr**	**Ti**	**Zn**	**Zr**
A-1	52	-	4	1908	17	18	25	9	1268	311	112	3	49	-	-
A-2	33	-	6	1499	13	-	25	3	1302	98	91	4	61	-	-
A-3	91	-	-	1457	48	39	33	10	1396	77	286	2	42	-	5
A-4	61	-	-	1444	17	20	21	3	1401	162	122	3	52	-	5
B-1	6	14	-	554	-	-	15	2	852	174	19	1	68	-	-
B-2	8	-	-	677	-	-	16	1	729	130	19	-	25	-	-
B-3	29	-	-	1165	12	5	20	2	783	104	99	4	42	-	-
B-4	37	58	-	4369	19	10	24	7	1045	87	178	10	8	-	-
R	95	-	-	1570	4	11	63	2	-	5	92	3	111	1	-

Figure 3.5 presents the results from FT-IR analysis. Peaks of considerable intensity

level within the investigated spectrum were found and could be interpreted according to known molecular motions (Jakubowicz et al., 1992; Noda et al., 2007; Wypych, 2015). The examined reference pipe demonstrated peaks at the same wavelengths as the old ones. In detail, these peaks appeared at circa 2970 cm^{-1} (CH stretch next to Cl), 2913 cm^{-1} (CH_2 asymmetric stretch), 1427 cm^{-1} (CH_2 wag), 1354 cm^{-1} (CH_2 wag), 1255 cm^{-1} (CH bend), 1100 cm^{-1} (C-C stretch), 960 cm^{-1} (CH_2 rock), 876 cm^{-1} ($CaCO_3$), and 687 cm^{-1} (C-Cl stretch). Discrepancies in the intensity levels among different samples are mainly caused by the high sensitivity of the applied method, especially since the tested samples were rigid and slightly curved instead of fine powder, inhibiting absolute crystal contact. Peaks at the same wavelengths were observed irrespectively of the tested surface (i.e. interior, exterior and middle of pipe thickness). Besides expected peaks, small abnormalities at wavelengths 1711 and/or 1739 cm^{-1} were found during testing on the exterior of excavated pipes, indicating the existence of carbonyl groups (Matuana et al., 2001; Wypych, 2015). Depending on the installation area, the pipes demonstrated different peaks at 1711 cm^{-1} (Figure 3.5, upper) and 1739 cm^{-1} (Figure 3.5, lower).

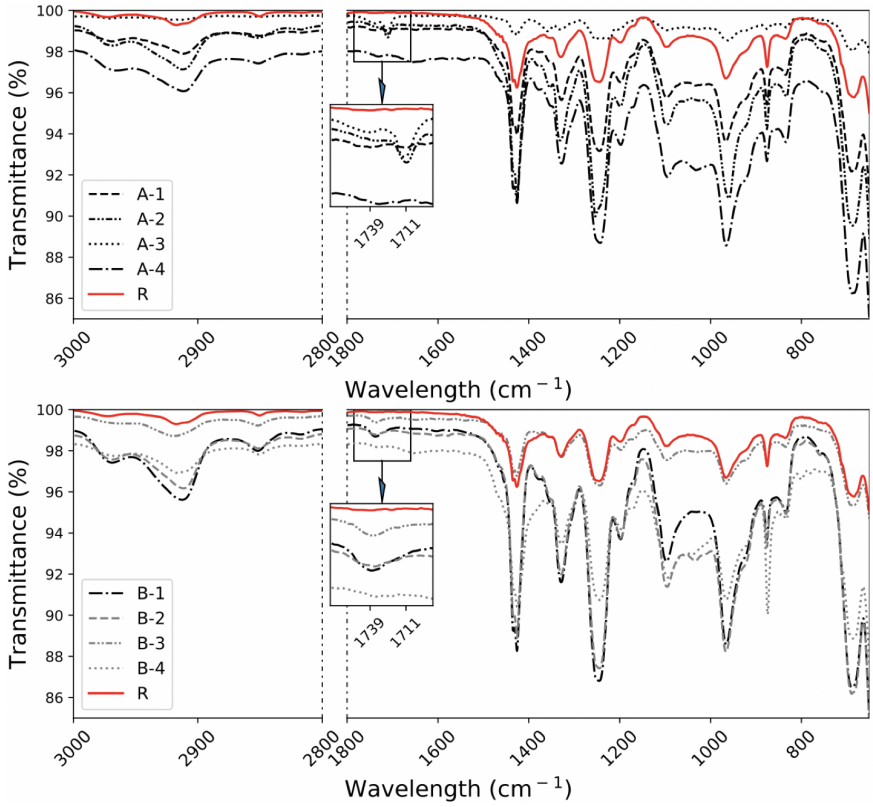

Figure 3.5: FTIR-ATR transmittance spectra of the exterior of examined pipes from Almere (upper graph) and Breda (lower graph). Only wavelengths with peaks are displayed. The wavelengths that denote carbonyl groups are magnified in built-in graphs.

Tensile testing indicated high variability among different pipes (Figure 3.6). Concerning single layer PVC pipes (B-1 & B-2), a translation was observed compared to the reference pipe towards higher values of ultimate strength and elastic modulus, and lower values of strain at break. Nonetheless, elongations at break remained high (136.9 ± 44.1% for pipe B-1 and 175.3 ± 20.1% for pipe B-2). Regarding pipe B-3, with a recycled core, the average ultimate tensile strength was in proximity to the reference pipe although break occurred earlier. Pipe B-4, incorporating a foamed core, showed the lowest values of ultimate strength and strain at break. Variations between samples from the same pipe may have originated due to the wide range of temperature (±2 °C) at which tensile testing was performed, rising the testing uncertainties, as indicated by the respective standard deviations.

In the explored specimens, two cases of premature failure during tensile testing were analyzed with SEM, samples B-1 and B-3 which failed at 53.4 and 23.4% elongation at break, respectively. Magnification of the cross-sections at break revealed that both failures were initiated due to cavities within the structure (Figure 3.7). Especially concerning sample B-3, numerous cavities were found in the recycled core and, in particular, near the interface between virgin and recycled PVC (Figure 3.7, right). Chemical analysis via EDS indicated that no foreign elements were traced at the inspected areas.

Flexural testing revealed that the same pattern as in tensile testing exists for single layer pipes, with older pipes demonstrating higher values of ultimate flexural strength and flexural (elastic) modulus compared to the reference pipe (Figure 3.8). However, high variability was noticed in some cases among samples coming from the same pipe, especially regarding pipe B-1. Further, pipe B-4 showed relatively low values in terms of flexural stress but similar to single layer pipes in terms of flexural modulus. Pipes with a void core (A-3 & A-4) exhibited the lowest flexural modulus values. Pipe B-2 was not tested due to insufficient material. The average values of the tensile and flexural properties for each pipe are presented in Appendix B.

3.4. DISCUSSION

3.4.1. EXTENT OF DEGRADATION ON EXCAVATED PIPES

A series of material tests were conducted based on methods described in scientific literature particularly for PVC pipes (Makris et al., 2020). Since material properties are influenced by several factors, comprehensive testing was necessary in order to identify how physical ageing interacts with potential chemical and mechanical degradation. Table 3.5 presents a comparison between the acquired properties and those dictated in NEN-EN 1401-1 for new non-pressure PVC pipes. The required parameter values for new pipes denote the threshold above which the initial properties should be, but their actual values still remain unknown.

Measurements of physical properties showed that the density values of the investigated pipes were similar and within the expected range for PVC (Orwoll, 2007; Cardarelli, 2008) and new PVC sewer pipes (Table 3.5). The fact that the density of older pipes is not higher than the newer ones as expected (Hutchinson, 1995) implies that physical ageing

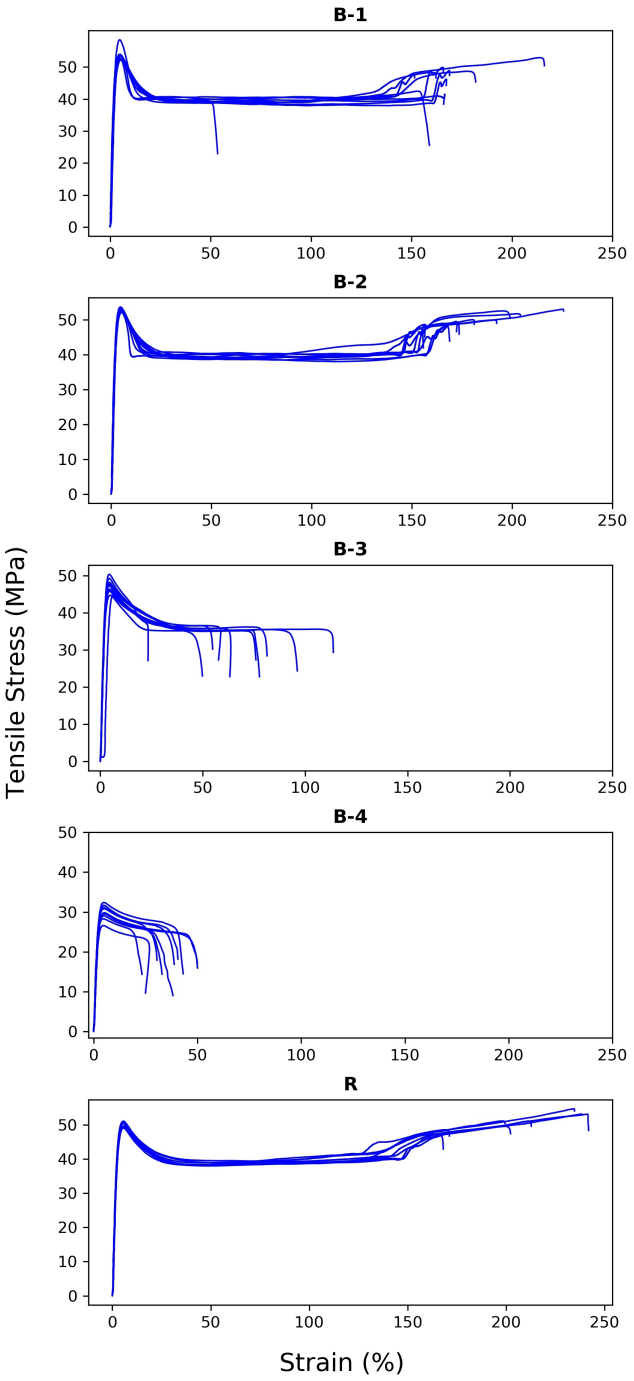

Figure 3.6: Stress – Strain curves derived by uniaxial tensile testing on ten specimens per pipe: B-1 (41 years, DN 250), B-2 (39 years, DN 250), B-3 (23 years, DN 200 with a recycled core), B-4 (16 years, DN 160 with a foamed core), and R (new pipe). Displacement rate = 5mm/min. Testing temperature = 24 ± 2 °C.

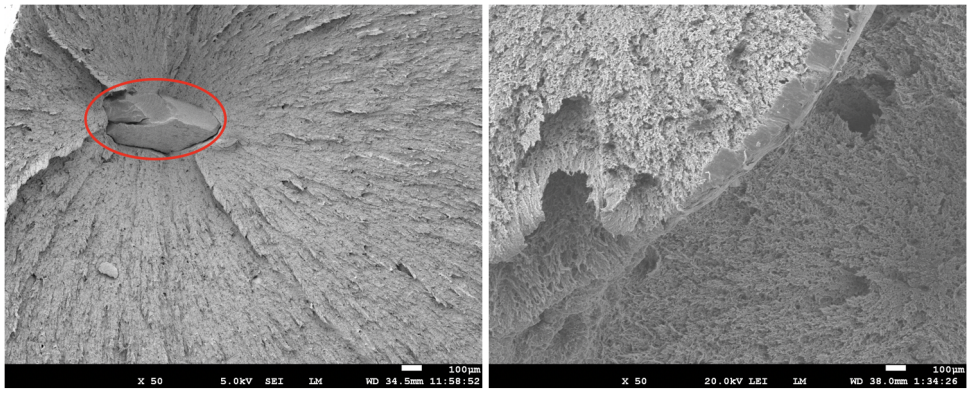

Figure 3.7: Images obtained via a scanning electron microscope at prematurely failed cross-sections during tensile testing for samples of B-1 (left) and B-3 (right). The cavity found in B-1 pipe sample (within red circle) is covered with the coating material needed for this analysis.

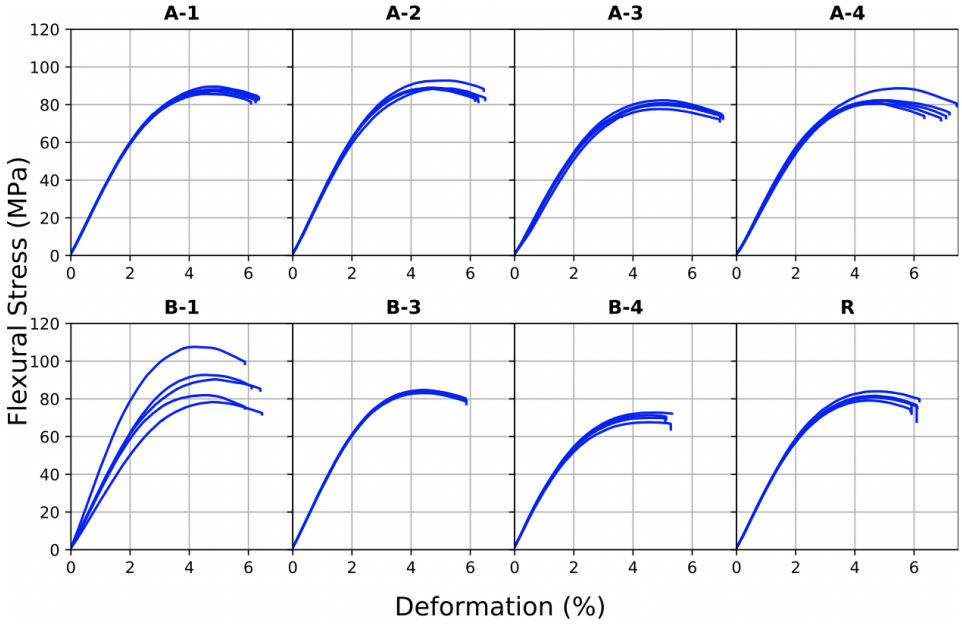

Figure 3.8: Flexural Stress – Deformation curves derived by repeated 4-point flexural testing on five different specimens per pipe. Displacement rate = 15 mm/min (B-3: displacement rate = 14mm/min, B-4: displacement rate = 11mm/min). Testing temperature = 20 ± 0.2 °C.

is not so clearly detected via density measurements as with other methods (e.g. tensile testing). Intrinsic viscosity of pipe B-4 proved to be noticeably less when compared to the rest of tested pipes, which was a precursor of lower tensile properties, although the embedded foamed core seemed to be of higher significance. Nonetheless, lower values

Table 3.5: Comparison between measured properties of excavated pipes and required values for new PVC sewer pipes given in NEN-EN 1401-1.

	Required value	Mean measured value								
Property	**(NEN-EN 1401-1)**	**A-1**	**A-2**	**A-3**	**A-4**	**B-1**	**B-2**	**B-3**	**B-4**	**R**
PVC content (%)[a]	≥ 80	78.9	81.6	82.1	80.5	84.7	83.2	82.8	73.6	80.4
Density (g/cm^3)	1.35 ≤ density ≤ 1.6	1.42	1.41	1.41	1.41	1.41	1.41	1.41	1.49	1.41
Processing temperature (°C)[b]	≥ 185	174.1	169.3	174.7	175.1	179.8	179.9	185.7	192.4	185.7
Strain at break (%)	≥ 80[c]	-	-	-	-	136.9	175.3	53.3	24.5	212.0

[a] This parameter is obtained via Thermogravimetric Analysis (TGA)
[b] This parameter is obtained via Differential Scanning Calorimetry (DSC)
[c] This value is given for tensile tests performed at 23±2 °C

of intrinsic viscosity may be yielded due to removing higher order molecules during filtering.

Furthermore, no distinct signs of degradation were detected via thermal analyses. The magnitude of glass transition temperature (T_g) is likely to decrease as degradation proceeds (Hamid et al., 1992), while the same tendency is expected for the characteristic temperature values (T_{onset} and T_{SD}) derived by TGA. Nonetheless, all the investigated pipes demonstrated values relatively close to the reference one, being similar to those of unaffected pipes (Fumire, 2008). Moreover, the degree of gelation is usually assessed based on the area of the two endotherms observed in the DSC graphs (Gramann et al., 2010; Real et al., 2018). However, this process was not conducted in the current study due to uncertainties of the applied method (i.e. sample preparation and variations through the pipe thickness) and the limited number of tested samples (maximum 4). Besides that, a clear connection between the level of gelation assessed with the mentioned methods and the performance of PVC pipes does not seem to prevail (Alferink et al., 1995; Real et al., 2018).

XRF analysis indicated that certain elements, which constitute common stabilizers, fillers and pigments for PVC pipes (Wilkes et. al, 2005), were found in all samples. At the same time, PVC proved to be a polydisperse material with various elemental compositions. Discrepancies were detected even in pipes which originate from the same production period and manufacturing company, such as pipes B-1 and B-2. However, it should be stressed that XRF is mainly a surface analysis as it penetrates only $2-20\,\mu m$ within the material. The variability in the type and concentration of inorganic elements combined with the range of processing temperatures revealed the disparate processing procedures followed by different manufacturers and through separate production periods. Only recently produced pipes (B-3, B-4 and R) obey to the levels of required processing temperature for PVC sewer pipes, while most pipes (except for A-1 and B-4) have the required level of PVC content (Table 3.5). These factors are generally expected to result in varying pipe properties and quality levels (Weller et al., 2016).

The main compositional structure of PVC seems to be intact (Noda et al., 2007), albeit the detected peaks at 1711 and 1739 cm^{-1} in the FTIR graphs indicate oxidation expressed via the existence of carbonyl functional groups on several pipes (Hamid et al., 1992). The fact that similar results were found also at the external surface of water dis-

tribution PVC pipes in another study (Kowalska et al., 2014) leads to the speculation that certain soil parameters potentially affect the chemical stability of PVC material. Additionally, the pipes manifested discolorization, an indication of dehydrochlorination, at several points of the outer surface and at the inner bottom surface at the area of sewage flow. Nonetheless, discolorization was definitely limited at the surface level while overall testing on discolored specimens proved that material properties were not affected.

Moreover, tensile tests showed a variability between pipes, as a consequence of the pipes' age and the construction materials. There was an evident indication of physical ageing regarding single layer pipes, as a transition was observed towards higher ultimate tensile strength and elastic modulus values, followed by lower strains at break. These values were of similar or higher magnitude compared to old PVC sewer pipes investigated in other studies (Bauer, 1990; Alferink et al., 1995; Whittle et al., 2005). Ductility of old pipes was found to be reduced but still remained at high levels. However, it has to be stressed that service temperatures can be lower than the tested ones, resulting in a more brittle behaviour and a reduced capacity of the pipe to absorb energy before fracturing (McGarry et al., 1985; Visser et al., 2011; Scholten et al., 2016). It is expected that, after a certain point, this brittleness will potentially cause issues concerning the pipe inspection and the placement of new household connections. Moreover, the existence of a core within the pipe wall thickness led to a decrease in all tensile properties, yielding lower values of elongation at break than required (Table 3.5). SEM indicated that more cavities are prone to be created in pipes with embedded cores, although a noticeable cavity was also found to be responsible for the failure of a sample of a single layer pipe (B-1). Consequently, poor installation quality or differential ground sedimentations could be critical factors as excessive tension of such pipes could lead to premature failures.

Four-point flexural testing was considered as more appropriate than tensile testing in order to describe the stress conditions of gravity sewers in the ground. In addition, the flexural modulus is highly correlated with ring stiffness, as shown in Eq. 2.3. Ring stiffness is an important parameter for gravity flow pipes as it is a measure of resistance against deflection (Eq. 2.1) and its estimation is used for the design and classification of thermoplastic pipes (ISO 9969). Since the available lengths of unaffected pipe segments were not sufficient to perform ring stiffness tests, flexural tests were preferred in order to estimate and compare the flexural moduli of the tested pipes. However, deriving actual values for ring stiffness of a cross-section via the obtained elastic modulus values would be assigned with substantial uncertainties, given that the samples were taken from the pipes crown and not from the whole cross-section.

Results from flexural tests revealed that a foamed or recycled core did not affect the performance against bending, yielding similar results with single layer pipes. However, pipes with a void core (A-3 and A-4) demonstrated lower flexural modulus values. Although several factors may have led to this outcome (for instance soil composition, backfill quality, traffic load), samples from these pipes (A-3, A-4) performed at the same level in a series of tests (density, intrinsic viscosity, thermal analyses) as single layer pipes subject to similar conditions (A-1, A-2). Therefore, the presence of the void core is considered as the main parameter for lower flexural properties. It should also be emphasized that both tensile and flexural testing on different samples of single layer pipe B-1 showed

high variability, denoting high heterogeneity levels within the pipe.

3.4.2. CAUSES OF PIPE FAILURE

Investigation of material properties provided sufficient information about the structural integrity of the affected pipes, without justifying the origins of the occurred failures. The actual causes were exposed either during excavation or via careful interpretation of inspection data. The cause of failure of pipe A-1 could be attributed to joint bending. Inspection footage clearly indicated angular bending at the joint (Figure 3.1a) leading to the development of contact points between the pipes. Such contact points impose excessive bending moments and local peaks in tensile stresses on the pipe during operation. This state may have initiated by poor installation quality and/or differential soil settling (Arsénio, 2013), a known phenomenon at the installation site due to the type of native soil (clay). Settling conditions and/or poor soil compaction are considered as a plausible justification also for the deformed top observed in pipe A-2. This pipe was also installed approximately 0.8 m deeper in the ground compared to the other tested pipes and under a paved street, increasing the vertical load at the crown of the pipe. The combined effect of soil conditions and the low bending stiffness of plastic pipes could lead to such pre-buckling conditions (Stein, 2001).

In case of pipe A-3, no sharp object (e.g. rock) was found to be in contact with the pipe near the pointy break, while deep scratches were observed in the deformed area above the defect (Figure 3.9, left). Based on this fact, it can be safely assumed that this defect is caused by human activity, conceivably third-party impact. A more evident indication of a similar situation was provided via visual examination of the break at pipe B-2, as the footprint of an excavator's bucket was recognized on the pipe (Figure 3.9, middle). The likelihood of such a failure cause was increased by the existence of several installed pipes destined for other purposes close to the affected one, hinting at extensive digging activity during the service life of the pipe under consideration. The source of the failure of pipe B-3 could be traced back to the installation of the pipe. The crack detected via the inspection was found to be initiated at the contact point between the affected pipe and the concrete protection of a warm water distribution pipe. Nonetheless, the interaction of these two types of infrastructure was trivial compared to the installation practice, as an extra piece of pipe was found around the cracked part of the pipe (Figure 3.9, right). This fact revealed the human interference regarding the failure and the poor installation quality.

Further, visual inspection of pipe A-4 revealed that only the inside layer of the bottom of the pipe was cracked; hence no exfiltration of sewage occurred during operation. This crack was apparently formed by the combination of deflection and the fact that pipes with void core demonstrated lower flexural modulus values. Pipe ovalization results in high tensile stresses at the 6 and 12 o' clock position of the inner surface, justifying the location of the crack. Finally, as mentioned in section 3.2.1, pipes B-1 and B-4 had no structural defects but suffered from root intrusion via elastomeric joints.

Figure 3.9: In-situ footage after excavation of pipes A-3 (left) and B-2 (middle) with break due to third party impact, and pipe B-3 (right) with crack due to poor installation quality.

3.5. CONCLUSIONS

Excavation and comprehensive testing of eight PVC sewer pipes (exposed to 16-43 service years) with known defects (fissures, breaks, root intrusion) revealed factors that affect the pipe's operational lifetime. Physical ageing was the most profound mechanism, resulting in an increase in ultimate tensile and flexural stresses followed by lower levels of ductility compared to a brand-new pipe. However, such a comparison can be only indicative given the polydispersity of PVC material and the updated production process.

One critical factor for premature failures was the existence of inherent defects. Especially the incorporation of a recycled or foamed core within the pipe acted as numerous inherent defects, while the core itself reduced significantly the strength and toughness of the pipe. This reduction could imply that excessive pipe bending or deflection is a potential threat to the longevity of the system. However, flexural testing showed that the investigated pipes could bare excessive bending, although pipes with an embedded void core had a comparatively lower flexural modulus. Moreover, there was a slight indication that oxidation on the external surface of the pipes had commenced. Signs of discolorization which could suggest potential chemical degradation were also limited to the pipe surface level only. Comprehensive testing led to the conclusion that alterations in properties among pipes originate from different production procedures, rather than a modified molecular structure or chain scission.

This study identified that the most important cause of failure for the examined pipes is related to poor installation quality and human activities. Such activities include excavation in the surroundings of the pipe, most likely due to installation or maintenance of other underground infrastructure. Therefore, it is inadequate to develop sewer asset management strategies based only on the age of the pipe and the pipe material properties. Incorporation of detailed protocols for handling and construction, close supervision during construction and measures against third party impacts are a precondition for long-lasting sewer pipelines.

4

ACOUSTIC WAVES FOR ESTIMATING THE STORAGE MODULUS OF PLASTIC PIPES

4.1. INTRODUCTION

Knowledge of a structure's elastic or storage modulus is crucial as it includes information concerning the level of stiffness and it allows predictions regarding the behaviour of the structure under certain loads, making it a crucial design parameter. In the case of plastic pipes, this characteristic is expressed via the pipe (or ring) stiffness which is directly related to the elastic modulus (Moser et al., 2008) and it is a measure of resistance to deflection under vertical loads (ISO 9969, 2016). In urban drainage, NEN 1401-1 (Table 4) dictates the required ring stiffness value depending on the desired application, namely 2, 4 or 8 kN/m/m, and the required thickness according to the nominal diameter in order to achieve these stiffness values. As shown in Chapter 3, the elastic modulus can also be used as a measure of ageing of plastic pipes as it's increase depicts the transition towards higher brittleness levels. Infrastructure ageing is a major concern for sewer asset managers since simultaneous pipe failures could result in extreme replacement costs and workloads. Therefore, there is a need for methods which will be capable of estimating the storage modulus and at the same time will be sensitive enough to detect changes in the storage modulus due to ageing.

A common way to estimate the linear properties of materials in the lower strain non-destructive regime is ultrasound (Ivey et al., 1949; Perepechko et al., 1973; Koda et al., 1993; Lionetto et al., 2008). Nonetheless, the capability of detecting ageing with high fre-

Parts of this chapter have been published in: Makris, K. F., Langeveld, J. G., Clemens-Meyer, F. H. L. R., Watts, J., Begum, H., & Horoshenkov K. V. (2022). Sonic assessment of physical ageing of plastic pipes. *Journal of Sound and Vibration.* DOI: 10.1016/j.jsv.2022.117393

quency sound waves has proved to be challenging. Demcenko et al. (2014) used the conventional pulse-echo ultrasonic method at 2 MHz to measure the bulk wave velocity and attenuation of PVC samples which were annealed for periods of 3 up to 124 days. However, the differences among samples in terms of both measured velocity and attenuation values were insignificant and did not allow to draw conclusions on material ageing. Furthermore, Read et al. (1992) measured the storage and loss modulus of PVC specimens of different ageing durations over a frequency range of 0.01 Hz to 5 MHz. Results revealed that discrepancies in the amplitude of the storage and loss modulus were observed due to ageing, although they became less distinguishable as the testing ultrasonic frequency increased. Similar findings are published concerning other polymer materials, such as high-density polyethylene, polypropylene and polycarbonate (Read et al., 1988, 1989).

Additionally, there is no recorded attempt so far to track a pipe's storage modulus with low frequency acoustics. The term "low frequency" denotes frequencies at which the compressional wavelength in the pipe wall is larger than the inner circumference of the pipe (Baik et al., 2010). Apart from higher sensitivity to ageing, a shift to lower frequencies would also limit the number of propagating acoustic modes to the axisymmetric ones that emerge first at low frequencies. Figure 4.1 gives an example of the number and types of modes that can propagate in a pipe suspended in vacuum. Each curve in this graph represents a propagating mode, indicating how its phase velocity changes according to frequency. The axisymmetric modes are also depicted in this figure, namely the longitudinal L(0,1) and torsional T(0,1) modes. For fluid-filled pipes, an additional mode, the fluid-borne wave, can also be detected at low frequencies. In literature, application of the latter mode has been studied mainly in order to locate the position of a leakage in water distribution systems via correlation of the received signals from the leakage at two known locations and corresponding time delay (Long et al., 2003; Gao et al., 2004; Scussel, 2021). Other applications of axisymmetric waves include the estimation of soil parameters around the pipe (Scussel et al., 2019) and locating buried pipes via ground surface vibration (Gao et al., 2017). Nonetheless, all the discussed applications are based on solutions of the considered propagation waves which include simplifications, aiming to reduce the complexity of the derived non-linear equation.

In this chapter, the general solution of wave propagation of a fluid-filled pipe surrounded by soil is derived from the equations of motion, while assuming that the coupled system is harmonically oscillated in the low-frequency regime. Initially, the wave propagation in each medium is analyzed and coupling is performed based on the shell boundary conditions. The considered equations are also reduced for the case of axisymmetric wave propagation and the case of a fluid-filled pipe in vacuum. The validity of assumptions found in literature to derive simplified forms of these analytical solutions are evaluated and discussed. Additionally, the theory behind the development of a finite element model (FEM) in COMSOL Multiphysics® is presented. Subsequently, the developed FEM is used for comparison with the demonstrated analytical solution, as well as for the analysis of the effect of soil and pipe deflection on wave propagation. Additionally, an uncertainty analysis reveals the factors that affect mostly the accuracy in estimating the storage modulus of a pipe with the axisymmetric waves. In essence, herein lies the theoretical part of low frequency wave propagation, as a basis of a technique for estimating the storage modulus and physical ageing, presented in Chapter 5.

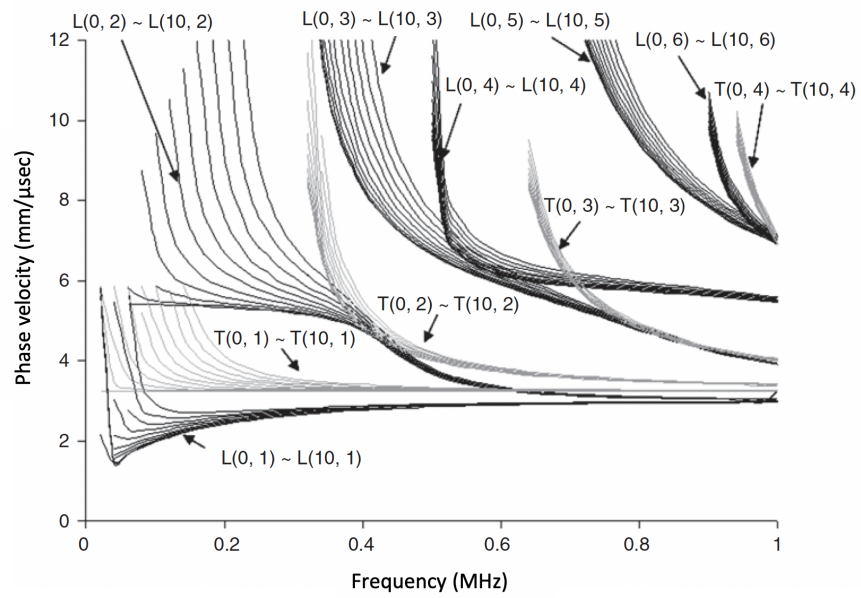

Figure 4.1: Dispersion curves for the propagating modes in a hollow three inch (76.2 mm) steel pipe. Both longitudinal L(n,m) and torsional T(n,m) modes are depicted (n,m=0, 1, ...). Each curve denotes a propagating mode and how its velocity changes as a function of frequency. The axisymmetric modes are obtained when n=0, while for n>0 flexural modes are obtained. The index m refers to different groups of modes and is increasing by moving to higher frequencies. This figure is retrieved from Rose (2014).

4.2. WAVE PROPAGATION IN THE EMBEDDED DOMAINS

This section includes the derivation of the dispersion equation for a fluid-filled pipe surrounded by soil, hereafter called "fluid-pipe-soil" system. The general equation is reduced for the case of axisymmetric modes and for a fluid-filled pipe in vacuum, hereafter called "fluid-pipe-vacuum" system. Figure 4.2 presents the applied coordinate system and the notation of the displacement fields used for this analysis.

4.2.1. PIPE SHELL DOMAIN

The equations of motion for an infinitesimal element of the pipe shell in cylindrical coordinates (Figure 4.3) under in vacuum boundary conditions are given by Gazis (1959):

$$\frac{\partial \sigma_{zz}}{\partial z} + \frac{1}{r}\frac{\partial \sigma_{z\theta}}{\partial \theta} + \frac{\sigma_{rz}}{r} = \rho \frac{\partial^2 u_z}{\partial t^2} \tag{4.1a}$$

$$\frac{1}{r}\frac{\partial \sigma_{\theta\theta}}{\partial \theta} + \frac{\partial \sigma_{r\theta}}{\partial r} + \frac{2\,\sigma_{r\theta}}{r} + \frac{\partial \sigma_{z\theta}}{\partial z} = \rho \frac{\partial^2 u_\theta}{\partial t^2} \tag{4.1b}$$

$$\frac{\partial \sigma_{rr}}{\partial r} + \frac{1}{r}\frac{\partial \sigma_{r\theta}}{\partial \theta} + \frac{\sigma_{rr} - \sigma_{\theta\theta}}{r} + \frac{\partial \sigma_{rz}}{\partial z} = \rho \frac{\partial^2 u_r}{\partial t^2} \tag{4.1c}$$

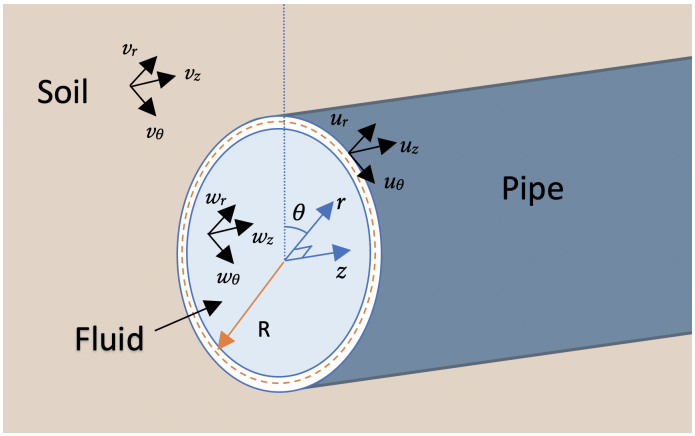

Figure 4.2: Sketch of the water-pipe-soil coupled system with indication of the coordinate system. The vectors u, v and w correspond to the pipe, soil and fluid propagation media respectively, and the subscripts (z, θ, r) correspond to the displacements in the respective directions.

where σ denotes the stress applied on a pipe shell element (Figure 4.3), ρ is the shell density, and u_z, u_θ and u_r are the displacements in the z, θ, and r direction, respectively. Utilizing the stress-displacement relationships for thin hollow cylinders and integrating Eq. 4.1 over the pipe thickness leads to the equations of motion for the whole shell.

Alternatively, the equations of motion for the pipe shell can be written in a matrix form (Leissa, 1973):

$$[Q][u_j] = 0 \tag{4.2}$$

where $[Q]$ is a matrix differential operator, and u_j is the displacement (j=z, θ, r).

Eq. 4.2 could be reformed with respect to the displacement amplitudes (U_j), if general wave solutions are assumed for the pipe displacement components:

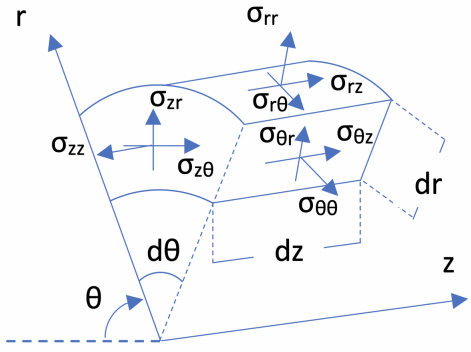

Figure 4.3: Stresses applied on a pipe shell element shown in the cylindrical coordinate system.

$$[u_j] = [U_j] e^{in\theta} e^{i(\omega t - k_z z)} \tag{4.3}$$

where U_j is the shell displacement amplitude for $j = z, \theta$ and r, n is the circumferential order (=0 for axisymmetric modes), ω is the angular frequency, k_z is the axial wavenumber and $i = \sqrt{-1}$.

Various theories describing the motion of thin cylindrical shells have been established. Depending on the adopted shell theory, a different operator $[Q]$ has been proposed. The discrepancies found among different theories originate from the way and/or location that the assumed simplifications (Love's approximations) are applied during derivation (Leissa, 1973). Operators of the most frequently used theories found in (Leissa, 1973) have been modified according to Eq. 4.3 and are presented in Appendix C. The form of Eq. C.1-C.7 leads to the conclusion that the elements between different operators remain identical or are modified by terms which are proportionate to the non-dimensional thickness parameter β^2:

$$\beta^2 = \frac{h^2}{12R^2} \tag{4.4}$$

where h is the pipe wall thickness and $R = R_i + h/2$ (R_i being the pipe's internal radius).

In the studied cases (i.e. buried plastic pipes), the geometric characteristics of the pipes are bound to a specific diameter-thickness ratio (SDR) in order to guarantee enough stiffness against vertical soil loading. In urban drainage, the usually required nominal stiffness (SN = 8 N/m/m) is achieved with a low SDR value, minimizing β^2. For instance, SDR should be 34 for PVC pipes and 21 for PE pipes (NEN 1401-1, NEN 12666-1), which implies that $\beta^2 \approx 3 \cdot 10^{-4}$ and $8 \cdot 10^{-4}$, respectively. Additionally, the majority of terms that include β^2 vanish if axisymmetric mode is considered (n=0). Therefore, any chosen theory would essentially lead to a similar operator. According to the simplest Donnel-Mushtari theory, the operator Q used for the subsequent analyses is (Leissa, 1973):

$$Q = \begin{bmatrix} \Omega^2 - k_z^2 R^2 - n^2 \frac{(1-\nu)}{2} & k_z R n \frac{(1+\nu)}{2} & -k_z R \nu i \\ k_z R n \frac{(1+\nu)}{2} & \Omega^2 - k_z^2 R^2 \frac{(1-\nu)}{2} - n^2 & n i \\ -k_z R \nu i & n i & -\Omega^2 + 1 + \beta^2 (n^2 + k_z^2 R^2)^2 \end{bmatrix} \tag{4.5}$$

where ν is the Poisson ratio, and $\Omega = \omega R \sqrt{\rho(1-\nu^2)/E}$ where E is the complex modulus ($E = E'(1 + \eta_s i)$, E' being the storage modulus and η_s the loss factor).

4.2.2. SOIL DOMAIN

Making a strong assumption of a homogeneous, isotropic and linear elastic soil medium, the equation of motion in the soil domain can be expressed via the Navier's governing wave equation (Rose, 2014):

$$(\mu_s + \lambda_s)\nabla(\nabla \cdot \vec{V}) + \mu_s \nabla^2 \vec{V} = \rho_s \frac{\partial^2 \vec{V}}{\partial t^2} \tag{4.6}$$

where $\vec{V}$ is the soil displacement vector, μ_s and λ_s are the Lamé constants, ρ_s is the soil density, $\nabla \cdot \vec{V}$ is the divergence of $\vec{V}$, ∇ is the gradient, and ∇^2 is the Laplace operator.

Moreover, the soil displacement components can be expressed by means of three functions Φ, X, Ψ (Liu et al., 2005):

$$v_z = \frac{\partial \Phi}{\partial z} - \frac{1}{r}\frac{\partial (r\frac{\partial X}{\partial r})}{\partial r} - \frac{1}{r^2}\frac{\partial^2 X}{\partial \theta^2} \tag{4.7a}$$

$$v_\theta = \frac{1}{r}\frac{\partial \Phi}{\partial \theta} - \frac{\partial \Psi}{\partial r} + \frac{1}{r}\frac{\partial^2 X}{\partial z \partial \theta} \tag{4.7b}$$

$$v_r = \frac{\partial \Phi}{\partial r} + \frac{1}{r}\frac{\partial \Psi}{\partial \theta} + \frac{\partial^2 X}{\partial z \partial r} \tag{4.7c}$$

The equation of motion (Eq. 4.6) is satisfied if the above functions satisfy the following three uncoupled equations of wave propagation:

$$\nabla^2 \Phi = \frac{1}{c_d^2}\frac{\partial^2 \Phi}{\partial t^2} \tag{4.8a}$$

$$\nabla^2 X = \frac{1}{c_\tau^2}\frac{\partial^2 X}{\partial t^2} \tag{4.8b}$$

$$\nabla^2 \Psi = \frac{1}{c_\tau^2}\frac{\partial^2 \Psi}{\partial t^2} \tag{4.8c}$$

where c_d and c_τ are the soil compressional and shear wave propagation velocities, respectively (Eq. 4.9):

$$c_d = \sqrt{\frac{2\mu_s + \lambda_s}{\rho_s}} \tag{4.9a}$$

$$c_\tau = \sqrt{\frac{\mu_s}{\rho_s}} \tag{4.9b}$$

Furthermore, the solutions of Eq. 4.8 can be expressed via the general wave solution formulation and by utilizing Hankel functions of the second kind so that the solutions approach 0 as r approaches infinity (Junger et al., 1986):

$$\Phi = A\, H_n(k_{d,r} r)\, e^{(in\theta)}\, e^{(i(\omega t - k_z z))} \tag{4.10a}$$

$$\Psi = B\, H_n(k_{\tau,r} r)\, e^{(in\theta)}\, e^{(i(\omega t - k_z z))} \tag{4.10b}$$

$$X = C\, H_n(k_{\tau,r} r)\, e^{(in\theta)}\, e^{(i(\omega t - k_z z))} \tag{4.10c}$$

where A, B and C are constant coefficients, H_n is the Hankel function of order n, ω is the angular frequency, k_z is the axial wavenumber and $i = \sqrt{-1}$. The terms $k_{d,r}$ and $k_{\tau,r}$ are

radial wavenumbers related to the compressional (k_d) and shear (k_τ) wavenumbers via the relationships:

$$k_{d,r} = \sqrt{k_d^2 - k_z^2} \tag{4.11a}$$

$$k_{\tau,r} = \sqrt{k_\tau^2 - k_z^2} \tag{4.11b}$$

Substitution of Eq. 4.10 into Eq. 4.7 leads to functions of the soil displacement components with respect to the coefficients A, B and C:

$$\begin{bmatrix} v_z \\ v_\theta \\ v_r \end{bmatrix} = \begin{bmatrix} K_{11} & K_{12} & K_{13} \\ K_{21} & K_{22} & K_{23} \\ K_{31} & K_{32} & K_{33} \end{bmatrix} \begin{bmatrix} A \\ B \\ C \end{bmatrix} e^{in\theta}\, e^{i(\omega t - k_z z)} \tag{4.12}$$

where

$$K_{11} = -k_z\, H_n(k_d^r\, r)\, i$$

$$K_{12} = 0$$

$$K_{13} = -\tfrac{1}{r}\, k_\tau^r\, H_n'(k_\tau^r\, r) - (k_\tau^r)^2\, H_n''(k_\tau^r\, r) + \tfrac{1}{r^2}\, n^2\, H_n(k_\tau^r\, r)$$

$$K_{21} = \tfrac{1}{r}\, n\, H_n(k_d^r\, r)\, i$$

$$K_{22} = -k_\tau^r\, H_n'(k_\tau^r\, r)$$

$$K_{23} = \tfrac{1}{r}\, k_z\, n\, H_n(k_\tau^r\, r)$$

$$K_{31} = k_d^r\, H_n'(k_d^r\, r)$$

$$K_{32} = \tfrac{1}{r}\, n\, H_n(k_\tau^r\, r)\, i$$

$$K_{33} = -k_z\, k_\tau^r\, H_n'(k_\tau^r\, r)\, i$$

Furthermore, the stress – strain relationships based on the Hooke's law for an isotropic medium are given by:

$$\begin{aligned} \sigma_{rr} &= (\lambda_s + 2\mu_s)\, \epsilon_{rr} + \lambda_s\, \epsilon_{\theta\theta} + \lambda_s\, \epsilon_{zz} = \lambda_s\, \nabla^2\Phi + 2\mu_s\, \epsilon_{rr} \\ \sigma_{r\theta} &= \mu_s\, \gamma_{r\theta} \\ \sigma_{rz} &= \mu_s\, \gamma_{rz} \end{aligned} \tag{4.13}$$

where the strains are expressed via the soil displacement components through the relationships:

$$\begin{aligned}
\epsilon_{rr} &= \frac{\partial v_r}{\partial r} \\
\epsilon_{zz} &= \frac{\partial v_z}{\partial z} \\
\epsilon_{\theta\theta} &= \frac{v_r}{r} + \frac{1}{r}\frac{\partial v_\theta}{\partial \theta} \\
\gamma_{r\theta} &= \frac{\partial v_\theta}{\partial r} + \frac{1}{r}\frac{\partial v_r}{\partial \theta} - \frac{v_\theta}{r} \\
\gamma_{rz} &= \frac{\partial v_z}{\partial r} + \frac{\partial v_r}{\partial z}
\end{aligned} \tag{4.14}$$

Consequently, the stresses can be expressed via the coefficients A, B and C:

$$\begin{bmatrix} \sigma_{rz} \\ \sigma_{r\theta} \\ \sigma_{rr} \end{bmatrix} = \begin{bmatrix} L_{11} & L_{12} & L_{13} \\ L_{21} & L_{22} & L_{23} \\ L_{31} & L_{32} & L_{33} \end{bmatrix} \begin{bmatrix} A \\ B \\ C \end{bmatrix} e^{in\theta}\, e^{i(\omega t - k_z z)} \tag{4.15}$$

where

$$\begin{aligned}
L_{11} &= -2\mu_s\, k_z\, k_d^r\, H_n'(k_d^r\, r)\, i \\
L_{12} &= \mu_s\, \tfrac{1}{r}\, k_z\, n\, H_n(k_\tau^r\, r) \\
L_{13} &= -\mu_s\, (k_z^2\, k_\tau^r\, H_n'(k_\tau^r\, r) + \tfrac{1}{r}\, (k_\tau^r)^2\, H_n''(k_\tau^r\, r) - \tfrac{1}{r^2}\, k_\tau^r\, H_n'(k_\tau^r\, r) + \\
&\quad + (k_\tau^r)^3\, H_n'''(k_\tau^r\, r) - \tfrac{1}{r^2}\, n^2\, k_\tau^r\, H_n'(k_\tau^r\, r) + \tfrac{2}{r^3}\, n^2\, H_n(k_\tau^r\, r)) \\
L_{21} &= \mu_s\, (\tfrac{2}{r}\, n\, k_d^r\, H_n'(k_d^r\, r) - \tfrac{2}{r^2}\, n\, H_n(k_d^r\, r))\, i \\
L_{22} &= \mu_s\, (\tfrac{1}{r}\, k_\tau^r\, H_n'(k_\tau^r\, r) - \tfrac{1}{r^2}\, n^2\, H_n(k_\tau^r\, r) - (k_\tau^r)^2\, H_n''(k_\tau^r\, r))\, i \\
L_{23} &= \mu_s\, (\tfrac{2}{r}\, k_z\, n\, k_\tau^r\, H_n'(k_\tau^r\, r) - \tfrac{2}{r^2}\, k_z\, n\, H_n(k_\tau^r\, r))\, i \\
L_{31} &= (\lambda_s + 2\mu_s)\, ((k_d^r)^2\, H_n''(k_d^r\, r)) + \lambda_s\, (\tfrac{1}{r}\, k_d^r\, H_n'(k_d^r\, r) - \tfrac{1}{r^2}\, n^2\, H_n(k_d^r\, r) - \\
&\quad - k_z^2\, H_n(k_d^r\, r)) \\
L_{32} &= 2\mu_s\, (\tfrac{1}{r}\, n\, k_\tau^r\, H_n'(k_\tau^r\, r) - \tfrac{1}{r^2}\, n\, H_n(k_\tau^r\, r))\, i \\
L_{33} &= -2\mu_s\, k_z\, (k_\tau^r)^2\, H_n''(k_\tau^r\, r)\, i
\end{aligned}$$

4.2.3. FLUID DOMAIN

Figure 4.4 illustrates a fluid element excited by the sound pressure wave. By applying Newton's second law with respect to the r direction, the following relationship between pressure and displacement is obtained (Junger et al., 1986):

$$(P_s + p)\, S - (P_s + p + \frac{\partial p}{\partial r} dr)\, S = \rho_f\, \frac{\partial^2 w_r}{\partial t^2}\, S\, dr$$

$$\frac{\partial p}{\partial r} = -\rho_f \frac{\partial^2 w_r}{\partial t^2} \tag{4.16}$$

where S is the cross-section of the fluid element perpendicular to the r direction and ρ_f is the fluid density, P_s is the static pressure, p is the acoustic pressure, and w_r is the displacement of the fluid in the r direction.

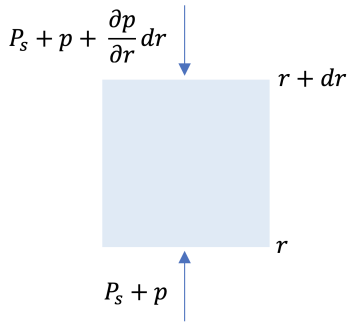

Figure 4.4: Pressure components acting on a fluid element in the r direction.

Similarly, for the θ and z directions it could be proven that:

$$\frac{1}{r}\frac{\partial p}{\partial \theta} = -\rho_f \frac{\partial^2 w_\theta}{\partial t^2} \tag{4.17}$$

$$\frac{\partial p}{\partial z} = -\rho_f \frac{\partial^2 w_z}{\partial t^2} \tag{4.18}$$

Further, the pressure field is expected to be in the form of modal series with a radial configuration expressed via Bessel functions of the first kind (Junger et al., 1986; de Jong, 1994). Assuming axial travelling waves, the pressure field in the fluid can be represented as:

$$p_{in} = P_{in}\, J_n(k_{f,r}\, r)\, e^{in\theta}\, e^{i(\omega t - k_z z)} \tag{4.19}$$

where P_{in} is the pressure amplitude, J_n is the Bessel function of the first kind and order n, and $k_{f,r}$ is the fluid radial wavenumber given by $k_{f,r} = \sqrt{k_f^2 - k_z^2}$.

4.3. COUPLED EQUATIONS OF MOTION

4.3.1. COUPLING AT THE PIPE - SOIL INTERFACE

The coupling between the pipe and soil is performed under the assumption of absolute contact, which implies that the following boundary conditions are applied at the pipe-soil interface:

$$u_i = v_i, \qquad i = z, \theta, r \tag{4.20}$$

Substituting Eqs. 4.3 and 4.12 into Eq. 4.20 yields:

$$\begin{bmatrix} U_z \\ U_\theta \\ U_r \end{bmatrix} e^{in\theta}\ e^{i(\omega t - k_z z)} = \begin{bmatrix} K_{11} & K_{12} & K_{13} \\ K_{21} & K_{22} & K_{23} \\ K_{31} & K_{32} & K_{33} \end{bmatrix} \begin{bmatrix} A \\ B \\ C \end{bmatrix} e^{in\theta}\ e^{i(\omega t - k_z z)}$$

Rearranging terms in the above leads to:

$$\begin{bmatrix} A \\ B \\ C \end{bmatrix} = \begin{bmatrix} U_z \\ U_\theta \\ U_r \end{bmatrix} \begin{bmatrix} K_{11} & K_{12} & K_{13} \\ K_{21} & K_{22} & K_{23} \\ K_{31} & K_{32} & K_{33} \end{bmatrix}^{-1} \tag{4.21}$$

Hence, the pressure exerted from the pipe shell towards the soil can be written with the aid of Eq. 4.15 in the following form:

$$\begin{bmatrix} \sigma_{rz} \\ \sigma_{r\theta} \\ \sigma_{rr} \end{bmatrix} = \begin{bmatrix} L_{11} & L_{12} & L_{13} \\ L_{21} & L_{22} & L_{23} \\ L_{31} & L_{32} & L_{33} \end{bmatrix} \begin{bmatrix} K_{11} & K_{12} & K_{13} \\ K_{21} & K_{22} & K_{23} \\ K_{31} & K_{32} & K_{33} \end{bmatrix}^{-1} \begin{bmatrix} U_z \\ U_\theta \\ U_r \end{bmatrix} e^{in\theta}\ e^{i(\omega t - k_z z)} \tag{4.22}$$

4.3.2. COUPLING AT THE FLUID - PIPE INTERFACE

Similar conditions are assumed to apply at the pipe-fluid interface (i.e. perfect contact):

$$u_i = w_i, \qquad i = z, \theta, r \tag{4.23}$$

This method is developed by regarding water as the internal fluid medium, which is considered to be inviscid. Hence, it cannot sustain shear stresses and substitution of Eq. 4.3 (in the r direction) and Eq. 4.19 into Eq. 4.16 leads to a relationship between the pressure amplitude P_{in} and the displacement amplitude W_r:

$$P_{in} = \frac{\rho_f\ \omega^2}{k_{f,r}\ J_n'(k_{f,r}\ r)}\ W_r \tag{4.24}$$

Therefore, Eq. 4.19 is expressed with respect to the shell amplitude U_r:

$$p_{in} = U_r\ P\ e^{in\theta}\ e^{i(\omega t - k_z z)} \tag{4.25}$$

where $P = \frac{\rho_f\ \omega^2\ J_n(k_{f,r}\ r)}{k_{f,r}\ J_n'(k_{f,r}\ r)}$.

4.3.3. GENERAL SOLUTION

The complete equations of motion are structured based on the formulation of Eq. 4.2 and by adopting the opposite sign convention in the matrix form concerning r direction:

$$\left[Q\right]\begin{bmatrix} u_z \\ u_\theta \\ u_r \end{bmatrix} + \frac{(1-\nu^2)\,R^2}{E\,h}\left\{\begin{bmatrix} p_z \\ p_\theta \\ -p_r \end{bmatrix} + \begin{bmatrix} 0\,0 & 0 \\ 0\,0 & 0 \\ 0\,0 & -p_{in} \end{bmatrix}\right\} = 0 \tag{4.26}$$

Considering Eqs. 4.22 and 4.25, Eq. 4.26 can be expressed by means of the displacement amplitudes U_z, U_θ and U_r:

$$\left\{\left[Q\right] + \frac{(1-\nu^2)\,R^2}{E\,h}\left(\begin{bmatrix} L_{11} & L_{12} & L_{13} \\ L_{21} & L_{22} & L_{23} \\ -L_{31} & -L_{32} & -L_{33} \end{bmatrix}\begin{bmatrix} K_{11} & K_{12} & K_{13} \\ K_{21} & K_{22} & K_{23} \\ K_{31} & K_{32} & K_{33} \end{bmatrix}^{-1} + P\begin{bmatrix} 0\,0 & 0 \\ 0\,0 & 0 \\ 0\,0 & -1 \end{bmatrix}\right)\right\}\begin{bmatrix} U_z \\ U_\theta \\ U_r \end{bmatrix} = 0 \tag{4.27}$$

A non-trivial solution of Eq. 4.27 exists only if the determinant of the coefficients is equal to zero. The solutions of Eq. 4.27 define the characteristic dispersion equation of the studied system. Although this equation is an 8^{th} order linear polynomial equation in case the pipe shell is (internally and externally) in vacuum, the fully coupled equation is deprived of linearity due to the inclusion of the required axial wavenumber k_z in the Bessel and Hankel functions. Therefore, solutions have to be sought recursively. Plotting the (angular) frequency versus the wavenumber leads to the so-called dispersion curves of the studied system. For measured axial wavenumbers, the determinant of Eq. 4.27 can be solved with respect to the pipe's storage modulus, which is a simpler task. The same equation (Eq. 4.27) can be also used for the system "fluid-pipe-vacuum" by setting $L_{ij} = K_{ij} = 0$ $(i, j = 1,2,3)$.

4.3.4. AXISYMMETRIC WAVE PROPAGATION

In axisymmetric wave propagation, the displacement field is independent of the circumferential angle (n=0). Eq. 4.27 can be further simplified by neglecting the dependence of the displacements on the θ direction. This leads to the following coupled equations of motion for the mode n=0:

$$\left\{\left[Q\right] + \frac{(1-\nu^2)\,R^2}{E\,h}\left(\begin{bmatrix} L_{11} & L_{13} \\ -L_{31} & -L_{33} \end{bmatrix}\begin{bmatrix} K_{11} & K_{13} \\ K_{31} & K_{33} \end{bmatrix}^{-1} + P\begin{bmatrix} 0 & 0 \\ 0 & -1 \end{bmatrix}\right)\right\}_{n=0}\begin{bmatrix} U_z \\ U_r \end{bmatrix} = 0 \tag{4.28}$$

The solutions of Eq. 4.28 can be traced by setting:

$$det\left\{\left[Q\right]+\frac{(1-\nu^2)\,R^2}{E\,h}\left(\begin{bmatrix}L_{11} & L_{13}\\ -L_{31} & -L_{33}\end{bmatrix}\begin{bmatrix}K_{11} & K_{13}\\ K_{31} & K_{33}\end{bmatrix}^{-1}+P\begin{bmatrix}0 & 0\\ 0 & -1\end{bmatrix}\right)\right\}_{n=0}=0 \tag{4.29}$$

In literature, a series of simplifications has been imposed in order to arrive at dispersion equations similar to Eq. 4.29, resulting in dispersion equations which can be solved analytically in a more straightforward way. Pinnington et al. (1994) explored the equations for the case of a fluid-filled pipe in vacuum. They obtained the equation for the fluid-borne wave by assuming that the axial wavenumber k_z is much larger than the dilatational shell wave number k_p which is included in the operand Q_0 via Ω. Further, the equation for the longitudinal L(0,1) wave was obtained by assuming that the axial wavenumber k_z is much smaller than the fluid wavenumber k_f. Additional simplifications were applied regarding the Bessel functions and their derivatives. Based on the same assumptions, Gao et al. (2016) developed the equation of the fluid-borne wave for the case of a pipe surrounded by soil. The solutions including the discussed simplifications are compared to the general analytical solution (Eq. 4.29) in Section 4.5.

4.4. DISPERSION CURVES VIA NUMERICAL ANALYSIS

This section presents the theory behind the development of a 2D finite element model (FEM) in COMSOL Multiphysics® for deriving dispersion curves of the systems "fluid-pipe-vacuum" and "fluid-pipe-soil" (Figure 4.5). The 2D model represents a cross-section of the system characterized by harmonic modes in space and uniform extension in the out-of-plane direction (COMSOL, 2017b). Solutions of the out-of-plane wavenumber for a given frequency are obtained via the modal analysis built on a built-in frequency domain eigensolver. Therefore, all the given equations in this section are considered in the frequency domain.

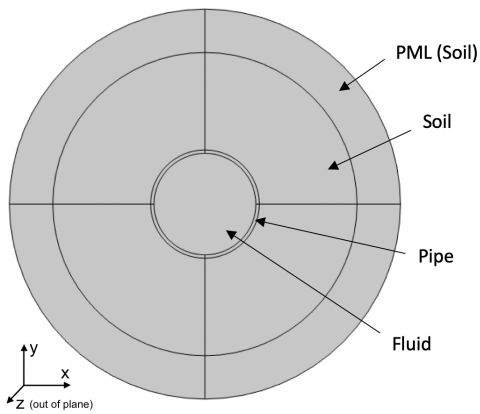

Figure 4.5: Geometry of the COMSOL® model ("fluid-pipe-soil") used for deriving the dispersion curves.

Within the fluid domain, the solutions for the out-of-plane wavenumber k_z are sought by the solver in the Helmholtz equation:

$$\nabla\,(-\frac{1}{\rho_f}\nabla p) - \frac{k_{f,r}^2\ p}{\rho_f} = 0 \tag{4.30}$$

where $k_{f,r}^2 = (\frac{\omega}{c_f})^2 - k_z^2$, p is the acoustic pressure, ρ_f is the fluid density, and c_f is the fluid sound velocity.

Within the pipe and soil domain, the solutions for k_z are found via Eq. 4.31 by assuming linear elasticity and that $u(x,y,z) = u(x,y)\ e^{-k_z z}$, where x, y, z are the cartesian space coordinates:

$$-\rho\ \omega^2\ \overrightarrow{u} = \nabla\ S \tag{4.31}$$

where ρ is the density of the medium, $\overrightarrow{u}$ is the solid displacement vector, ω is the angular frequency, $S = C_{jk}\ \epsilon_{jk}$ (C_{jk} being the elasticity tensor and ϵ_{jk} the elastic strain for $j,k = x,y,z$).

Further, the coupling at the acoustic-structure interface is implemented by applying Eq. 4.32 on the inner and outer boundary of the interface (COMSOL, 2017a):

$$\begin{gathered} -\overrightarrow{n}\,(-\frac{1}{\rho_f}\nabla p) = -\overrightarrow{n}\ \frac{\partial^2 \overrightarrow{u}}{\partial t^2} \\ \overrightarrow{F_A} = p\ \overrightarrow{n} \end{gathered} \tag{4.32}$$

where $\overrightarrow{n}$ is the surface normal, and $\overrightarrow{F_A}$ is the load applied on the pipe.

In case the pipe is surrounded by soil, a perfectly matched layer (PML) is applied at the external edge of the soil domain in order to model the infinite extents of the system. PML is used in order to dissipate the propagating waves with minimal reflections back to the system. This is achieved by applying a polynomial stretching function within the PML (COMSOL, 2017a):

$$f_p(\xi) = s\ \xi^c\ (1-i) \tag{4.33}$$

where ξ is a dimensionless coordinate (from 0 to 1) which extents along the PML, s is the scaling factor, c is the curvature parameter, and $i = \sqrt{-1}$.

The performance of the PML is dependent on the input values for the scaling factor and the curvature parameter. The scaling factor is multiplied with the longest wavelength of the propagating waves in order to generate an effective scaled width for the applied PML. The curvature parameter rearranges the meshing inside the PML so that the resolution near the boundary between PML and physical domain is increased and, hence, wavemodes of smaller wavelengths can be effectively treated. Since FEM is used in this research for comparison, the default values (equal to 1) are used for both scaling factor and curvature parameter without further tuning.

4.5. PERFORMANCE OF THE ANALYTICAL SOLUTION

The performance of the analytical solution was assessed via comparing its results with the results obtained from the COMSOL® model. FEM is used here as a reference for the evaluation of the developed analytical method and of simplified methods available in literature, as it solves the complete equations of motion. One major limitation that exists in FEM concerning the accuracy of solution is the quality of meshing. In the developed models, the maximum size of each element was one twelfth of the smallest wavelength based on a proposed rule of thumb (https://www.comsol.com) and a convergence analysis, while around the interfaces between domains the meshing was even finer.

Table 4.1 contains the properties used for the analyses in the remaining sections. The values of the properties are retrieved from Chapter 3 or from literature (Gao et al., 2017). The dimensions of the considered pipe are extensively used for PVC sewer pipes, following the specifications according to NEN 1401-1 for ring stiffness of 8 kN/m/m, with 250 mm external diameter and 7.8 mm wall thickness. The ring frequency, which denotes the low-frequency regime, is ~2.9 kHz for the given geometric and material properties (wavelength = 0.736 m). The following analyses are conducted for frequencies up to 1 kHz, so within the low-frequency regime.

Table 4.1: Material properties used for analyses.

	Density (kg/m^3)	Elastic modulus (GPa)	Poisson ratio (-)	Loss factor (-)	Compressional wave velocity (m/s)	Shear wave velocity (m/s)
Pipe (DN250)	1410	3	0.4	0.06	2135.2	871.7
Water	1000	-	-	-	1481.4	-
Soil	1500	-	-	-	200	100

Initially, the case of a water-filled pipe in vacuum is explored. Figures 4.6 and 4.7 present the real and imaginary part, respectively, of the analytical solution (Eq. 4.29), the simplified analytical solutions for longitudinal L(0,1) and water-borne waves given by Pinnington et al. (1994), and the numerical solution obtained by COMSOL®. The imaginary part is included as it is associated with the attenuation of propagating modes. Results revealed that the general analytical solution follows the numerical one with deviations up to 0.8% and 1.2% for the real part, and 0.9% and 1.3% for the imaginary part of the L(0,1) and water-borne mode, respectively. No actual deviation between the analytical and numerical solutions was observed regarding the torsional T(0,1) mode. Concerning the simplified solution, although the L(0,1) mode is close with the numerical solution (<0.5% discrepancy), the water-borne mode deviates from the beginning, an issue that exacerbates as the frequency increases. The same pattern is observed for both the real and imaginary parts of the solution, with deviations up to 30% and 45%, respectively.

In the system "fluid-pipe-soil", the number of propagating axisymmetric waves is reduced to only the fluid-borne wave due to the presence of soil, a topic which is further discussed in Section 4.6. Figure 4.8 demonstrates the real and imaginary parts of the solutions. It is again noticed that the general analytical solution follows the numerical one, while deviations observed among the solutions (maximum 2% for both real and imagi-

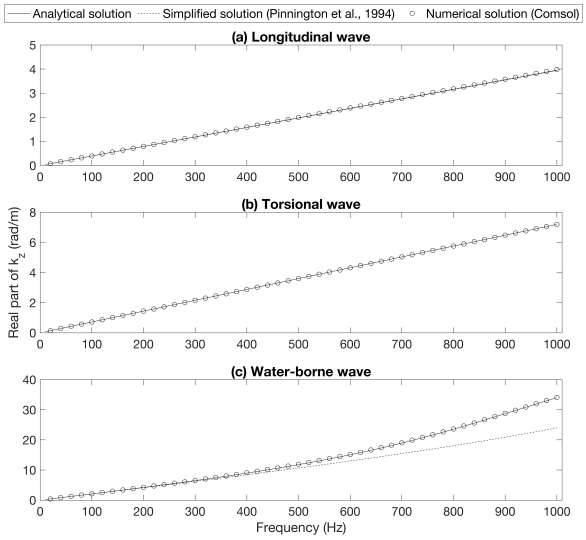

Figure 4.6: A comparison of the real part of the axial wavenumber k_z between different solutions of the axisymmetric propagating waves for the system "fluid-pipe-vacuum": a) Longitudinal L(0,1) wave, b) Torsional wave T(0,1), c) Water-borne wave. The real part of the axial wavenumber denotes the number of wavelengths per unit distance.

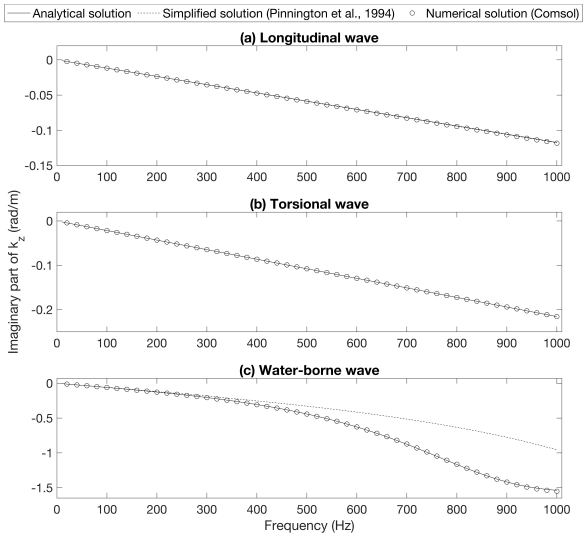

Figure 4.7: A comparison of the imaginary part of the axial wavenumber k_z between different solutions of the axisymmetric propagating waves for the system "fluid-pipe-vacuum": a) Longitudinal L(0,1) wave, b) Torsional wave T(0,1), c) Water-borne wave. The imaginary part of the axial wavenumber denotes the wave attenuation per unit distance.

nary parts) could be attributed to the fact that the PML of the FEM was not tuned. The simplified solution deviates at a larger extent almost within the whole tested frequency range, especially concerning the imaginary part which increasingly diverges (up to 40% at 1000Hz). The effect of the magnitude of the observed discrepancies on the estimation of storage modulus is analyzed in depth in Section 4.7.

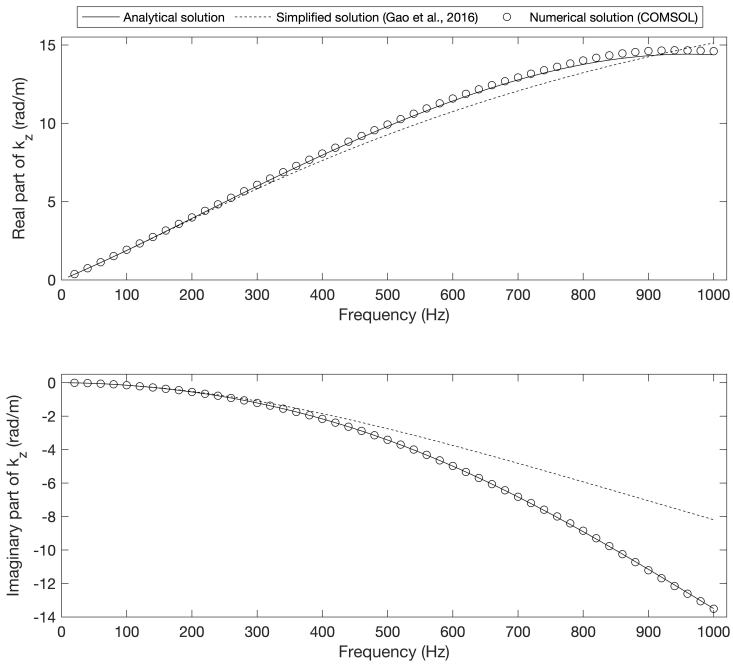

Figure 4.8: A comparison between different solutions for the real (top graph) and imaginary (bottom graph) part of the water-borne propagating wave for the system "fluid-pipe-soil". The real part of the axial wavenumber denotes the number of wavelengths per unit distance and the imaginary part denotes the wave attenuation per unit distance.

4.6. EFFECT OF SOIL ON WAVE PROPAGATION

Solving the dispersion equations for the system "fluid-pipe-soil" reveals that there is only one axisymmetric propagating mode, the fluid-borne wave. On the contrary, if the fluid-filled pipe is in vacuum, then the longitudinal L(0,1) and torsional T(0,1) modes are also existent. This section explores the reason behind this fact via different scenarios of coupling at the interface between pipe and soil. The analysis is based on a 2D axisymmetric model developed in COMSOL® (Figure 4.9) in which one end of the pipe shell is excited in the longitudinal direction with a harmonic sound pressure wave of 1 Pa at 100 Hz, while modifying the soil's ability to sustain shear stresses. The model is solved in the frequency domain. The material properties are given in Table 4.1 and PML's parameters remain at their default values (both scaling factor and curvature parameter are equal to 1).

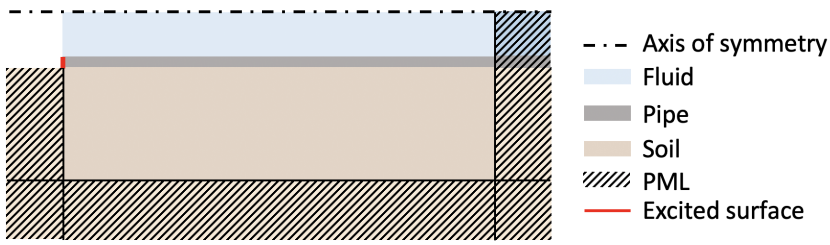

Figure 4.9: Geometry of 2D axisymmetric COMSOL® model ("fluid-pipe-soil") used to study the effect of soil on wave propagation. The scale is different to the actual for visual clarity.

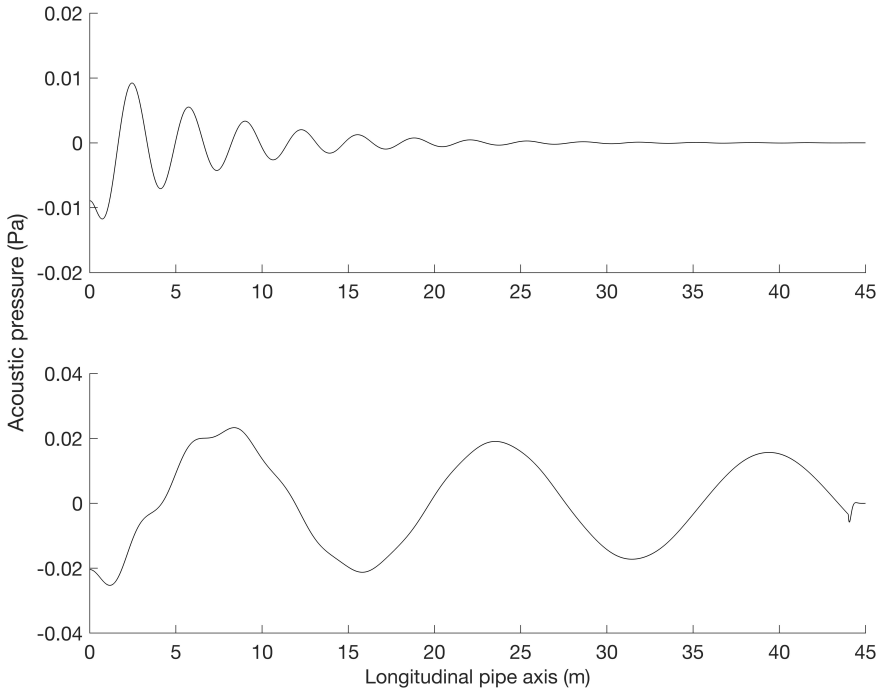

Figure 4.10: The effect of shear coupling between pipe and soil on wave propagation: Variation of acoustic pressure in water along the longitudinal pipe axis with pipe-soil shear coupling (top) and without pipe-soil shear coupling (bottom). The results are obtained at 100 Hz.

Figure 4.10 demonstrates how the sound pressure in water varies along the longitudinal axis of the pipe. In this simulation the soil's shear velocity is equal to 100 m/s (as in Table 4.1) or equal to zero. In fact, from Figure 4.10 the wavelength of a propagating wave can be estimated as the distance at which the signal shape repeats. If the soil sustains shear stresses ($c_\tau = 100 m/s$), then the wavelength of the propagating mode is equal to 3.27 m which yields an axial wavenumber of 1.92 rad/m (Figure 4.10, top). This value is equal to the wavenumber of the fluid-borne wave given by the numerical solution (Figure 4.8). If the soil is unable to sustain a shear wave ($c_\tau = 0$), then the wavelength is equal to 15.75 m which yields an axial wavenumber of 0.4 rad/m (Figure 4.10, bottom). This value is equal to the wavenumber of the longitudinal L(0,1) wave given by the numerical solution in Figure 4.6a when the pipe is in vacuum. Therefore, shear coupling at the pipe-soil interface is the factor that hinders shell-dominated waves from propagating. Additionally, in Figure 4.10 (bottom), it is also observed that close to the excitation source (< 15 m) the coupling with water affects the recorded acoustic pressure, although the pattern of axial wave's propagation persists.

4.7. UNCERTAINTY ANALYSIS OF THE ANALYTICAL SOLUTION

The aim of this section is to evaluate the relative significance of the accurate knowledge of parameters that affect the estimation of a pipe's storage modulus. Solving Eq. 4.29 with respect to the storage modulus leads to a function f of various properties (Eq. 4.34):

$$E = f(\nu, \rho, \eta_s, R_i, h, \rho_f, c_f, \rho_s, c_d, c_\tau, k_z^{re}, k_z^{im}) \tag{4.34}$$

where ν is the Poisson ratio of the pipe material, ρ is the pipe density, η_s is the pipe loss factor, R_i is the pipe internal radius, h is the pipe wall thickness, ρ_f is the fluid density, c_f is the fluid sound velocity, ρ_s is the soil density, c_d is the soil compressional velocity, c_τ is the soil shear velocity, k_z^{re} is the real axial wavenumber, and k_z^{im} is the imaginary axial wavenumber.

When putting this methodology into practice, each of the mentioned parameters shall be measured or taken from recorded measurements in other sources (e.g. literature, textbooks). Each parameter shall also have its own uncertainty, since measurements are always couped with errors (e.g. instrumental or observational errors). The combined effect of individual standard uncertainties can be expressed via the Law of Propagation of Uncertainties (LPU) under the condition that all parameters with their respective uncertainty distribution are known (Bertrand-Krajewski et al. 2021):

$$u(E)^2 = \sum_{n=1}^{N} u(x_i)^2 \left(\frac{\partial f}{\partial x_i}\right)^2 + 2 \sum_{i=1}^{N-1} \sum_{j=i+1}^{N} u(x_i, x_j) \left(\frac{\partial f}{\partial x_i}\right) \left(\frac{\partial f}{\partial x_j}\right) \tag{4.35}$$

where $u(x_i)$ is the standard uncertainty of each individual parameter x_i, N is the total number of parameters in the function f, and $u(x_i, x_j)$ is the covariance between two parameters x_i and x_j. All the parameters in Eq. 4.34 are considered independent, and therefore all the covariances are assumed to be zero.

The main focus here was on conducting a type of sensitivity analysis, hence Eq. 4.35

was applied by assessing the individual effect of each parameter's uncertainty on the uncertainty of the storage modulus. Additionally, the uncertainty of each parameter was considered to be the parameter's value itself (Table 4.1). The normalization was implemented with respect to the maximum uncertainty contribution at each considered frequency. The normalized uncertainty of the storage modulus ($u(E)_{norm}$) for every parameter x_i is defined as:

$$u(E)_{norm} = \frac{u(E)_{x_i}}{max(u(E)_{x_i}, \dots, u(E)_{x_N})} \tag{4.36}$$

where $u(E)_{x_i}$ is the uncertainty of the storage modulus caused by the individual uncertainty of parameter x_i at a given frequency. It should be stressed that the reported results (Figures 4.11 and 4.12) are scaled by the utilized values in the analysis and may differ for different parameter settings.

Figure 4.11 demonstrates the factors that affect mostly the accuracy of the estimation of the pipe's storage modulus for the three types of axisymmetric waves that propagate in the system "fluid-pipe-vacuum". Based on this figure, it is highlighted that the accurate estimation of the storage modulus based on the shell-dominated waves (L(0,1) and T(0,1)), is affected mainly by the uncertainty in the real part of the axial wavenumber and in the pipe shells properties (i.e. density and Poisson ratio). In the case of the waterborne wave, the accuracy is dependent on the fluid properties (fluid density and fluid's compressional wave velocity) and geometry of pipe (internal radius and thickness). The dependence on the real part of the axial wavenumber remains also high, albeit at high frequencies (e.g. 1000 Hz) it's relative significance is surpassed by that of the internal radius. As the frequency increases, the relative influence of the pipe's Poisson ratio on the overall uncertainty also increases.

Figure 4.12 presents the relative significance of the uncertainty of each parameter concerning the estimation of pipe's storage modulus for the fluid-borne wave of the "fluid-pipe-soil" system. As in the case of no soil, the accuracy is affected by the uncertainties in the geometrical properties of the pipe, the fluid's properties and the real axial wavenumber. However, in this case there are additional contributing parameters. In detail, soil density and shear wave velocity have an effect at lower frequencies, while soil compressional wave velocity has a relatively higher impact at higher frequencies. There is an increasing contribution of the imaginary axial wavenumber with increasing frequency on the overall uncertainty.

In general, it should be noted that in all studied cases the relative contribution of the real axial wavenumber is higher, a fact that requires extreme caution and repeated measurements when estimating the pipe's storage modulus in practice. Nonetheless, it also denotes a high sensitivity among wavenumber and storage modulus. This correlation could prove crucial when using the proposed method for detecting physical ageing in pipes from acoustical data. Figure 4.13 presents the relationship between the uncertainty in storage modulus and real and imaginary axial wavenumber uncertainties, given the considered properties (Table 4.1). In general, at higher frequencies the uncertainty in the storage modulus is less sensitive to the wavenumber uncertainty, an outcome that is expected, since at such frequencies the wavenumber values are considerably larger.

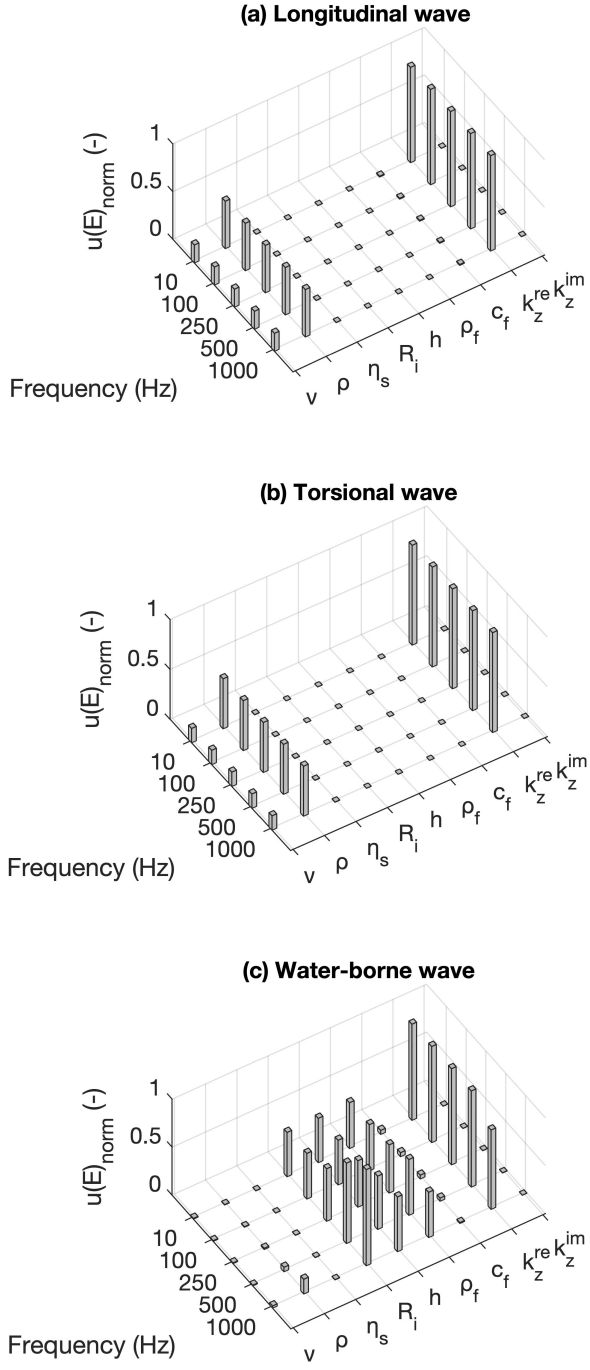

Figure 4.11: Relative contribution of each parameter's uncertainty to the overall uncertainty of the storage modulus $u_{(E)}$ of the pipe for the system "fluid-pipe-vacuum": a) Longitudinal wave L(0,1), b) Torsional wave T(0,1), c) Water-borne wave. $u_{(E)}$ is normalized according to Eq. 4.36 (ν: pipe's Poisson ratio, ρ: pipe density, η_s: pipe loss factor, R_i: pipe internal radius, h: pipe wall thickness, ρ_f: fluid density, c_f: fluid sound velocity, k_z^{re}: real axial wavenumber, k_z^{im}: imaginary axial wavenumber).

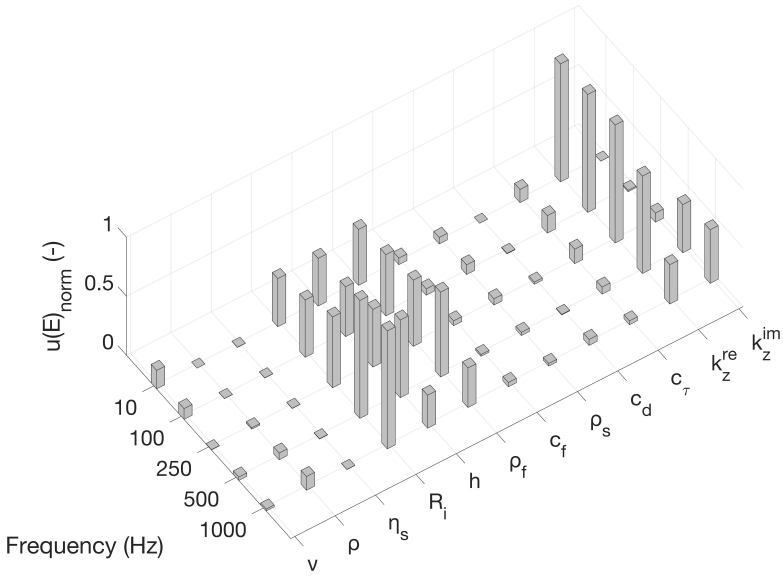

Figure 4.12: Relative contribution of each parameter's uncertainty to the overall uncertainty of the storage modulus $u_{(E)}$ of the pipe for the water-borne wave of the system "fluid-pipe-soil". $u_{(E)}$ is normalized according to Eq. 4.36 (υ: pipe's Poisson ratio, ρ: pipe density, η_s: pipe loss factor, R_i: pipe internal radius, h: pipe wall thickness, ρ_f: fluid density, c_f: fluid sound velocity, ρ_s: soil density, c_d: soil compressional velocity, c_τ: soil shear velocity, k_z^{re}: real axial wavenumber, k_z^{im}: imaginary axial wavenumber).

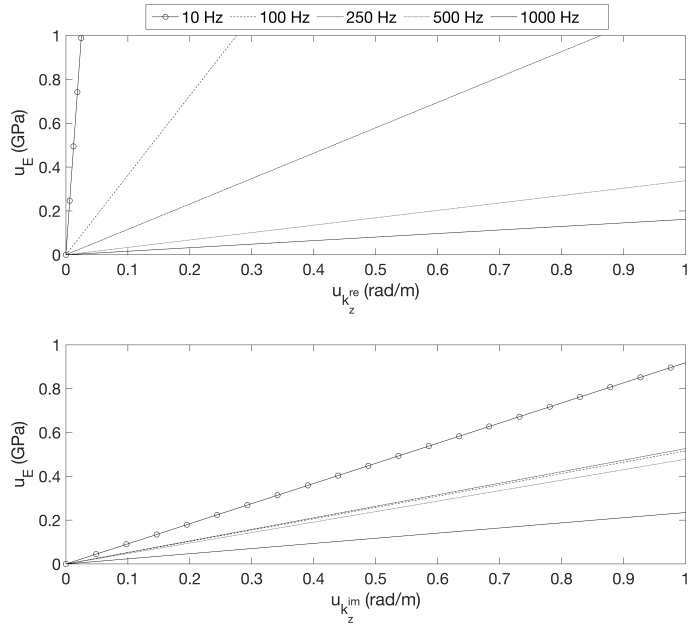

Figure 4.13: Uncertainty of the pipe's storage modulus as a function of the real (top) and imaginary (bottom) axial wavenumber uncertainty. This figure is generated based on the property values presented in Table 4.1.

Further, the importance of accurate estimation of the imaginary part of axial wavenumber is also depicted in Figure 4.13. These results could also be used to evaluate the discrepancies noticed among the various solutions presented in section 4.5. For instance, only the difference between the imaginary part of the simplified solution and other solutions (Figure 4.8) would yield a deviated estimation of storage modulus of around 0.8 GPa based on Figure 4.13.

4.8. EFFECT OF PIPE DEFLECTION ON WAVE PROPAGATION

Deflection in plastic sewer pipes is a defect that appears even directly after installation (Kuliczkowska & Zwierzchowska, 2016) and, depending on the quality of bedding and soil compaction, it can be mild or excessive. Significant deflection levels in water or gas distribution plastic pipes are not expected due to the lower pipe diameter-thickness ratio used for pressurized piping applications. According to NEN 1401-1 protocol for non-pressure pipe specifications, the expected average pipe deflection is less than 8%, while deflections up to 15% are allowed. These values along with 3%, used for ring stiffness evaluation (NEN 9969), are considered in this analysis. The aim of this section is to evaluate whether the presented methodology in this chapter can be used for deflected pipes, albeit the geometry is altered. Since deflection is a defect caused by soil, the analysis is limited to the water-borne wave of the "fluid-pipe-soil" system.

Initially, the capability of COMSOL® to solve for arbitrary geometries was utilized. The cross-section of a deflected pipe was assumed to be a perfect ellipse (Figure 4.14). Deflection was defined as y/D_o, where y is the vertical dispacement and D_o is the external diameter. Based on that relation, the vertical displacement of the pipe's crown and, subsequently, the semi-minor axis "b" of the resulting ellipse is estimated ($2\,b = D_o - y$). The semi-major axis "a" is then determined based on the condition that the ovalized pipe has no loss or addition of material compared to the non-deflected circular one, and, therefore, the circumference remains intact. In Figure 4.14, the eccentricity ($=\sqrt{(1-b/a)}$) of each ellipse is given for the considered deflections.

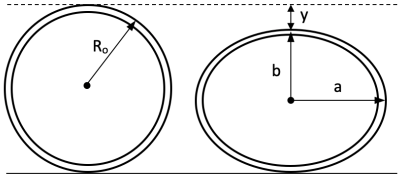

Deflection (%)	Eccentricity (-)
0	0
3	0.34
8	0.53
15	0.69

Figure 4.14: Geometry of non-deflected (left) and deflected (right) pipes used for analysis: R_o is the external radius, y is the vertical displacement at the pipe crown, a and b are the semi-major and semi-minor axis of the ovalized pipe, respectively.

Figure 4.15 presents the real and imaginary part of the solutions for a circular pipe and for ovalized pipes deflected at 3, 8 and 15%. The properties used for this analysis are found in Table 4.1. In general, it is observed that higher deflection levels result in larger deviations and this escalates in a non-linear way. Compared to the solution for

the non-deflected pipe, the deviation in the real part of the solution at 3% deflection is close to 2% for frequencies up to 100 Hz (maximum difference in storage modulus of ~ 0.15 GPa according to Figure 4.13), whereas above 200 Hz the obtained discrepancies (<1%) correspond to maximum deviations of ~ 0.03 GPa. Similarly, the imaginary part of the solution deviates more in low frequencies (maximum 15% at around 150Hz) but, due to the different sensitivity of the storage modulus to the imaginary part, the discrepancy in terms of modulus remains below 0.03 GPa for the whole frequency range.

When the pipe is subjected to 8% deflection, the real part of the solution deviates from the reference solution (0% deflection) up to 14% (at 80 Hz). This is translated into a mismatch of estimated storage modulus of up to 1 GPa. Above 200 Hz, deviations between the solutions (0% and 8% deflection) decrease rapidly and the maximum difference in the estimated storage modulus does not surpass 0.1 GPa (see Figure 4.13). Further, although the discrepancy concerning the imaginary part of the solutions is considerably high for low frequencies (up to 107% at 140 Hz), the effect on the accuracy of the storage modulus estimation is relatively minimal (<0.04 GPa) for the whole frequency range. At a deflection level of 15% the axial wavenumber deviates at larger extents from the reference solution within most of the tested frequency range (Figure 4.15), generating discepancies of up to 45% (at 80 Hz) and 340% (at 140 Hz) concerning the real and imaginary parts of the solution, respectively.

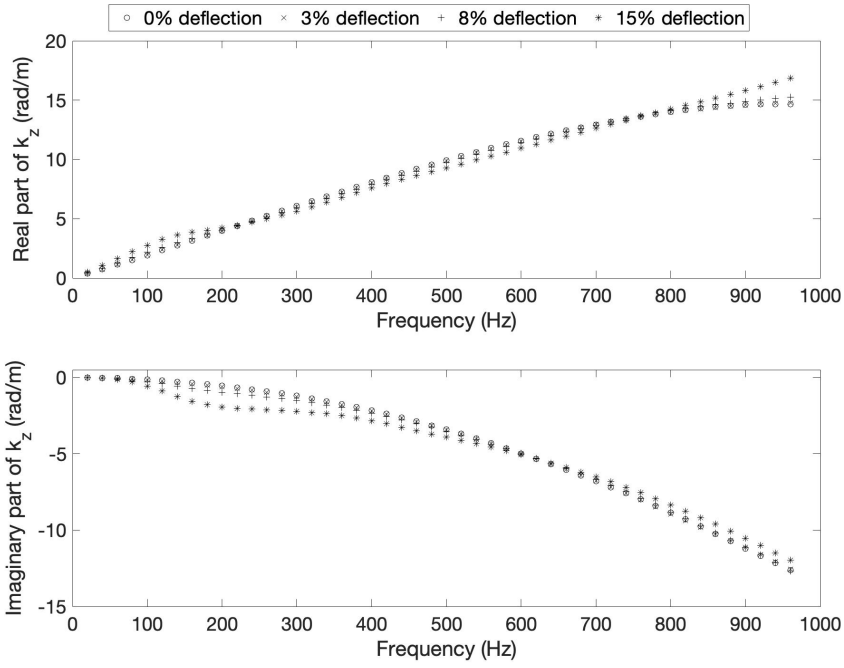

Figure 4.15: The effect of pipe deflection on the real and imaginary parts of the wavenumber for the fluid-borne acoustic wave. This figure is generated based on the property values presented in Table 4.1.

4.9. CONCLUSIONS

The dispersion curve equations have been developed analytically from the equations of motion by assuming harmonic oscillation of the whole system. The cases of a fluid-filled pipe in vacuum and a fluid-filled pipe surrounded by soil have been studied, while focus has been given only on axisymmetric modes (n=0), namely the axial L(0,1), torsional T(0,1) and water-borne modes. Comparison of the proposed methodology with a finite element model (FEM) showed in all cases insignificant or no deviations between the analytical and numerical solutions. Simplified analytical solutions available in literature followed closely the results from the numerical model only regarding the longitudinal L(0,1) propagating mode, for the same considered material properties. Furthermore, when soil surrounds the pipe, a reduction in the number of propagating modes to just the water-borne wave was observed, an effect which originates from the shear coupling at the pipe-soil interface.

Uncertainty analysis of each propagating mode revealed the relative contribution of the uncertainty of each parameter to the accuracy estimation of a pipe's storage modulus. In general, if the shell-dominated waves (i.e. L(0,1) and T(0,1)) can propagate, then the accurate knowledge of shell properties leads to a lower uncertainty of the estimated storage modulus. When utilizing fluid-borne waves to estimate the storage modulus, the geometry of the pipe becomes more important. In all cases, the uncertainty of the real axial wavenumber should be kept as low as possible since it contributes crucially to the overall uncertainty especially at lower frequencies (<500 Hz). If the pipe is surrounded by soil, then uncertainty in the imaginary axial wave increases significantly as the frequency increases. Additionally, uncertainties in soil density and shear wave velocity have an impact at lower frequencies.

Finally, the applicability of the developed solution for the axisymmetric fluid-borne mode was tested for three deflection values (3, 8 and 15%) with the aid of a FEM model, simulating deformed pipes surrounded by soil. The results revealed that solutions of lower deflection values (3 and 8%) show deviations from the solution of the circular pipe which can constrain the accuracy in the estimation of the storage modulus within 0.1 GPa, under the condition that testing frequencies are higher than 200 Hz. Larger deflections (15%) showed that applicability of the proposed solution would be challenging at any frequency given the level of the observed deviations.

5

THE POTENTIAL OF VIBRO-ACOUSTICS TO DETECT AGEING OF PLASTIC PIPES

5.1. INTRODUCTION

There are several available methods that can be used to detect physical ageing in thermoplastic materials. Most methods correspond to destructive techniques, such as conventional tensile testing (Visser, 2009), impact tests (Struik, 1977; Fillot et al., 2007), differential scanning calorimetry (Fillot et al., 2007), dynamic mechanical analysis (Flores et al., 1994; Fillot et al., 2007), and tensile/ torsional creep compliance measurements (Struik, 1977; Read et al., 1992). However, the development of non-destructive, single-sided (from the pipe's interior) techniques is essential concerning the inspection of pipes in operation, in order to ensure lower costs and minimal disruption of the system. Non-collinear ultrasonics and micro-indentation are such techniques with demonstrated ability to track ageing (Visser, 2009; Demcenko et al., 2014; Delgadillo et al., 2019). Nonetheless, significant limitations exist in both methods, since micro-indentation focuses only on the surface of the material, while non-collinear ultrasonics require continuous precise alignment and known acoustic properties of the inspected medium.

This chapter proposes a new method by exploring the potential of low frequency vibro-acoustics to track the ageing levels of plastic pipes, putting the theory developed in Chapter 4 into practice. An impact hammer was used to excite low frequency waves in two water-filled high-density polyethylene (HDPE) pipes (one above and another below ground), while the propagated wave signal was received by one or two hydrophones

Parts of this chapter have been published in: Makris, K. F., Langeveld, J. G., Clemens-Meyer, F. H. L. R., Watts, J., Begum, H., & Horoshenkov K. V. (2022). Sonic assessment of physical ageing of plastic pipes. *Journal of Sound and Vibration.* DOI: 10.1016/j.jsv.2022.117393

placed within the pipes. The raw signals were processed in order to estimate the real part of the axial wavenumber of the propagating water-borne wave. Subsequently, the proposed equation for axisymmetric waves (Eq. 4.29) was applied based on the vibro-acoustic experimental results, reaching an estimation for the storage modulus of the pipe material. Furthermore, dynamic mechanical analysis (DMA) was utilized on samples from the HDPE pipes to verify the magnitude of the estimated storage modulus. DMA was also conducted on samples from PVC pipes with extrusion age difference of 41 years, in order to study how the storage modulus behaves with respect to frequency and pipe age. The comparison between the storage moduli of these two samples along with the incorpotation of the measurement uncertainty levels found in the tested experimental configurations, allowed to draw conclusions on the potential of the axisymmetric water-borne wave to detect ageing and to recommend optimizing alterations in the used set-ups.

5.2. MATERIALS AND METHODS

5.2.1. EXPERIMENTAL SETUPS

Two different setups were used to examine the propagation of the water-borne wave in a water-filled HDPE pipe surrounded by air ("Set-up A") and water-filled HDPE pipe surrounded by sand ("Set-up B"). These pipes had an external diameter of 110 mm and wall thickness of 11 mm and were installed in a 40 m long, 3 m wide and 5 m deep sandpit in the The Integrated Civil and Infrastructure Research Centre at the University of Sheffield. The excitation of waves in the system was achieved via an impact hammer (PCB 086C03, 0.16 kg). The rubber tip of the hammer was carefully selected to generate low frequency modes of interest. A built-in load cell connected to the tip of hammer was capable of recording the force applied to the pipe at every hit. The acoustic signal was captured with hydrophones (B&K 8103) connected to a condition amplifier (B&K Nexus 2693-0S4). Figure 5.1 shows the two experimental setups including the hydrophone arrangements in the pipes. Set-up A was a straight pipe (see Figure 5.1(a)). In this set-up, just one hydrophone was used as the distance between the excitation point and hydrophone could be directly measured 5.3 m. Set-up B was a combination of a straight section and elbow section tilted at an angle (see Figure 5.1(c)). In this set-up, a second hydrophone was added 0.3 m away from the first one to help to resolve the uncertainty in the measurement of the effective distance between the impact and receiver points. Both vibration and acoustic signals were recorded with the same data acquisition module (NI USB-4431).

The measured or assumed values and their standard deviations in the properties of the pipe material, water and soil are given in Table 5.1. The density of the pipe material was measured from extracted samples according to ISO 1183-1 (immersion method) and was found to be 957.6 kg/m^3. The geometry of the pipe shell (wall thickness and internal radius) was determined in-situ with a measuring tape, accepting an uncertainty of 0.5 mm. Regarding the properties of water, reported values were used (Pang, 2013) with suitable uncertainties to compensate for temperature changes within a certain temperature range (10 − 20 °C). The values of the remaining properties were retrieved from lit-

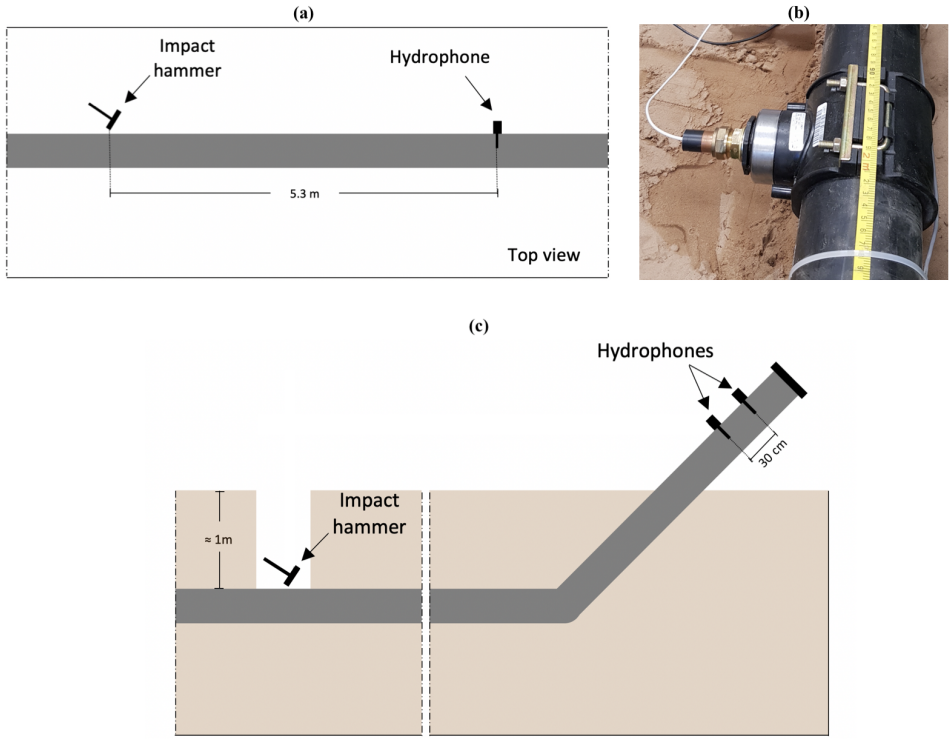

Figure 5.1: An illustration of the experimental set-ups: Set-up A (a); hydrophone installation method (b); and Set-up B (c).

erature. The magnitude of their uncertainties was based on the variability of the values observed in different scientific sources (Kubat et al., 1990; Men et al., 2003; Nitta, 2012; Gao et al., 2017) and expected variability in practice, rather than the prevailed laboratory conditions in the current study.

The soil in the below-ground section was washed silica sand and assumed properties were retrieved from Gao et al. (2017). The uncertainties of the soil parameters were considered higher compared to these of other media, since soil is expected to be the medium with the highest parameter variability. These uncertainties are high enough to reach the properties measured by Long et al. (2002) ($\rho_s = 2100 kg/m^3$, $c_d = 350 m/s$, and $c_\tau = 72 m/s$) for typical soil.

5.2.2. SIGNAL ANALYSIS

Figure 5.2 presents the process that was followed to estimate the real part of the axial wavenumber k_z^{re} of the water-borne mode from the raw signals. Depending on the set-up, raw signals could refer to signals from the impact hammer and single hydrophone (Set-up A) or exclusively to signals from two hydrophones (Set-up B). A Hanning time

Table 5.1: Measured or assumed pipe, water and soil properties and their standard uncertainties used in the following analyses.

Medium	Property	Symbol (Units)	Value	Standard Uncertainty
Pipe shell	Density	ρ (kg/m^3)	957.6	1.4
	Poisson ratio	ν (-)	0.4	0.05
	Loss factor	η_s (-)	0.05	0.01
	Internal radius	R_i (mm)	44	0.5
	Wall thickness	h (mm)	11	0.5
Fluid	Density	ρ_f (kg/m^3)	998	2
	Compressional wave velocity	c_f (m/s)	1481.4	35
Soil	Density	ρ_s (kg/m^3)	1500	600
	Compressional wave velocity	c_d (m/s)	200	150
	Shear wave velocity	c_τ (m/s)	100	28

window was applied to the signals in order to isolate the desired mode (i.e. the water-borne wave) from other present modes or signals reflected from various artefacts. The Hanning window was selected as it ensures the smoothing of abrupt ends and reduction of the spectral leakage. Moreover, the application of a bandpass Butterworth frequency filter allowed the consideration of a specific frequency range. The choice of the cut-off frequencies used in the filter (f_b and f_e) was informed by the coherence analysis of the raw signals to help identify the frequency range in which the two recorded signals were linearly related. The coherence is defined as (Carter et al., 1975):

$$CH(\omega) = \frac{|S_{12}(\omega)|^2}{|S_{11}(\omega)||S_{22}(\omega)|} \tag{5.1}$$

where S_{12} is the mean cross spectral density between the two signals, S_{11} and S_{22} are their mean autospectral densities, and ω is the angular frequency.

The transition to the frequency domain was achieved by applying the Discrete Fourier Transform (DFT) to each signal and then extracting the phase. The real axial wavenumber was estimated on the basis of the difference in phase between the two signals and distance between the points of their reception. In total, the experiments were repeated 10 times for each experimental set-up, and signals were recorded at a sampling rate of 12 kHz.

The application of the Law of Propagation of Uncertainties (LPU) to the formula for the real part of the axial wavenumber k_z^{re} (Figure 5.2) allows the estimation of its standard uncertainty u(k_z^{re}) (Eq. 5.2). LPU, presented in Section 4.7, was applied based on the assumption that all the measurements were independent and having a Gaussian uncertainty:

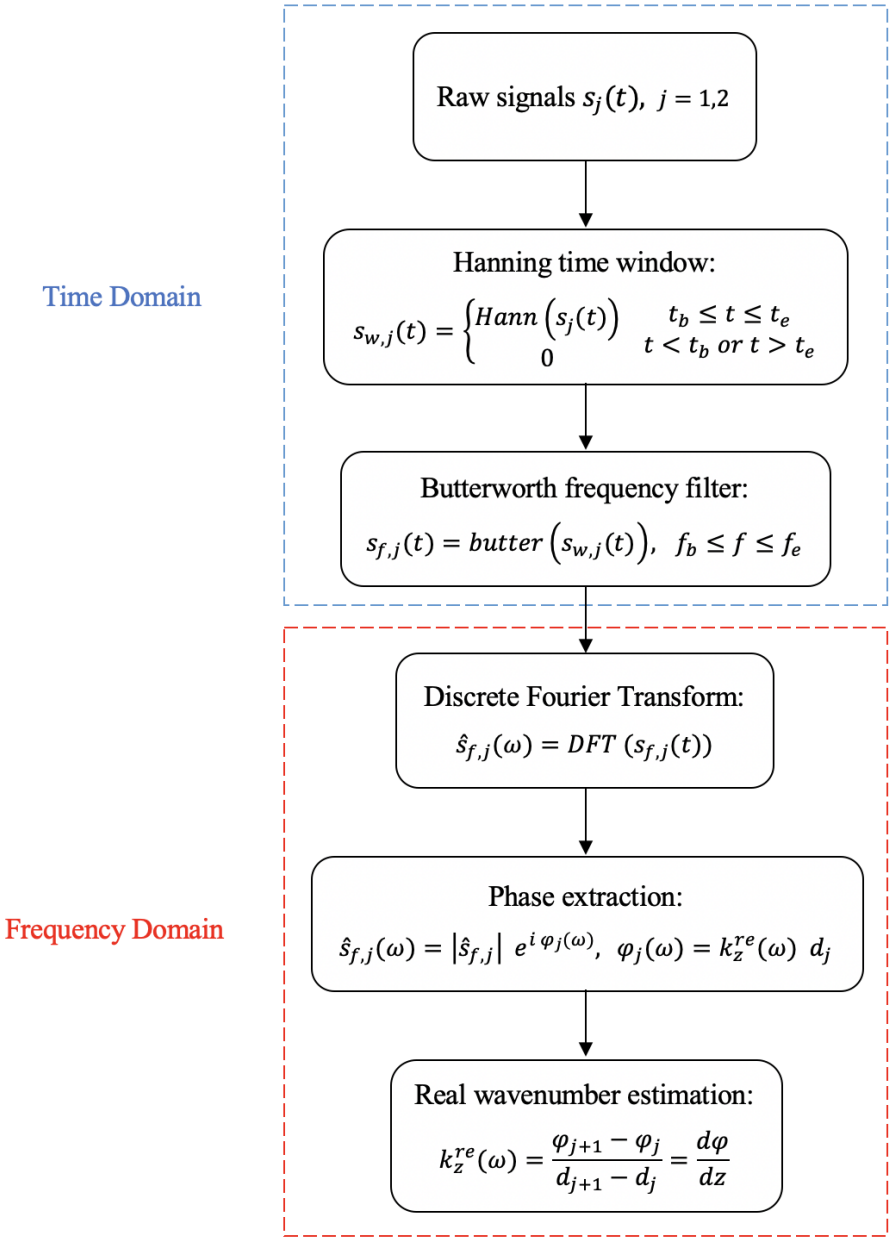

Figure 5.2: The flowchart of the process followed to estimate the real wavenumber k_z^{re} from the received raw signals. The subscripts "b" and "e" stand for "begin" and "end", respectively, and are used to denote upper and lower limits in time windowing and frequency filtering. ϕ_j is the extracted phase of a signal, d_j is the distance between the excitation point and the point of signal reception, $d\phi$ and dz are the phase difference and distance between two signals respectively, and i=$\sqrt{-1}$.

$$u(k_z^{re}) = \sqrt{\frac{1}{dz^2}u^2(d\phi) + \frac{d\phi^2}{dz^4}u^2(dz)} \tag{5.2}$$

where $u(k_z^{re})$ is the uncertainty of the real axial wavenumber, dz is the distance between the two considered sensors (impact hammer and/or hydrophone(s)), $u(dz)$ is the uncertainty of the distance dz, $d\phi$ is the phase difference between the received signals, and $u(d\phi)$ is the uncertainty of the phase difference $d\phi$.

Further, the presented signal analysis offers a process to extract only the real part of the axial wavenumber (k_z^{re}). In this study, the imaginary part k_z^{im} was difficult to extract accurately from the experiments and it was considered to be zero irrespectively of frequency. In order to evaluate the effect of this choice, the two setups were simulated in COMSOL Multiphysics®. Subsequently, the uncertainty of the imaginary part of the axial wavenumber was considered to be equal to the value of the imaginary part itself ($u(k_z^{im}) = k_z^{im}$). Details on the development of the models along with the solutions are given in Appendix D. The effect of this choice is discussed in Section 5.4.

5.2.3. DYNAMIC MECHANICAL ANALYSIS AND AGEING

Dynamic mechanical analysis (DMA) was performed in order to study the viscoelastic behaviour of samples taken from the HDPE pipes which were used in the described experiments in this chapter and from two PVC pipes extensively tested in Chapter 3. The samples were milled along the longitudinal pipes axis and through the whole pipe wall thickness. The sample dimensions were 20 mm x 10 mm x 11 mm for the HDPE samples and 20 mm x 10 mm x 8 mm for the PVC samples. The desired parameter was the frequency-dependent storage modulus of the pipe material. DMA was conducted with a Metravib (VA 2000) analyzer at frequencies between 1 and 50 Hz, within a temperature range of −10 °C to 20 °C at 5 °C steps. Subsequently, time-temperature superposition was applied in order to track the storage modulus at a wider frequency range and at a specific reference temperature (10 °C for the HDPE pipe in lab conditions and 20 °C for the PVC samples).

In the case of the HDPE pipes, the storage modulus from DMA was compared to the storage modulus calculated from the vibro-acoustic method presented in Chapter 4 (Eq. 4.29). In the case of the PVC pipes, the storage modulus from DMA was used to explore the capability of the water-borne axisymmetric wave to detect physical ageing at low frequencies while considering the uncertainty levels measured from the actual vibro-acoustic experiments. The measured uncertainty of the storage modulus for the two different setups was expressed as a percentage which was thereafter applied to the modulus values obtained from the DMA results. The PVC pipes concern one 3 years old unused pipe ("R") and one 44 years old pipe ("B-1") that had served as a foul sewer.

5.3. RESULTS

5.3.1. ESTIMATION OF THE PIPE STORAGE MODULUS USING VIBRO-ACOUSTICS

An example of received raw signals from the two hydrophones in Set-up B is given in Figure 5.3. With such raw signals, the coherence for a wide range of frequencies (up to 6kHz) was determined for both setups (Figure 5.4). The presented coherence values were evaluated based on the average cross-spectral and auto-spectral densities of the signals received during ten repeated independent measurements.

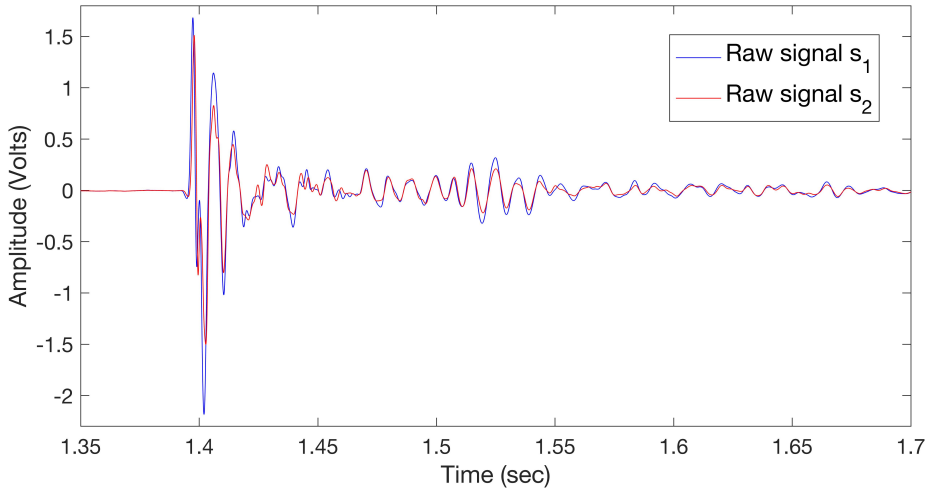

Figure 5.3: An example of raw signals, s_1 and s_2, received on the two hydrophones in Set-up B.

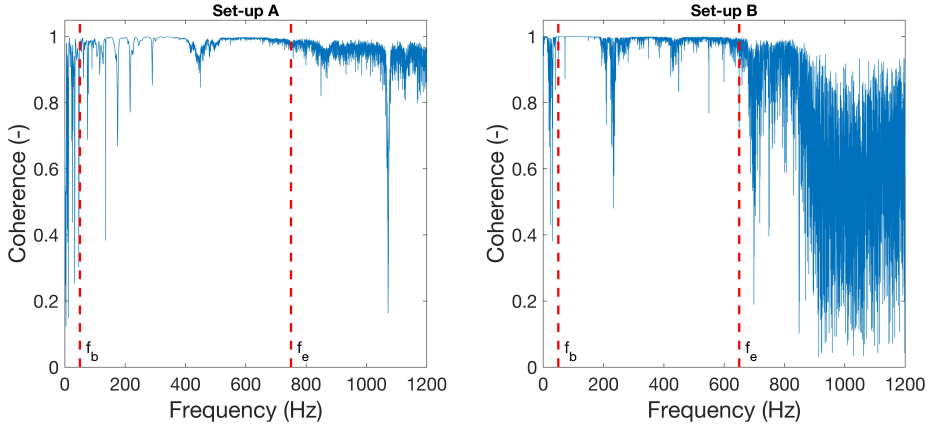

Figure 5.4: The coherence as a function of frequency between the hammer and the single hydrophone signal in Set-up A (left) and between the two hydrophone signals Set-up B (right). In each case, the coherence is estimated from Eq. 5.1. The red dashed lines show the frequencies f_b and f_e used in the Butterworth frequency filter.

Subsequently, a Hanning time window was applied. The shape and extent of the time window is presented in Figure 5.5 (left graph), and Figure 5.5 (right) presents an example of its application on the raw signals. The frequency limits used for the Butterworth frequency filtering of the signals were determined at the points in which the coherence deviated consistently from unity as illustrated in Figure 5.4. Following the notation given in Figure 5.2, f_b and f_e were set to 50 and 750 Hz, respectively, for Set-up A, and 50 and 650 Hz for Set-up B.

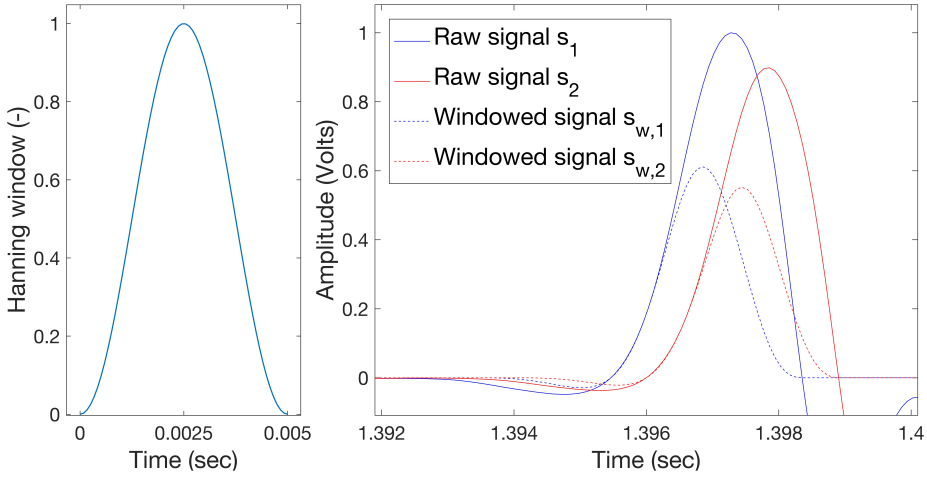

Figure 5.5: Left: The Hanning window used in the processing of raw signals according to the procedure described in Figure 5.2. Right: Example of windowed signals $s_{w,1}$, $s_{w,2}$ after applying the Hanning window to raw signals s_1, s_2.

Figure 5.6 presents the real part of the wavenumber of the axisymmetric water-borne mode for Set-up A and Set-up B. The mean value represents the average of 10 experiments and the 95% confidence interval is twice the standard uncertainty calculated via Eq. 5.2. Set-up B demonstrates a lower mean wavenumber (or higher mean phase velocity) within the examined frequency range, which indicates the added stiffness from the surrounding soil. Further, the results for Set-up B show relatively wider confidence intervals, which imply higher uncertainty levels compared to Set-up A.

The values of the storage modulus estimated from the vibro-acoustic data and respective uncertainty levels (95% confidence interval) are depicted in Figure 5.7. Irrespectively of the used set-up, the mean value of the storage modulus lies around 2.2 GPa within the considered frequency range. The results from the pipe section buried in sand show a relatively high uncertainty which is frequency dependent with the maximum between 200 and 400 Hz.

5.3.2. ESTIMATION OF THE PIPE STORAGE MODULUS BASED ON DMA

Figure 5.8 presents the storage modulus for the HDPE sample measured with the DMA method. Figure 5.8(left) shows the dependence of the modulus as a function of temperature for the range of frequencies used in DMA. Figure 5.8(right) shows the frequency-

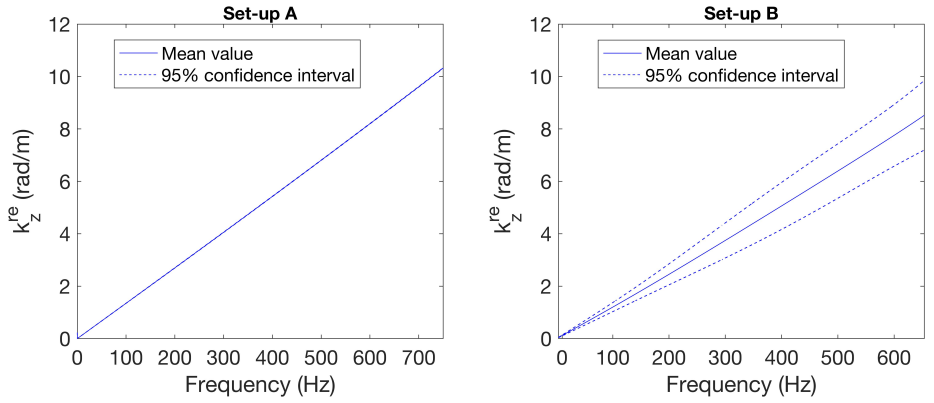

Figure 5.6: The real part of the axial wavenumber k_z^{re} as a function of frequency for Set-up A (left) and Set-up B (right). k_z here represents the wavenumber of the axisymmetric water-borne wave. The results were obtained by processing the raw signals according to the procedure described in Figure 5.2.

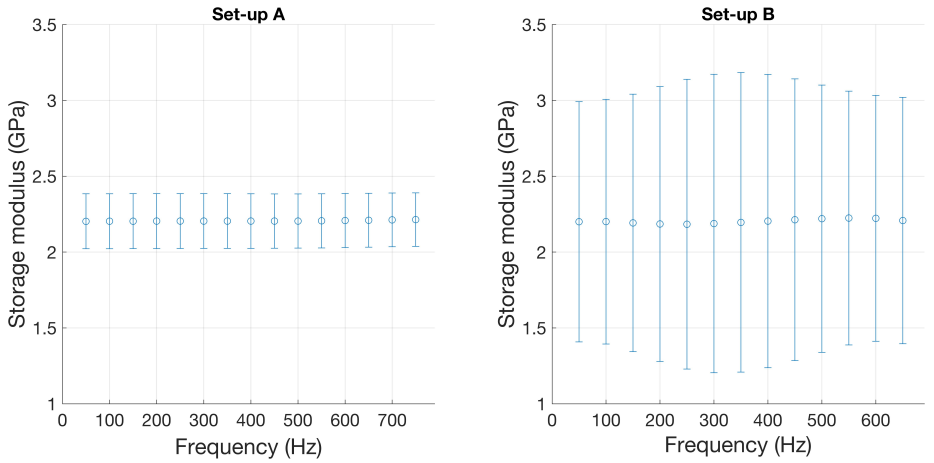

Figure 5.7: The estimated pipe storage modulus as a function of frequency for Set-up A (left) and Set-up B (right). The error bars denote the 95% confidence interval. The results are based on the parameters given in Table 5.1 and Eq. 4.29 derived for the axisymmetric water-borne wave.

dependent storage modulus predicted via the time-temperature superposition for the reference temperature of 10 °C. The storage modulus rises rapidly from its DC value to stabilize between 1.7 and 1.8 GPa at frequencies higher than 50 Hz. Compared to the values estimated via the vibro-acoustic method (see Figure 7), the DMA results predict the storage modulus that is 0.4-0.5 GPa lower than that obtained via the vibro-acoustic method.

DMA was also applied on two PVC samples, sample R (3 years old) and sample B-1 (44 years old). Figure 5.9 depicts the DMA data after the application of time-temperature superposition. The deviation between the data of the PVC samples decreases as the fre-

quency increases, from 22.2% at 10 Hz to 19% at 500 Hz. Additionally, if the uncertainty levels of the storage modulus of Set-up A are applied (Figure 5.9, left), there is a clear distinction between the estimated moduli. On the contrary, application of the uncertainty levels of Set-up B on the DMA data demonstrates that the overlap of the confidence intervals is so wide that they include both datasets (Figure 5.9, right).

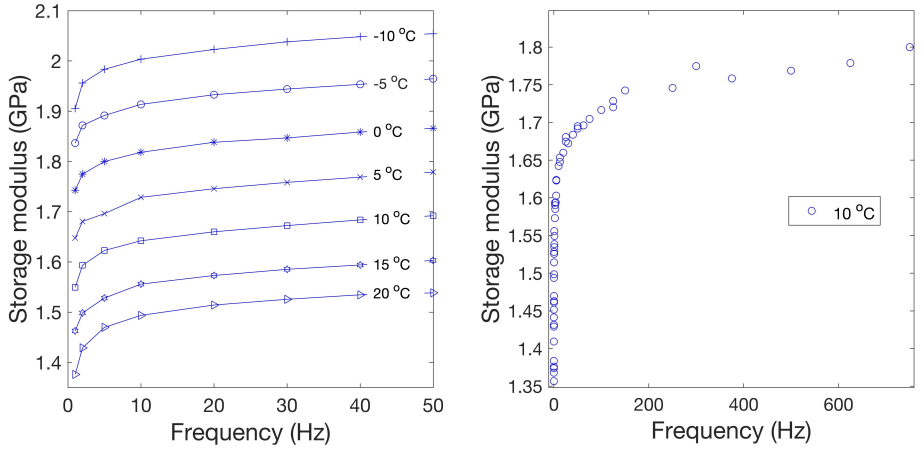

Figure 5.8: Left: The storage modulus of a HDPE pipe sample as a function of frequency for various temperatures obtained by dynamic mechanical analysis. Right: The storage modulus of a HDPE pipe sample as a function of frequency after applying time-temperature superposition for a reference temperature of 10 °C.

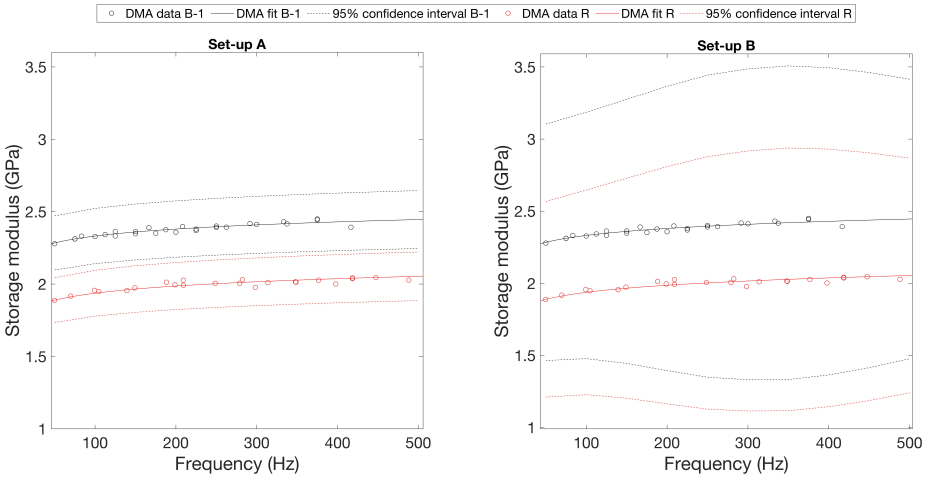

Figure 5.9: The storage modulus of two pipe samples, sample R (3 years old) and sample B-1 (44 years old), as a function of frequency after the application of time-temperature superposition on data obtained by dynamic mechanical analysis. The confidence intervals are the uncertainties in the acoustically estimated storage modulus for Set-up A (left) and Set-up B (right).

5.4. DISCUSSION

Successful applicability of vibro-acoustics in order to detect physical ageing of plastic pipes relies on two assumptions: i) vibro-acoustics can be used to estimate the storage modulus of a plastic pipe, and ii) the frequency-dependent storage modulus is sensitive to pipe ageing. Applications of this method are also affected by the measurement uncertainty. In this section the uncertainty is discussed based on the findings from the conducted experiments and analyses.

A comparison between the results from the DMA and vibro-acoustic experiments shows a systematic difference in the storage modulus of up to 0.5 GPa. This discrepancy could be attributed to a series of causes. Initially, the theory of acoustic waves was developed based on the conditions that all the elements of the system are isotropic and homogeneous, while the contact at the interface pipe-soil was assumed to be full and continuous. The inclusion of the mentioned prerequisites was necessary in order to produce a simpler and solvable system of equations. Nonetheless, it has to be realized that meeting these assumptions in practice would be very unlikely even in controlled laboratory conditions. Furthermore, depending on the method of measurement different estimates of the storage modulus can be obtained. For instance, when sample B-1 has been subjected within this thesis to conventional tensile tests, flexural tests and DMA, demonstrating an elastic modulus of 3.09, 3.33, and 2.3 - 2.45 GPa (within 50-500 Hz), respectively. Consequently, it is crucial that the same technique is applied consistently in order to draw safe conclusions concerning changes in the pipe condition (e.g. ageing detection and pipe stiffness). For the tested HDPE pipe samples, the value of the storage modulus estimated via vibro-acoustics (~2.2 GPa) was close to that quoted for HDPE pipes by Gao et al. (2016) (2 GPa).

The DMA results for the two PVC pipe samples with an age difference of 41 years demonstrated a clear deviation in terms of measured storage modulus. The older sample showed a higher value of the storage modulus due to a lower ductility (Visser, 2009; Makris et al., 2020). The observed deviation decreased with increased frequency, a pattern that follows the findings in literature concerning the difficulty of ageing detection at higher frequencies (Read et al., 1988, 1989, 1992; Demcenko et al., 2014). However, estimating the storage modulus vibro-acoustically via the water-borne mode involves a higher uncertainty originating from individual uncertainties in the parameters in each medium of which the system consists. This affects the capability of the method to track ageing accurately. Results in this study showed that it is challenging to distinguish between different storage modulus values for the configuration when the pipe was surrounded by sand (Figure 5.9, right). Nonetheless, the considered uncertainty is not affected only by the addition of new parameters due to the presence of soil and their respective uncertainties. There is also a difference in the distance dz between the points at which the signals were recorded (5.3 m between the hammer and the single hydrophone in the above-ground section (Set-up A) and 0.3 m between the two hydrophones in the below-ground section (Set-up B)).

Figure 5.10 presents the normalized relative contribution of each parameter's uncertainty to the overall uncertainty of the storage modulus estimation for Set-up A (top graph) and Set-up B (bottom graph). In the case of Set-up A the derived uncertainty in

the storage modulus (Figure 5.7, left) originates mostly from a lack of accurate data on the pipe geometry, especially the pipe wall thickness. In the considered frequency range (50 - 750Hz), the relative contribution of the uncertainty in the pipe wall thickness and internal radius to the overall uncertainty is ~90% and 6-8%, respectively. It should be noted that if the uncertainty in the wall thickness and internal radius decreases from 0.5 to 0.1 mm, then the overall uncertainty in the estimation of the pipe's storage modulus drops from ~0.2 to ~0.04 GPa, a characteristic that would allow the proposed method to become significantly more sensitive to the modulus changes due to ageing. The rest of the parameters have a minor effect.

In the case of Set-up B, most of the overall uncertainty (~90%) is attributed to the uncertainty in the real part of the axial wavenumber ($u(k_z^{re})$). Eq. 5.2 reveals the factors that contribute to an increase in the uncertainty of k_z^{re}. The distance between the hydrophones is an influencing parameter as it is in both denominators while being raised in the power of 2 and 4. Therefore, values of dz lower than unity are expected to increase $u(k_z^{re})$, whereas values larger than unity would have the opposite effect. This finding is also reflected in the width of confidence intervals of k_z^{re} in Figure 5.6 for the considered values of 5.3 and 0.3 m (left and right graph, respectively). Additionally, in the case of Set-up B a higher uncertainty in the phase difference $d\phi$ was predicted, although there is not a clear proof regarding the origin of it. Possible reasons can include inconsistent coupling at the pipe-sand interface, elastomeric joint and/or transition from a fully covered by soil pipe section to a section surrounded only by air required to provide easy access to the two hydrophones (see Figure 5.1, bottom).

This study assumed considerably higher uncertainties in the soil parameters compared to those quoted for the pipe material and water (Table 5.1). However, the results presented in Figure 5.10 (bottom) suggest that the contribution to the overall uncertainty from the uncertainties in the soil parameters is similar to or less than that from the uncertainty in the pipe wall thickness (~5%). Therefore, a lack of accurate knowledge of the parameters of surrounding soil is unlikely to hinder the applicability of the presented vibro-acoustic method, although a lower uncertainty of the soil's shear wave velocity and density at specific frequencies would be beneficial. Finally, the assumption that the imaginary part of the axial wavenumber (k_z^{re}) was zero proved to have minimal effect on the overall uncertainty in the estimated storage modulus. It should be stressed that applying such a condition requires that the values of $u(k_z^{im})$ are similar to the magnitude of the expected true values of k_z^{im} at each considered frequency.

5.5. CONCLUSIONS

This study explored the use of the vibro-acoustic axisymmetric water-borne mode to estimate the storage modulus of two high-density polyethylene pipes and to relate it to ageing. This was based on the measurement of the real part of the modal wavenumber in a pipe surrounded by air and a pipe buried in sand. The both experimental configurations (above and below ground) proved to be capable of identifying similar values for the pipe's storage modulus (~ 2.2 GPa). A 0.4-0.5 GPa higher value of the storage modulus was obtained via acoustic data compared to the results from dynamic mechanical

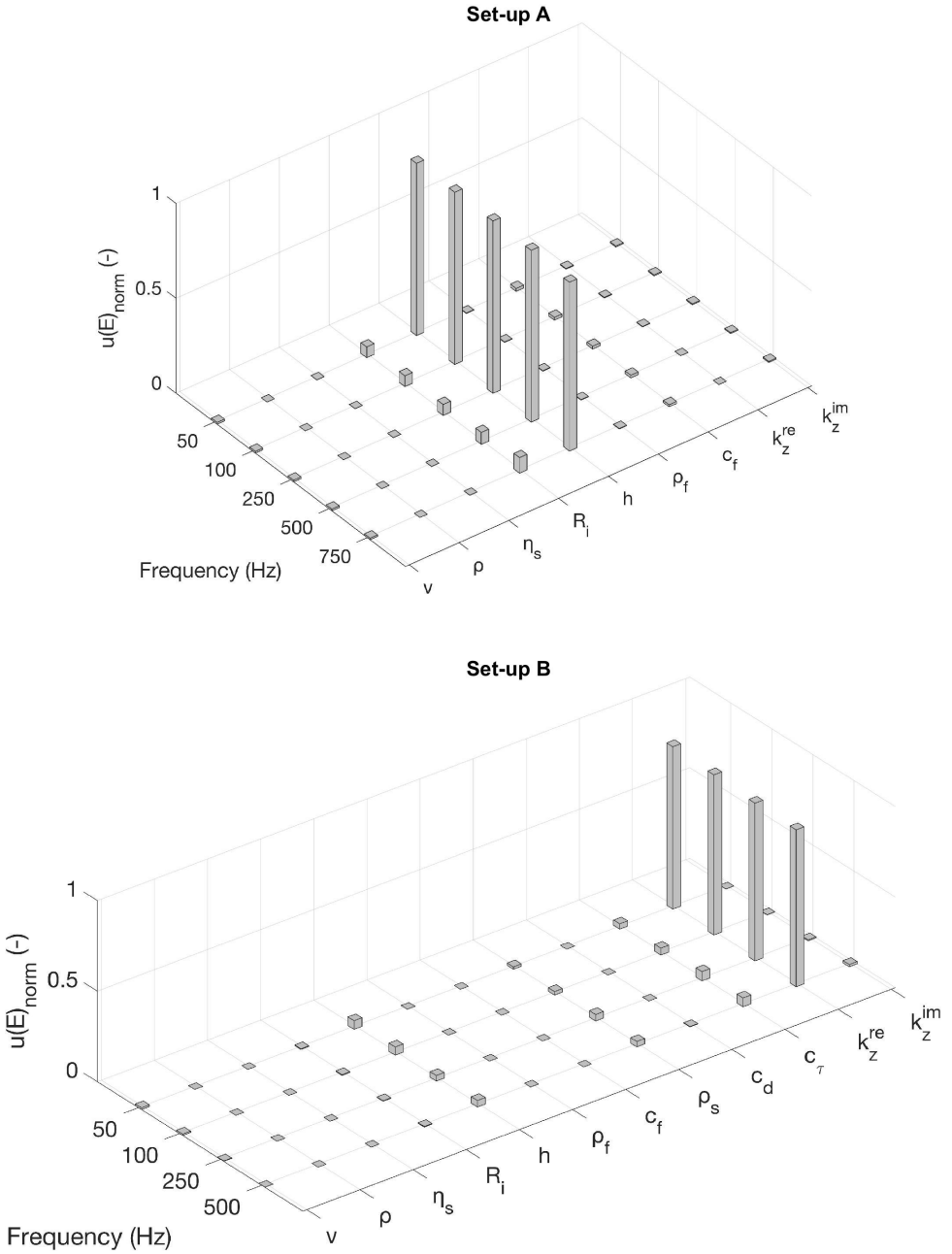

Figure 5.10: The relative contribution of each parameter's uncertainty to the overall uncertainty of the pipe storage modulus $u(E)$ estimated via the axisymmetric water-borne wave for: Set-up A (top graph) and Set-up B (bottom graph). $u_{(E)}$ is normalized according to Eq. 4.36 (ν: pipe's Poisson ratio, ρ: pipe density, η_s: pipe loss factor, R_i: pipe internal radius, h: pipe wall thickness, ρ_f: fluid density, c_f: fluid sound velocity, ρ_s: soil density, c_d: soil compressional velocity, c_τ: soil shear velocity, k_z^{re}: real axial wavenumber, k_z^{im}: imaginary axial wavenumber).

analysis (DMA).

DMA on samples from two PVC pipes with 41 years extrusion age difference revealed that ageing can be detected via the storage modulus estimated from vibro-acoustic data at low frequencies (<500 Hz). Nevertheless, applicability of the vibro-acoustic method yields results with an overall uncertainty that depends on a combination of uncertainties in the parameters of the embedded media (pipe, water, soil). A larger distance between the locations of the two receiving signals results in a lower overall uncertainty in the real part of the modal wavenumber. The accurate knowledge of the pipe's geometry (wall thickness and internal radius) is paramount, as it is a key parameter that contributes to the overall uncertainty. Especially the uncertainty in the pipe wall thickness affects significantly the overall uncertainty. The presence or absence of soil around the pipe has a relatively small effect in comparison with the uncertainty in the wall thickness. However, a better knowledge of the true shear wave velocity in soil and soil density would be beneficial to reduce the overall uncertainty. The uncertainty analysis suggests that the knowledge of the imaginary part of the axial wavenumber is unimportant to estimate the pipe's storage modulus and associated uncertainties.

6

CONCLUSIONS AND RECOMMENDATIONS

6.1. OVERALL CONCLUSIONS

The objective of this thesis is to provide the appropriate knowledge and tools in order to understand the failure mechanisms and quantify the parameter(s) that express the ageing of PVC pipes used in urban drainage systems. Most of the conducted research explored degradation mechanisms that are shared generally by buried plastic pipes, regardless of their material and use. This section presents the main conclusions that are drawn from the preceding chapters, initially focusing on PVC sewer pipes and subsequently on methods that can be applied on plastic pipes universally.

DURABILITY OF PVC SEWER PIPES: SCIENTIFIC LITERATURE VS. PRACTICE

The condition assessment of PVC sewer pipes relies on three different but interacting aspects: i) the physical state, ii) the chemical resistance, and iii) the mechanical durability. A holistic view on sewer systems reveals that there is also a fourth aspect which plays a contributing role: iv) the leak tightness of elastomeric joints. Based on these four aspects, researchers and practitioners can make estimates concerning the residual operational lifetime of a system.

Research on the physical and mechanical properties of PVC pipes proves that PVC is a durable material. Additionally, PVC material shows no signs of degradation when tested against substances which are found in sewers, such as sulfuric acid, sodium sulfate and drinking water chlorine-based disinfectants. Concerning the elastomeric joints, only extreme values of deflection and bending of the joint cause leakages. Based on these points, some researchers suggest that the operational lifetime of PVC pipes will exceed 100 years.

However, inspection data reveals that all kinds of known defects have surfaced, af-

fecting in many cases the structural stability, flow regime and/or leak tightness of the system. The level of severity of these defects is increasing at a relatively fast pace, depicting a high degradation rate. Further, defects corresponding to the integrity of elastomeric joints suffer from the highest occurrence rates. Therefore, a noticeable gap is observed between the findings in scientific literature and in practice, raising questions about the actual lifetime of PVC sewer systems. Additionally, throughout Chapter 2, it is highlighted that only comprehensive testing of material properties can help understand the origins and levels of degradation.

FAILURE FACTORS OF OPERATING PVC SEWER PIPES

The conclusions reported in this section are based on the specific case studies of excavated PVC sewer pipes presented in Chapter 3. Heterogeneity prevails concerning the number and types of inorganic elements found in the composition of PVC pipes manufactured from different companies or during different periods. Deviations in properties between pipes stem from this heterogeneity. Mild signs of chemical degradation are limited exclusively to the surface, proving the overall chemical resistance of PVC material against potentially harmful substances in the sewage. Further, modern production techniques facilitate the construction of non-pressurized PVC pipes with a built-in recycled or foamed core. Albeit such a core offers some merits (e.g. sustainability, less weight), it could be the main reason for premature pipe failures under certain conditions. In particular, tensile stresses seem to have a tremendous impact on pipes with an embedded core. The same effect applies for flexural stresses in case of PVC pipes with a "void" core (the pipe is perforated across its longitudinal axis).

The common and most profound detected mechanism is physical ageing, being expressed by an increase in stiffness and a decrease in ductility. Although physical ageing offers higher values of pipe stiffness, in the long term it is a potential threat for the structural integrity of plastic pipes. The increasing brittleness could cause issues during pipe inspection, the placement of household connections in the existing system or any other activity that could subject the pipe to a sudden impact. Finally, the most common cause of failure for the examined pipes in this study originated from human activities in the surroundings of the pipe and/or poor installation quality, demonstrating that the innate degradation mechanisms of plastic pipes are not the sole or most significant ones.

AXISYMMETRIC WAVE PROPAGATION AND AGEING DETECTION

Physical ageing is an inevitable degradation mechanism of viscoelastic pipes and the level of ageing is associated with an increase in the storage modulus of the pipe material. Low-frequency vibro-acoustics proved to be sofar the best working method for the non-destructive evaluation of the storage modulus, while changes in the values of the modulus due to ageing become more distinguishable as the frequency decreases. Additionally, mainly axisymmetric modes propagate at lower frequencies, which makes it practical to find the storage modulus from the vibro-acoustic data. In total, three types of axisymmetric waves propagate in a water-filled pipe within the low frequency range: the longitudinal L(0,1), torsional T(0,1), and water-borne wave. In the case of the pipe surrounded by soil, only the water-borne wave is able to propagate since shear coupling

at the pipe-soil interface hinders the propagation of the other two modes.

For an accurate estimation of the pipe's storage modulus, different parameters have to be more accurately known for each propagating wave. Concerning the shell-waves (L(0,1) and T(0,1)), accurate knowledge of the density and Poisson ratio of the pipe shell is required, whereas, the radius and wall thickness of the pipe are the most affecting parameters regarding the water-borne wave. Further, irrespectively of the explored mode, the standard uncertainty of the axial wavenumber of the propagating wave always has to be as low as possible. The minimization is dependent on the configuration of the sensors that receive the wave signals, requiring the largest possible distance between them. Further, the uncertainties of the shear wave velocity and the density of the surrounding soil also contribute to the overall uncertainty in the estimation of the storage modulus, although at a lower degree compared to the already discussed parameters.

Vibro-acoustics can be used for all visco-elastic pipe materials, although filling of the pipe with water is a prerequisite in order to sustain the propagating wave if the pipe is surrounded by soil. This requirement holds for the vast majority of sewer and drinking water pipes since they are buried. Besides this precondition, the applicability of the method is straightforward as low-frequency acoustic waves can be excited and received by utilizing an impact hammer and hydrophones, as conducted in this study (Chapter 5).

6.2. RECOMMENDATIONS AND FUTURE RESEARCH

Based on the findings of this thesis, the most significant factor that affects the longevity of plastic (PVC) pipes is human activity, either in the form of accidental third party impacts or in the form of low installation quality. Addressing this issue was not part of this thesis, since it escapes from the framework of technical scientific research. Proposed tackling measures include stricter protocols for handling and installation of pipes, followed by close supervision during construction and the incorporation of adequate protection against third party impacts. Additionally, it was noticed that inspection databases refer to PVC pipes universally, regardless of the embedded core. Nevertheless, especially in the case of an existing "void" core, extra caution should be exercised concerning higher levels of pipe deflections or bending. The existence of a core could lead to a specific failure pattern in areas that share similar characteristics of soil inconsistency, such as differential settling.

The biggest challenge regarding asset management of (plastic) sewer systems is to estimate their residual lifetime. This would allow infrastructure managers to develop asset management strategies with predefined, apt pipe replacement/ rehabilitation schedules. This has driven a considerable amount of research towards modeling a specific degradation mechanism based on the age and specific material properties of the studied pipe (e.g. Whittle et al., 2005; Frank et al., 2009; Gould et al., 2013). However, the large number of different degradation mechanisms, their potential interaction, and different levels of interaction are some of the reasons why such models can be disputed. If the different conditions that prevail in practice at every pipe are also taken into consideration (e.g. traffic loads, soil parameters, soil cover, level of watertable, installation quality),

then it is obvious that every pipe is a different system that has to be encountered separately. Based on these arguments, it is safe to claim that estimating the residual lifetime of a pipe is very challenging, if not impossible in practice.

Furthermore, the discussed heterogeneity and peculiarities affect also any published and proposed methods or techniques concerning the condition assessment of a pipe. For instance, the development of a vibro-acoustic method for ageing detection in this thesis was based on the assumptions that the solid media (pipe and soil) are homogeneous, isotropic and (visco)elastic, while the contact between pipe and soil is perfect and the pipe's cross-section is totally circular. Deviation from these conditions, which is much anticipated in practice, would yield also a deviation in the estimation of the storage modulus of the pipe's material from the true value. Nevertheless, estimating the true value would be less useful when the failure point is not known or it is known for a specific pipe in laboratory conditions. Therefore, the use of the proposed method consistently over time could produce a database of pipes with certain recorded properties (e.g. diameter, thickness, soil type) and the storage modulus estimated by the described method. Correlation of future pipe failures with the magnitude of the recorded storage modulus could allow to draw conclusions for other pipes that are subjected to similar conditions.

Moreover, further research in the proposed method would be advantageous for its successful deployment in practice. It would be useful to test its applicability in a system that generates reflections from elastomeric joints or household connections (with different levels of intrusion in the main pipe). Additionally, the use of a more precise technique to measure thickness (e.g. ultrasonics) and internal radius of the pipe (e.g. laser scanning) could decrease significantly the uncertainty in the end result, allowing for the detection of lower discrepancies in the storage modulus of a pipe over time. For the same reason, caution is required concerning the distance between the signal receiving sensors, keeping it optimal to reduce uncertainty. Further, the addition of more sensors (like hydrophones) would give the opportunity for better separation of different propagating modes and for the measurement of attenuation. The latter enables the estimation of the imaginary part of the axial wavenumber, a requirement for a more accurate determination of the axial wavenumber. Otherwise, the method can be applied by assuming that the imaginary wavenumber values are equal to zero and estimating the respective uncertainty via analytical or modeling solutions, as conducted in this thesis.

Finally, there is a crucial part regarding the operation of sewer systems which was not explored by this study. Elastomeric joints had the highest defect rates during exploration of inspection data of sewer systems. Despite the effect of pipe installation, which according to literature should not have a big impact (Meijering et al., 2004; Arsenio, 2013), it would be of great interest to test the performance of joints against typical chemicals and bacteria found in sewage. Therefore, it is recommended to conduct similar tests and analyses to those described in Chapter 3, but adjusted for elastomer materials. A practical technique to assess the integrity of elastomeric joints is by utilizing ultrasonics in a pulse-echo mode. A conceptual schematic is presented in Figure 6.1. The circumferential scanning could generate a 3D representation of the joint, depicting if there are points at which leak tightness is not optimum.

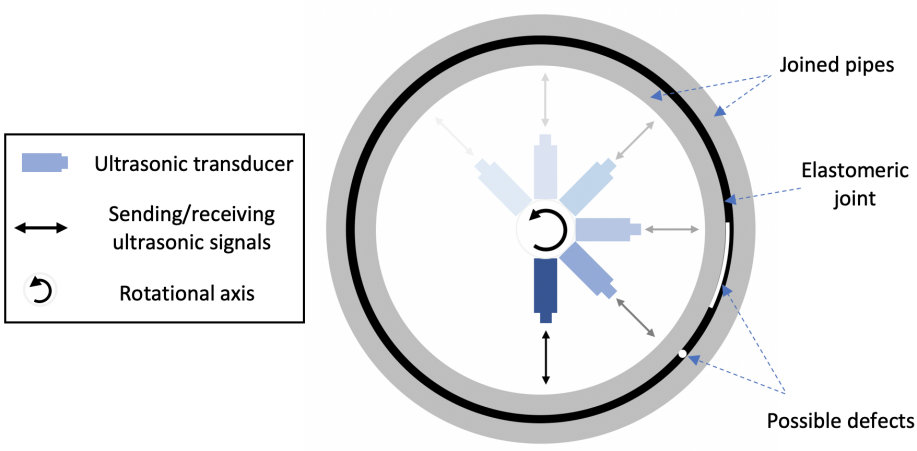

Figure 6.1: Conceptual schematic of an ultrasonic configuration within a pipe for assessment of the integrity of the elastomeric joints.

A

UNCERTAINTY IN VISCOSITY MEASUREMENTS

Uncertainty exists in all types of measurements. However, it is expected to be significant in viscosity measurements, as several steps are incorporated, each of which has its own uncertainty propagating through the final outcome. Application of the law of uncertainty propagation to Eq. 3.1 yields the uncertainty of inherent viscosity, assuming independent measurements each having a Gaussian uncertainty:

$$\begin{aligned}\delta_{\eta_{inh}} &= \sqrt{\left(\frac{\partial \eta_{inh}}{\partial \eta}\delta_{\eta}\right)^2 + \left(\frac{\partial \eta_{inh}}{\partial \eta_o}\delta_{\eta_o}\right)^2 + \left(\frac{\partial \eta_{inh}}{\partial \eta_c}\delta_{\eta_c}\right)^2} \\ &= \sqrt{\frac{1}{(\eta\ c)^2}\delta_{\eta}^2 + \frac{1}{(\eta_o\ c)^2}\delta_{\eta_o}^2 + \frac{\ln\left(\frac{\eta}{\eta_o}\right)^2}{c^4}\delta_c^2}\end{aligned} \tag{A.1}$$

where $\delta_{\eta_{inh}}$ is the uncertainty of the inherent viscosity (mL/g), δ_{η} is the uncertainty of the polymer solution's viscosity (Pa s), δ_{η_o} is the uncertainty of the solver's viscosity (Pa s), and δ_c is the uncertainty of the polymer solution concentration (g/mL).

Similarly, the uncertainty of the polymer solution concentration was estimated via Eq. A.2:

$$\delta_c = \sqrt{\left(\frac{\partial c}{\partial M}\delta_M\right)^2 + \left(\frac{\partial c}{\partial V}\delta_V\right)^2} = \sqrt{\frac{1}{V^2}\delta_M^2 + \frac{M^2}{V^4}\delta_V^2} \tag{A.2}$$

where M is the mass of the pipe sample (g) with its respective uncertainty δ_M, and V is the volume of the solver (mL) with its respective uncertainty δ_V. Uncertainty δ_M is considered as the last significant digit of the used balance (10^{-4} g) and δ_V is the standard error of the used pipette (0.02 mL). Uncertainties δ_{η} and δ_{η_o} were estimated as the standard deviation of 10 runs of the exact same procedure with the same solution (Figure

A.1). Subsequently, the shear rates with the lower uncertainties were considered (i.e. 38, 76, 115, 154, 193 and 231 s^{-1}).

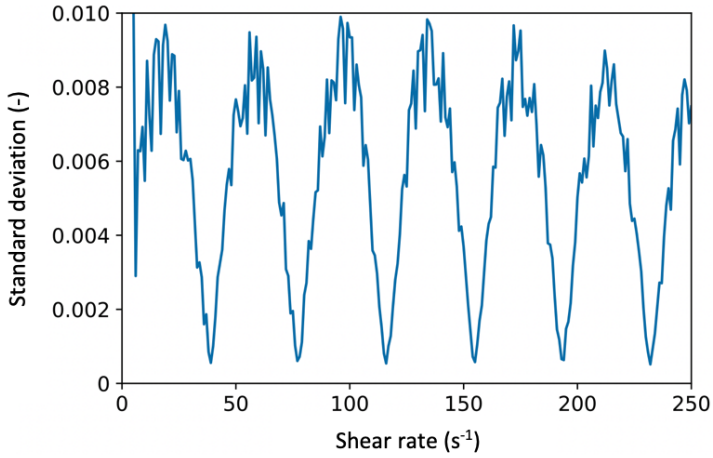

Figure A.1: Normalized standard deviation with respect to shear rate obtained by ten consecutive measurements on cyclohexanone at 20 °C with Anton-Paar 302. The same method was applied as for the viscosity measurements of the investigated polymer solutions in Chapter 3.

B

MECHANICAL PROPERTIES OF TESTED PVC PIPES

The detailed tensile and flexural properties of the tested pipe samples in Chapter 3 are summarized in Table B.1.

Table B.1: Mechanical properties of examined PVC samples derived by tensile (24 ± 2 °C) and 4-point bending testing (20 ± 0.2 °C)

Sample	Tensile Modulus (GPa)	Ultimate Stress (MPa)	Stress at break (MPa)	Elongation at break (%)	Flexural Modulus (GPa)	Ultimate Flexural Stress (MPa)
A-1	-	-	-	-	3.24 ± 0.02	87.7 ± 1.5
A-2	-	-	-	-	3.33 ± 0.07	88.7 ± 0.2
A-3	-	-	-	-	2.92 ± 0.10	79.6 ± 1.3
A-4	-	-	-	-	2.98 ± 0.12	83.0 ± 3.3
B-1	3.09 ± 0.02	54.3 ± 2.1	44.2 ± 3.8	136.9 ± 44.1	3.33 ± 0.74	89.5 ± 13.0
B-2	2.69 ± 0.30	53.2 ± 0.3	49.8 ± 1.8	175.3 ± 20.1	*	*
B-3	2.32 ± 0.15	47.8 ± 1.7	36.2 ± 0.2	53.3 ± 16.8	3.34 ± 0.04	84.1 ± 0.7
B-4	1.37 ± 0.07	28.9 ± 1.2	24.1 ± 0.7	24.5 ± 9.6	3.32 ± 0.07	70.4 ± 2.2
R	2.25 ± 0.19	49.3 ± 0.2	50.8 ± 2.3	212.0 ± 27.0	3.17 ± 0.01	80.7 ± 1.1

* Material was inadequate for specimen preparation

C

OPERATORS IN EQUATIONS OF MOTION FOR THE PIPE SHELL

Equations C.1 - C.7 present the operators used to describe the equations of motion for a pipe shell in a matrix (Leissa, 1973). The Donnel-Mushtari operator (Eq. C.1) is used as the basis, and only additional terms in the operators from other theories are presented. The included matrix elements refer to wave and pipe properties: k_z is the axial wavenumber, h is the pipe thickness, $R = R_i + h/2$ (R_i is the pipe internal radius), $\beta^2 = h^2/(12R^2)$, ν is the Poisson ratio, and $\Omega = \omega R\sqrt{\rho(1-\nu^2)/E}$, where ω is the angular frequency, ρ is the pipe density, and E is the complex modulus ($E = E'(1+\eta_s i)$, E' being the storage modulus, η_s the loss factor) and $i = \sqrt{-1}$.

Donnel-Mushtari:

$$Q_{DM} = \begin{bmatrix} \Omega^2 - k_z^2\, R^2 - n^2\, \frac{(1-\nu)}{2} & k_z\, R\, n\, \frac{(1+\nu)}{2} & -k_z\, R\, \nu\, i \\ k_z\, R\, n\, \frac{(1+\nu)}{2} & \Omega^2 - k_z^2\, R^2\, \frac{(1-\nu)}{2} - n^2 & n\, i \\ -k_z\, R\, \nu\, i & n\, i & -\Omega^2 + 1 + \beta^2\, (n^2 + k_z^2\, R^2)^2 \end{bmatrix} \tag{C.1}$$

Kennard (simplified):

$$Q = Q_{DM} + \beta^2 \begin{bmatrix} 0 & 0 & 0 \\ 0 & 0 & \frac{3\, n\, \nu\, (1-n^2)}{2\, (1-\nu)}\, i \\ 0 & 0 & \frac{\nu+2}{2\, (1-\nu)} + n^2\, \frac{\nu-4}{2\, (1-\nu)} \end{bmatrix} \tag{C.2}$$

Love - Timoshenko:

$$Q = Q_{DM} + \beta^2 \begin{bmatrix} 0 & 0 & 0 \\ 0 & -n^2 - k_z^2\, R^2\, (1-\nu) & [n^3 + k_z^2\, R^2\, n]\, i \\ 0 & [n^3 + k_z^2\, R^2\, n\, (2-\nu)]\, i & 0 \end{bmatrix} \tag{C.3}$$

Flügge – Byrne – Lur'ye (also Biezemo - Grammel):

$$Q = Q_{DM} + \beta^2 \begin{bmatrix} -n^2\, \frac{(1-\nu)}{2} & 0 & [k_z\, R\, n^2\, \frac{(1-\nu)}{2} - k_z^3\, R^3]\, i \\ 0 & -k_z^2\, R^2\, 3\, \frac{(1-\nu)}{2} & k_z^2\, R^2\, n\, \frac{3-\nu}{2}\, i \\ [k_z\, R\, n^2\, \frac{(1-\nu)}{2} - k_z^3\, R^3]\, i & k_z^2\, R^2\, n\, \frac{(3-\nu)}{2}\, i & -2\, n^2 + 1 \end{bmatrix} \tag{C.4}$$

Sanders:

$$Q = Q_{DM} + \beta^2 \begin{bmatrix} -n^2\, \frac{(1-\nu)}{8} & -k_z\, R\, n\, 3\, \frac{(1-\nu)}{8} & k_z\, R\, n^2\, \frac{(1-\nu)}{2}\, i \\ -k_z\, R\, n\, 3\, \frac{(1-\nu)}{8} & -n^2 - k_z^2\, R^2\, 9\, \frac{(1-\nu)}{8}] & [n^3 + k_z^2\, R^2\, n\, \frac{3-\nu}{2}]\, i \\ k_z\, R\, n^2\, \frac{(1-\nu)}{2}\, i & [n^3 + k_z^2\, R^2\, n\, \frac{(3-\nu)}{2}]\, i & 0 \end{bmatrix} \tag{C.5}$$

Vlasov:

$$Q = Q_{DM} + \beta^2 \begin{bmatrix} 0 & 0 & [k_z\, R\, n^2\, \frac{(1-\nu)}{2} - k_z^3\, R^3]\, i \\ 0 & 0 & k_z^2\, R^2\, n\, \frac{3-\nu}{2}\, i \\ [k_z\, R\, n^2\, \frac{(1-\nu)}{2} - k_z^3\, R^3]\, i & k_z^2\, R^2\, n\, \frac{(3-\nu)}{2}\, i & -2\, n^2 + 1 \end{bmatrix} \tag{C.6}$$

Reissner - Naghdi - Berry:

$$Q = Q_{DM} + \beta^2 \begin{bmatrix} 0 & 0 & 0 \\ 0 & -n^2 - k_z^2\, R^2\, \frac{(1-\nu)}{2} & (n^3 + k_z^2\, R^2\, n)\, i \\ 0 & (n^3 + k_z^2\, R^2\, n)\, i & 0 \end{bmatrix} \tag{C.7}$$

D

UNCERTAINTY INPUT OF THE IMAGINARY AXIAL WAVENUMBER

The imaginary part of the axial wavenumber could not be extracted from the conducted vibro-acoustic experiments described in Chapter 5. Consequently, the imaginary part of the axial wavenumber was assumed to be zero at all frequencies and the respective uncertainty was considered to be the expected value of imaginary wavenumber. The latter was given by solving a finite element COMSOL®model. The theory and general framework behind a COMSOL®model is explained in Section 4.4. The pipe shell, water and soil properties are given in Table 5.1. Further, the storage modulus of the pipe shells used as input in both models was obtained by the results of the dynamic mechanical analysis (Figure 5.7, right). Figure D.1 demonstrates the imaginary parts of the axial wavenumber for the water-borne mode concerning the two different setups utilized for this analysis (Set-up A and Set-up B).

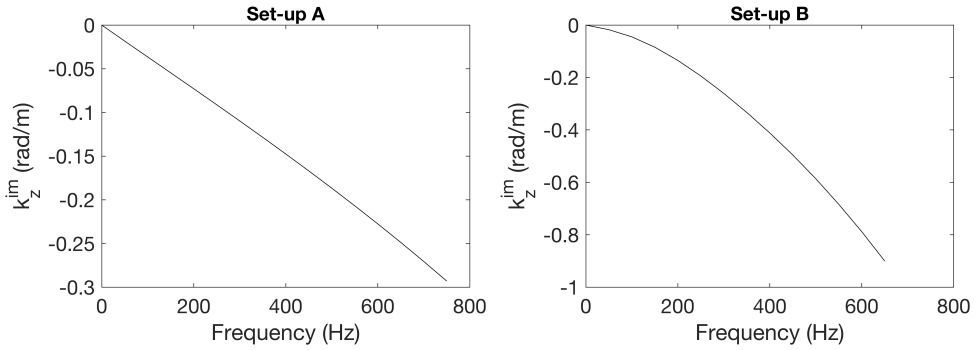

Figure D.1: Imaginary parts of the axial wavenumber solutions in COMSOL®for the experimental configurations Set-up A and Set-up B described in Chapter 5.

ACKNOWLEDGEMENTS

The end of my PhD finds me in a happy position in which I can say that I enjoyed very much the past 4 years in many aspects. Although it was a long period, it passed incredibly fast and it was full of contradictory emotions (changing even within the same day). I hope I managed to add my very small piece to this boundless and hard-to-define concept called science. At least I know that during this period I learned a lot of new things. The end result of my PhD is this thesis and I would like to thank explicitly most of those people who made this achievement possible.

Initially, I would like to thank Prof. François Clemens for our collaboration all these years, including technical and research-related discussions, as well as discussions around my concerns aiming for my phychological boosting. I would also like to thank Dr. Jeroen Langeveld for his guidance and help, for trusting me so much even from the very first days of my PhD and making my life easier when possible. I am also grateful to Prof. Kirill Horoshenkov for his participation in the supervisory team of my PhD. His input was paramount for helping me proceed with my research and finish in time, while he made my visit to Sheffield fruitful and memorable.

Further, I thank Mathieu Lepot for introducing me to the magical world of experimental research and for being always there to discuss anything. Our joint work during my MSc thesis was definitely a decisive factor for my acceptance in a PhD programme within this group. Of course, I could not leave out my colleagues at TU Delft who shared the office and their coffee/lunch time with me: Antonio, Adithya, Bram, Eva, Matthijs, Job, Alex, Elena, Juan and João. I would like to thank Drhuv for all the funny talks and for trying to keep me fit. I also thank Armand and Mohammed for all the help concerning my experimental activities, and Joanna and Hasina from the University of Sheffield for our nice collaboration and for being so hospitable.

I would also like to express my gratitude to Stavroula for all her support, understanding and constant encouragement. Lastly but certainly not least, I would like to thank my family for their continuous support and guidance (Ευχαριστώ τους γονείς μου για την κάθε είδους, συνεχή υποστήριξη).

ABOUT THE AUTHOR

Konstantinos Makris has studied Civil Engineering at the Polytechnic School of the University of Thessaly in Volos with specialization (M.Eng.) in hydraulics and environmental engineering. He graduated with the thesis titled "Reduction of non-revenue water in urban water supply systems via pressure management: the case of the city Kos". In 2014 he came to The Netherlands in order to follow the M.Sc. program of Water Management at TU Delft. He selected the track of Urban Drainage and completed his studies in 2016 by presenting the M.Sc. thesis titled "Detection and quantification of lateral, illicit connections and infiltration in sewers with Infra-Red camera: Conclusions after a wide experimental plan". After his graduation he worked on several projects, although his main focus had always been on urban water management. In April 2018, we was accepted for a PhD program in the group of urban drainage at the Water Management Department of TU Delft. During this period he studied the ageing of plastic pipes in urban drainage systems by assessing their durability and developing a vibro-acoustic inspection technique for physical ageing detection. This research was under the "Kennisprogramma Urban Drainage" scheme and the main findings are presented in this Thesis.

LIST OF PUBLICATIONS

Peer reviewed journal publications

Lepot, M., **Makris, K. F.**, & Clemens, F. H. L. R. (2017). Detection and quantification of lateral, illicit connections and infiltration in sewers with Infra-Red camera: Conclusions after a wide experimental plan. Water Research, 122, 678-691. DOI: 10.1016/j.watres.2017.06.030

Makris, K. F., Langeveld, J., & Clemens, F. H. L. R. (2020). A review on the durability of PVC sewer pipes: Research vs. practice. *Structure and Infrastructure Engineering, 16(6), 880–817*. DOI: 10.1080/15732479.2019.1673442

Makris, K. F., Langeveld, J., & Clemens, F. H. L. R. (2021). Extensive testing on PVC sewer pipes towards identifying the factors that affect their operational lifetime. *Structure and Infrastructure Engineering*. DOI: 10.1080/15732479.2021.1907601

Makris, K. F., Langeveld, J. G., Clemens-Meyer, F. H. L. R., Watts, J., Begum, H., & Horoshenkov K. V. (2022). Sonic assessment of physical ageing of plastic pipes. *Journal of Sound and Vibration*. DOI: 10.1016/j.jsv.2022.117393

International conferences

Kanakoudis, V., Gonelas, K., & **Makris, K.** (2014). Ex-ante evaluation of a pressure management pilot project in Kos Town water pipe network. In the proceedings of *12th International Conference on Protection and Restoration of the Environment*, 264-271, Skiathos, Greece.

Makris, K. F., Lepot, M., & Clemens, F. H. (2016). Potential uses of an IR camera to detect and quantify lateral connections in sewers. In the proceedings of *8th International Conference on Sewer Processes and Networks*, Delft, The Netherlands.

Makris, K. F., Langeveld, J., & Clemens, F. H. (2019). PVC sewer pipes: as invincible as suggested?. In the proceedings of *9th International Conference on Sewer Processes and Networks*, Aalborg, Denmark.

Makris, K. F., Langeveld, J., & Clemens, F. H. (2021). The biggest threat for PVC sewer pipes. In the proceedings of *15th International Conference on Urban Drainage (ICUD)*, Melbourne, Australia.

BIBLIOGRAPHY

Alferink, F., Guldback, E., and Grootook, J. (1995). Old PVC gravity sewer pipes: Long term performance. In *Proceedings of the 9th International Conference on Plastics Pipes*, Edinburgh, Scotland, UK.

Alferink, F., Janson, L. E., and Wolters, M. (2004). Combined loading of buried thermoplastics pressure pipes. In *Proceedings of the 12th International Conference on Plastics Pipes*, Milan, Italy.

Anders, U. (2014). Highlights on PVC stabilization for pipes - comparison and trends. In *Proceedings of the 17th International Conference on Plastics Pipes*, Chicago, USA.

Anton-Prinet, C., Mur, G., Gay, M., Audouin, L., and Verdu, J. (1999). Change of mechanical properties of rigid poly (vinylchloride) during photochemical ageing. *Journal of Materials Science*, 34:379–384. DOI: 10.1023/A:1004482328203.

Arbeiter, F., Schrittesser, B., Frank, A., Berer, M., and Pinter, G. (2015). Cyclic tests on cracked round bars as a quick tool to assess the long term behaviour of thermoplastics and elastomers. *Polymer Testing*, 45:83–92. DOI: 10.1016/j.polymertesting.2015.05.008.

Arnold, J. C. (2003). 6.06 Environmental effects on crack growth in polymers. *Comprehensive Structural Integrity*, 6:281–319. DOI: 10.1016/B0-08-043749-4/06123-1.

Arsenio, A. M. (2013). *Lifetime prediction of PVC push-fit joints (Doctoral Dissertation)*. PhD thesis, Delft University of Technology, Delft, The Netherlands. 10.4233/uuid:18a79a31-abd9-4f24-81f5-15935e3523d0.

Arsenio, A. M., Vreeburg, J. H. G., Pieterse-Quirijns, E. J., and Rosenthal, L. (2009). Overview of failure mechanism of joints in water distribution networks. In Boxall, J. and Maksimovic, C., editors, *Integrating water systems: Proceedings of computer and control in the water industry*, pages 607–612. CRC Press, Sheffield.

ASTM D2412-11 (2018). Standard test method for determination of external loading characteristics of plastic pipe by parallel-plate loading. Technical report, Pennsylvania: ASTM International.

Baik, K., Jiang, J., and Leighton, T. G. (2010). Acoustic attenuation, phase and group velocities in liquid-filled pipes: Theory, experiment, and examples of water and mercury. *The Journal of the Acoustical Society of America*, 128(5):2610–2624. DOI: 10.1121/1.3495943.

Balika, W. and Lang, R. W. (2002). Crack growth in a pipe grade PVC material under static and cyclic loading conditions. *Macromolecular Symposia*, 181:341–352. DOI: 10.1002/1521-3900(200205)181:1<341::AID-MASY341>3.0.CO;2-2.

Balkaya, M. and Moore, I. D. (2009). Analysis of a gasketed polyvinyl chloride pipe joint. *Transportation Research Record: Journal of the Transportation Research Board*, 2131:113–122. DOI: 10.3141/2131-11.

Balkaya, M., Moore, I. D., and Saglamer, A. (2012). Study of non-uniform bedding due to voids under jointed PVC water distribution pipes. *Geotextiles and Geomembranes*, 34:39–50. DOI: 10.1016/j.geotexmem.2012.01.003.

Bauer, D. (1990). 15 year old polyvinyl chloride (PVC) sewer pipe; A durability and performance review. In Buczala, G. and Cassady, M., editors, *STP1093-EB buried plastic pipe technology*, pages 393–401. ASTM International, West Conshohocken, PA. DOI: 10.1520/STP42134S.

Benjamin, P. (1980). The influence of the extrusion process on the quality of unplasticized polyvinyl chloride (UPVC) pressure pipe. *Journal of Vinyl and Additive Technology*, 2:254–258. DOI: 10.1002/vnl.730020412.

Bertrand-Krajewski, J.-L., Clemens-Meyer, F., and Lepot, M. (2021). *Metrology in urban drainage and stormwater management: Plug and pray*. IWA Publishing.

Bishop, R. (1990). Retention of pipe stiffness for polyvinyl chloride (PVC) pipe samples exposed to various environments and constant strain. In Buczala, G. and Cassady, M., editors, *STP1093-EB buried plastic pipe technology*, pages 7–20. ASTM International, West Conshohocken, PA. DOI: 10.1520/STP42110S.

Bishop, S., Isaac, D. H., Hinksman, P., and Morrissey, P. (2000). Environmental stress cracking of poly (vinyl chloride) in alkaline solutions. *Polymer Degradation and Stability*, 70:477–484. DOI: 10.1016/S0141-3910(00)00144-0.

Breen, J. (1993). Environmental stress cracking of PVC and PVC-CPE. *Journal of Materials Science*, 28:3769–3776. DOI: 10.1007/BF00353177.

Breen, J. (1994). Environmental stress cracking of PVC and PVC-CPE. *Journal of Materials Science*, 29:39–46. DOI: 10.1007/BF00356570.

Breen, J. (1995). Environmental stress cracking of PVC and PVC-CPE. *Journal of Materials Science*, 30:5833–5840. DOI: 10.1007/BF00356729.

Breen, J. (2006). *Expected lifetime of existing PVC water systems: Summary*. TNO, Eindhoven.

Broutman, L. J., Duvall, D. E., and So, P. K. (1990). Failure analysis of a PVC water pipe. *Journal of Vinyl and Additive Technology*, 12:53–56. DOI: 10.1002/vnl.730120112.

Brown, N. (2007). Intrinsic lifetime of polyethylene pipelines. *Polymer Engineering & Science*, 47:477–480. DOI: 10.1002/pen.20696.

Burn, L. S. (1991). Effect of installation damage on the lifetime of UPVC pipes subjected to cyclic pressures. *Polymer International*, 26:147–150. DOI: 10.1002/pi.4990260305.

Burn, L. S. (1992). Lifetime prediction of uPVC pipes: Experimental and theoretical comparisons. In *Proceedings of the 8th International Conference on Plastics Pipes*, Eindhoven, The Netherlands.

Butters, G. E. (1982). *Particulate nature of PVC: Formation, structure and processing*. Applied Science Publishers, London.

Cardarelli, F. (2008). Polymers and elastomers. In Cardarelli, F., editor, *Materials handbook: A Concise Desktop Reference (2nd ed)*, pages 691–750. Springer, London. DOI: 10.1007/978-1-84628-669-8_11.

Carter, G. and Knapp, C. (1975). Coherence and its estimation via the partitioned modified chirp-z transform. *IEEE Transactions on Acoustics, Speech, and Signal Processing*, 23(3):257–264.

Castagnetti, D., Mammano, G. S., and Dragoni, E. (2011). Effect of chlorinated water on the oxidative resistance and the mechanical strength of polyethylene pipes. *Polymer Testing*, 30:277–285. DOI: 10.1016/j.polymertesting.2010.12.001.

Castillo, J. L. (2016). Longitudinal crack in large PVC-U pressure pipes. Pipe gelation influence. Case study discussion (I). In *Proceedings of the 18th International Conference on Plastics Pipes*, Berlin, Germany.

Celina, M., Gillen, K. T., and Assink, R. A. (2005). Accelerated aging and lifetime prediction: Review of non-Arrhenius behaviour due to two competing processes. *Polymer Degradation and Stability*, 90:395–404. DOI: 10.1016/j.polymdegradstab.2005.05.004.

Celina, M. C. (2013). Review of polymer oxidation and its relationship with materials performance and lifetime prediction. *Polymer Degradation and Stability*, 98:2419–2429. DOI: 10.1016/j.polymdegradstab.2013.06.024.

Chaoui, K., Chudnovsky, A., and Moet, A. (1987). Effect of residual stress on crack propagation in MDPE pipes. *Journal of Materials Science*, 22:3873–3879. DOI: 10.1007/BF01133334.

Choi, B. H., Zhou, Z., Chudnovsky, A., Stivala, S. S., Sehanobish, K., and Bosnyak, C. P. (2005). Fracture initiation associated with chemical degradation: Observation and modeling. *International Journal of Solids and Structures*, 42:681–695. DOI: 10.1016/j.ijsolstr.2004.06.028.

Choi, P., Lynch, M., Rudin, A., Teh, J. W., and Batiste, J. (1992). Dsc analysis of fusion level of rigid PVC revisited: Filler effects on thermal analysis data. *Journal of Vinyl and Additive Technology*, 14:156–160. DOI: 10.1002/vnl.730140309.

COMSOL (2017a). *Acoustics Module User's Guide*.

COMSOL (2017b). *Structural Mechanics Module User's Guide*.

Davidovski, Z. (2016). Main drivers and barriers for plastic pipes in Europe. In *Proceedings of the 18th International Conference on Plastics Pipes*, Berlin, Germany.

Davis, P., Burn, S., Moglia, M., and Gould, S. (2007). A physical probabilistic model to predict failure rates in buried PVC pipelines. *Reliability Engineering & System Safety*, 92:1258–1266. DOI: 10.1016/j.ress.2006.08.001.

De Jong, C. A. F. (1994). *Analysis of Pulsations and Vibrations in Fluid-filled Pipe Systems (Doctoral Dissertation)*. Eindhoven University of Technology, Eindhoven, The Netherlands. DOI: 10.6100/IR423649.

Delgadillo, H. (2019). *Ultrasonic inspection of drinking water mains (Doctoral Dissertation)*. University of Twente, Enschede, The Netherlands. DOI: 10.3990/1.9789036548533.

Demčenko, A. (2014). *Development and analysis of noncollinear wave mixing techniques for material properties evaluation using immersion ultrasonics (Doctoral Dissertation)*. University of Twente, Enschede, The Netherlands. DOI: 10.3990/1.9789036537612.

Deveci, S. and Fang, D. (2017). Correlation of molecular parameters, strain hardening modulus and cyclic fatigue test performances of polyethylene materials for pressure pipe applications. *Polymer Testing*, 62:246–253. DOI: 10.1016/j.polymertesting.2017.07.007.

Dirksen, J., Clemens, F. H. L. R., Korving, H., Cherqui, F., Le Gauffre, P., T., E., ..., and Snaterse, C. T. M. (2013). The consistency of visual sewer inspection data. *Structure and Infrastructure Engineering*, 9:214–228. DOI: 10.1080/15732479.2010.541265.

Doshi, S. R. (1989). Prediction of residual stress distribution in plastic pipe extrusion. *Journal of Vinyl and Additive Technology*, 11:190–194. DOI: 10.1002/vnl.730110410.

Drenth, E. (2015). *Towards condition based asset management of uPVC pipes (Doctoral Dissertation)*. University of Twente, Enschede, The Netherlands. DOI: 10.3990/1.9789036539920.

Faulkner, P. G. (1975). The use of a temperature programmable brabender mixing head for the evaluation of the processing characteristics of poly (vinyl chloride). *Journal of Macromolecular Science, Part B: Physics*, 11:251–279. DOI: 10.1080/00222347508217863.

Fillot, L. A., Hajji, P., Gauthier, C., and Masenelli-Varlot, K. (2006). UPVC gelation level assessment, part 1: Comparison of different techniques. *Journal of Vinyl and Additive Technology*, 12:98–107. DOI: 10.1002/vnl.20077.

Fillot, L. A., Hajji, P., Gauthier, C., and Masenelli-Varlot, K. (2007). Thermomechanical history effects on rigid PVC microstructure and impact properties. *Journal of Applied Polymer Science*, 104:2009–2017. DOI: 10.1002/app.25688.

Fischer, I., Schmitt, W. F., Porth, H. C., Allsopp, M. W., and Vianello, G. (2014). *Poly (vinyl chloride)*. In Ullmann's encyclopedia of industrial chemistry. Wiley-VCH Verlag GmbH, Weinheim. Electronic Release. DOI: 10.1002/14356007.a21_717.pub2.

Flores, R., Pérez, J. Z., Cassagnau, P., Michel, A., and Cavaillé, J.-Y. (1994). α mechanical relaxation in poly(vinyl chloride): effect of ageing and crosslinking. *Polymer*, 35:2800–2807. DOI: 10.1016/0032-3861(94)90309-3.

Folkman, S. (2014). Validation of the long life of PVC pipes. In *Proceedings of the 17th International Conference on Plastics Pipes*, Chicago, USA.

Frank, A., Freimann, W., Pinter, G., and Lang, R. W. (2009). A fracture mechanics concept for the accelerated characterization of creep crack growth in PE-HD pipe grades. *Engineering Fracture Mechanics*, 76:2780–2787. DOI: 10.1016/j.engfracmech.2009.06.009.

Frank, A., Hutar, P., and Pinter, G. (2012). Numerical assessment of PE 80 and PE 100 pipe lifetime based on Paris-Erdogan equation. *Macromolecular Symposia*, 311:112–121. DOI: 10.1002/masy.201000096.

Fujiyama, M. and Kondou, M. (2004). Effect of degree of polymerization on gelation and flow processability of poly (vinyl chloride). *Journal of Applied Polymer Science*, 92:1915–1938. DOI: 10.1002/app.20181.

Fumire, J. (2008). Resistance of PVC pipes against disinfectants. In *Proceedings of the 14th International Conference on Plastics Pipes*, Budapest, Hungary.

Gao, Y., Brennan, M. J., Joseph, P. F., Muggleton, J. M., and Hunaidi, O. (2004). A model of the correlation function of leak noise in buried plastic pipes. *Journal of Sound and Vibration*, 277(1-2):133–148. DOI: 10.1016/j.jsv.2003.08.045.

Gao, Y., Muggleton, J. M., Liu, Y., and Rustighi, E. (2017). An analytical model of ground surface vibration due to axisymmetric wave motion in buried fluid-filled pipes. *Journal of Sound and Vibration*, 395:142–159. DOI: 10.1016/j.jsv.2017.02.022.

Gao, Y., Sui, F., Muggleton, J. M., and Yang, J. (2016). Simplified dispersion relationships for fluid-dominated axisymmetric wave motion in buried fluid-filled pipes. *Journal of Sound and Vibration*, 375:386–402. DOI: 10.1016/j.jsv.2016.04.012.

García, D. B., Cortés-Pérez, J., and Moore, I. D. (2016). Quality control testing of joints in gravity flow plastic pipes. In *Proceedings of the 18th International Conference on Plastics Pipes*, Berlin, Germany.

García, D. B. and Moore, I. D. (2013). Behavior of bell and spigot joints in buried thermoplastic pipelines. *Transportation Research Record: Journal of the Transportation Research Board*, 2332:29–40. DOI: 10.3141/2332-04.

Gazis, D. C. (1959). Three-dimensional investigation of the propagation of waves in hollow circular cylinders. I. Analytical foundation. *The journal of the Acoustical Society of America*, 31(5):568–573. DOI: 10.1121/1.1907753.

Ghabeche, W., Alimi, L., and Chaoui, K. (2015). Degradation of plastic pipe surfaces in contact with an aggressive acidic environment. *Energy Procedia*, 74:351–364. DOI: 10.1016/j.egypro.2015.07.625.

Gilbert, M. and Vyvoda, J. C. (1981). Thermal analysis technique for investigating gelation of rigid PVC compounds. *Polymer*, 22:1134–1136. DOI: 10.1016/0032-3861(81)90305-0.

Gladchenko, A. N., Shevelya, I. V., Kiyanitsa, E. V., and Derkach, V. V. (1997). Wear of working members of extruders for processing polymers. *Chemical and Petroleum Engineering*, 33:367–370. DOI: 10.1007/BF02416718.

Gould, S. J., Davis, P., Beale, D. J., and Marlow, D. R. (2013). Failure analysis of a PVC sewer pipeline by fractography and materials characterization. *Engineering Failure Analysis*, 34:41–50. DOI: 10.1016/j.engfailanal.2013.07.009.

Gramann, P., Cruz, J., and Ralston, B. (2010). Using differential scanning calorimetry to determine the quality of a PVC part. *The Madison Group*, pages 1–6.

Guerrero, S. J. and Keller, A. (1981). The gelation of PVC: Characterization and control. *Journal of Macromolecular Science, Part B: Physics*, 20:167–184. DOI: 10.1080/00222348108219435.

Hassinen, J., Lundbäck, M., Ifwarson, M., and Gedde, U. W. (2004). Deterioration of polyethylene pipes exposed to chlorinated water. *Polymer Degradation and Stability*, 84:261–267. DOI: 10.1016/j.polymdegradstab.2003.10.019.

Hawkins, T. W. and Mass, T. R. (1994). The effects of sulfuric acid on calcium carbonate filled PVC sewer pipe compounds. In Eckstein, D., editor, *STP1222 Buried plastic pipe technology (Vol. 2, pp. 167–179)*. ASTM International, Philadelphia, PA.

Headford, A. (1998). Jointing methods for plastics pipelines systems. In *Proceedings of the 10th International Conference on Plastics Pipes*, Gothenburg, Sweden.

Hsieh, C. W., Wu, J. H., and Huang, C. C. (2010). Plastic pipe long-term pipe stiffness by conventional and accelerated test methods. *Journal of GeoEngineering*, 5:69–76. DOI: 10.6310/jog.2010.5(3).2.

Hu, Y., Summers, J., Hiltner, A., and Baer, E. (2003). Correlation of fatigue and creep crack growth in poly (vinyl chloride). *Journal of Materials Science*, 38:633–642. DOI: 10.1023/A:1021899801981.

Hunt, L. E. (1979). Evaluation and usage of joint seals for UPVC pipe systems. In *Proceedings of the 4th International Conference on Plastics Pipes*, Brighton, England.

Hussain, I., Hamid, S. H., and Khan, J. H. (1995). Polyvinyl chloride pipe degradation studies in natural environments. *Journal of Vinyl and Additive Technology*, 1:137–141. DOI: 10.1002/vnl.730010305.n.

Hutař, P., Ševčík, M., Frank, A., Náhlík, L., Kučera, J., and Pinter, G. (2013). The effect of residual stress on polymer pipe lifetime. *Engineering Fracture Mechanics*, 108:98–108. DOI: 10.1016/j.engfracmech.2013.04.014.

Hutař, P., Ševčík, M., Náhlík, L., Pinter, G., and Frank, A. & Mitev, I. (2011). A numerical methodology for lifetime estimation of HDPE pressure pipes. *Engineering Fracture Mechanics*, 78:3049–3058. DOI: 10.1016/j.engfracmech.2011.09.001.

Hutchinson, J. M. (1995). Physical aging of polymers. *Progress in Polymer Science*, 20:703–760. DOI: 10.1016/0079-6700(94)00001-I.

ISO 1167-1 (2006). Thermoplastics pipes, fittings and assemblies for the conveyance of fluids - Determination of the resistance to internal pressure - Part 1: General method. Standard, Brussels: CEN.

ISO 1183-1 (2012). Plastics - methods for determining the density of non-cellular plastics - Part 1: Immersion method, liquid pyknometer method and titration method. Standard, Brussels: CEN.

ISO 9080 (2012). Plastics piping and ducting systems - Determination of the long-term hydrostatic strength of thermoplastics materials in pipe form by extrapolation. Standard, Brussels: CEN.

ISO 9969 (2016). Thermoplastic pipes - Determination of ring stiffness. Standard, Brussels: CEN.

Ivey, D. G., Mrowca, B. A., and Guth, E. (1949). Propagation of ultrasonic bulk waves in high polymers. *Journal of Applied Physics*, 20:486–492. DOI: 10.1063/1.1698415.

Janson, L. E. (1988). Physical ageing of buried PVC sewer pipes as affecting their long-term behaviour. In *Proceedings of the 7th International Conference on Plastics Pipes*, Bath, U.K.

Janson, L. E. (1995). Long-term behaviour of buried PVC sewer pipes. In *Proceedings of the 9th International Conference on Plastics Pipes*, Edinburgh, Scotland, UK.

Janson, L. E. (2003). *Plastics pipes for water supply and sewage disposal (4th ed.)*. Borealis, Stenungsund.

Joekes, D. and Elzink, W. J. (1985). Deflection of PVC sewer pipes and a new method of measuring and specifying stiffness of plastic pipes. In *Proceedings of the 6th International Conference on Plastics Pipes*, University of York, London, UK.

Johansson, L. and Törnell, B. (1986). Information about incomplete gelation in rigid PVC from SEM studies of fracture surfaces. *Journal of Materials Science Letters*, 5:279–281. DOI: 10.1007/BF01748077.

Johansson, L. and Törnell, B. (1987). Initiation of fractures in rigid PVC pipes by soft particles. *Journal of Vinyl and Additive Technology*, 9:103–107. DOI: 10.1002/vnl.730090304.

Junger, M. C. and Feit, D. (1986). *Sound, structures, and their interaction (2nd ed.)*. MIT Press, Cambridge, Massachusetts.

Khelif, R., Chateauneuf, A., and Chaoui, K. (2007). Reliability-based assessment of polyethylene pipe creep lifetime. *International Journal of Pressure Vessels and Piping*, 84:697–707. DOI: 10.1016/j.ijpvp.2007.08.006.

Kim, H. S., Cotterell, B., and Mai, Y. W. (1987). Unnotched impact bend test assessment of the degree of gelation in unplasticized poly (vinyl chloride) pipe. *Polymer Engineering and Science*, 27:277–281. DOI: 10.1002/pen.760270407.

Koda, S., Yamashita, K., Matsumoto, K., and Nomura, H. (1993). Characterization of Polyvinylchloride by Means of Sound Velocity and Longitudinal Modulus Measurements. *Japanese Journal of Applied Physics*, 32:2234–2237.

Koski, L. M. (1982). Relaxation modulus of PVC and PEH sewage pipes for evaluation of long-term ring stiffness. In *Proceedings of the 5th International Conference on Plastics Pipes*, University of York, London, UK.

Kowalska, B., Klepka, T., and Kowalski, D. (2016). Influence of chlorinated water on mechanical properties of polyethylene and polyvinyl chloride pipes. In Proverbs, D., Brebbia, C., Mambretti, S., and Ursino, N., editors, *WIT Transactions on The Built Environment*, volume 165, pages 63–74. WIT Press, Southampton. DOI: 10.2495/UW160061.

Kowalska, B., Rudawska, A., and Kowalski, D. (2014). Tests on a polyvinyl chloride pipe from an existing water distribution system. In Brebbia, S. M. . C. A., editor, *Urban Water II*, pages 3–14. WIT Press, Southampton. DOI: 10.2495/UW140011.

Kratochvilla, T. R., Frank, A., and Pinter, G. (2014). Determination of slow crack growth behaviour of polyethylene pressure pipes with cracked round bar test. *Polymer Testing*, 40:299–303. DOI: 10.1016/j.polymertesting.2014.10.002.

Krishnaswamy, R. K. (2005). Analysis of ductile and brittle failures from creep rupture testing of high-density polyethylene (HDPE) pipes. *Polymer*, 46:11664–11672. DOI: 10.1016/j.polymer.2005.09.084.

Kubat, J., Rigdahl, M., and Welander, M. (1990). Characterization of interfacial interactions in high density polyethylene filled with glass spheres using dynamic-mechanical analysis. *Journal of Applied Polymer Science*, 39(7):1527–1539. DOI: 10.1002/app.1990.070390711.

Kuliczkowska, E. (2014). Influence of PVC pipe deflection on the thickness of CIPP rehabilitation liners. In Madryas, C., Kolonko, A., Szot, A., and Nienartowicz, B., editors, *Underground infrastructure of Urban areas*, pages 63–72. CRC Press, (Vol. 3, pp.). London.

Kuliczkowska, E. and Zwierzchowska, A. (2016). A qualitative analysis of early defects present in PVC-U sewers but not observed in rigid pipes. *Tunnelling and Underground Space Technology*, 56:202–210. DOI: 10.1016/j.tust.2016.03.013.

Kunst, O. (2016). Het nut van stedelijk waterbeheer. Technical report, Stichting Rioned.

Kunststoffrohrverband (1997). *Kunststoffrohr Handbuch - Rohrleitungssysteme für die Ver-und Entsorgung sowie weitere Anwendungsgebiete*. Vulcan-Verlag, Essen.

Kuriyama, T., Narisawa, I., Shina, R., and Kotaki, M. (1998). Effects of morphology on the fracture toughness of PVC-U pipe. *Journal of Vinyl and Additive Technology*, 4:164–168. DOI: 10.1002/vnl.10035.

Laiarinandrasana, L., Gaudichet, E., Oberti, S., and Devilliers, C. (2011). Effects of aging on the creep behaviour and residual lifetime assessment of polyvinyl chloride (PVC) pipes. *International Journal of Pressure Vessels and Piping*, 88:99–108. DOI: 10.1016/j.ijpvp.2011.01.002.

Lang, R. W., Stern, A., and Doerner, G. (1997). Applicability and limitations of current lifetime prediction models for thermoplastics pipes under internal pressure. *Applied Macromolecular Chemistry and Physics*, 247:131–145. DOI: 10.1002/apmc.1997.052470109.

Lasfar, S., Mouallif, I., Latrach, A., Chergui, M., H., Choukir, A., and Diab, A. (2014). Resistance of different materials used in sewers systems: Polyvinyl chloride (PVC), polypropylene (PP) and high-density polyethylene (HDPE), to sulfuric acid and sodium sulfate attack. *International Journal Engineering Research and Applications*, 4:670–678.

Leissa, A. W. . N. A., Scientific, S. A., and Office, T. I. (1973). *Vibration of shells*. USGPO, Washington.

Lepot, M., Makris, K. F., and Clemens, F. H. (2017). Detection and quantification of lateral, illicit connections and infiltration in sewers with infra-red camera: Conclusions after a wide experimental plan. *Water Research*, 122:678–691. DOI: 10.1016/j.watres.2017.06.030.

Lionetto, F. and Maffezzoli, A. (2008). Polymer characterization by ultrasonic wave propagation. *Advances in Polymer Technology*, 27(2):63–73. DOI: 10.1002/adv.20124.

Liu, J. X., Li, T. Y., Liu, T. G., and Yan, J. (2005). Vibration characteristic analysis of buried pipes using the wave propagation approach. *Applied acoustics*, 66(3):353–364. DOI: 10.1016/j.apacoust.2004.06.010.

Long, R., Cawley, P., and Lowe, M. (2003). Acoustic wave propagation in buried iron water pipes. In *Proceedings of the Royal Society of London. Series A: Mathematical, Physical and Engineering Sciences*, volume 459(2039), pages 2749–2770. DOI: 10.1098/rspa.2003.1148.

Long, R., Vine, K., Lowe, M. J. S., and Cawley, P. (2002). The effect of soil properties on acoustic wave propagation in buried iron water pipes. *AIP Conference Proceedings*, 615(1):1310–1317. DOI: 10.1063/1.1472947.

Lu, J. P., Burn, L. S., and Whittle, A. J. (2000). Elastomeric joint performance of PVC, VC, and FRC pipes. *Polymer Engineering & Science*, 40:2217–2226. DOI: 10.1002/pen.11353.

Lu, J. P., Davis, P., and Burn, L. S. (2003). Lifetime prediction for ABS pipes subjected to combined pressure and deflection loading. *Polymer Engineering & Science*, 43:444–462. DOI: 10.1002/pen.10036.

Magnusson, J. (1982). Sealing systems for PVC pipes. In *Proceedings of the 5th International Conference on Plastics Pipes*, University of York, London, UK.

Maiti, S. K. (2015). *Fracture mechanics: Fundamentals and applications*. University Press, Cambridge.

Mandell, J. F., Darwish, A. Y., and McGarry, F. J. (1982). Effects of processing conditions and aging on the fracture toughness of rigid PVC pipe materials. *Journal of Vinyl and Additive Technology*, 4:95–100. DOI: 10.1002/vnl.730040303.

Marshall, G. P. and Birch, M. W. (1982). Criteria for high toughness in uPVC pressure pipes. In *Proceedings of the 5th International Conference on Plastics Pipes*, University of York, London, UK.

McGarry, F. J., Mandell, J. F., and Hsueh-Lee, L. (1985). Brittle fracture in PVC pipe material. *Journal of Polymer Science: Polymer Symposia*, 72:83–110. DOI: 10.1002/polc.5070720116.

Meerman, M. (2008). Lifetime expectancy of PVC-U pipelines for sewer systems. In *Proceedings of the 14th International Conference on Plastics Pipes*, Budapest, Hungary.

Meijering, T. G., Wolters, M., and Hermkens, R. J. (2004). The durability of a low-pressure gas distribution system of ductile PVC. In *Proceedings of the 12th International Conference on Plastics Pipes*, Milan, Italy.

Men, Y., Rieger, J., Endeler, H.-F., and Lilge, D. (2003). Mechanical α-process in polyethylene. *Macromolecules*, 36(13):4689–4691. DOI: 10.1021/ma0344902.

Moghri, M., Garmabi, H., and Akbarian, M. (2003). Effect of processing parameters on fusion and mechanical properties of a twin-screw extruded rigid PVC pipe. *Journal of Vinyl and Additive Technology*, 9:81–89. DOI: 10.1002/vnl.10067.

Mohamedzein, Y. E. and Al-Aghbari, M. Y. (2016). Experimental study of the performance of plastic pipes buried in dune sand. *International Journal of Geotechnical Engineering*, 10:236–245. DOI: 10.1080/19386362.2015.1124508.

Moser, A. and Folkman, S. (2008). *Buried pipe design*. McGraw-Hill, New York, 3rd ed. edition.

Moser, A. P., Shupe, O. K., and Bishop, R. R. (1990). Is PVC pipe strain limited after all these years. In Buczala, G. and Cassady, M., editors, *STP1093-EB buried plastic pipe technology*, pages 159–170. ASTM International, West Conshohocken, PA. DOI: 10.1520/STP42119S.

NEN 12666-1 (2011). Plastics piping systems for non-pressure underground drainage and sewerage. polyethylene (PE) - part 1: Specifications for pipes, fittings and the system. Standard, Brussels: CEN.

NEN 1277 (2003). Plastics piping systems - Thermoplastics piping systems for buried non-pressure applications - Test methods for leaktightness of elastomeric sealing ring type joints. Standard, Brussels: CEN.

NEN 1401-1 (2009). Plastics piping systems for non-pressure underground drainage and sewerage. unplasticized poly(vinyl chloride) (PVC-U) - part 1: Specifications for pipes, fittings and the system. Standard, Brussels: CEN.

NEN 3399 (2015). Sewerage systems outside buildings - Classification system for visual inspection of objects. Standard, Delft: Royal Netherlands Standardization Institute.

Nezbedová, E., Hutař, P., Zouhar, M., Knésl, Z., Sadílek, J., and Náhlík, L. (2013). The applicability of the Pennsylvania Notch Test for a new generation of PE pipe grades. *Polymer Testing*, 32:106–114. DOI: 10.1016/j.polymertesting.2012.09.009.

Nitta, K.-h. and Yamana, M. (2012). Poisson's ratio and mechanical nonlinearity under tensile deformation in crystalline polymers. *Rheology, Open Access; Vicente, JD, Ed.; Intec: Rijeka, Croatia*, pages 113 – 132.

Oosterom, G. and Hermans, R. (2013). Riolering in beeld. Technical report, Stichting Rioned.

Östberg, J., Martinsson, M., Stål, Ö., and Fransson, A. M. (2012). Risk of root intrusion by tree and shrub species into sewer pipes in Swedish urban areas. *Urban Forestry & Urban Greening*, 11:65–71. DOI: 10.1016/j.ufug.2011.11.001.

Pang, X.-F. (2013). *Water: molecular structure and properties*. World Scientific.

Perepechko, I. I. and Golub', P. D. (1973). Viscoelastic parameters of certain polymers in the temperature interval 4.2–240 °K. *Polymer Mechanics*, 9:534–538. DOI: 10.1007/BF00855890.

Pinnington, R. and Briscoe, A. (1994). Externally applied sensor for axisymmetric waves in a fluid filled pipe. *Journal of Sound and vibration*, 173(4):503–516. DOI: 10.1006/jsvi.1994.1243.

Pinter, G., Lang, R. W., and Haager, M. (2007). A test concept for lifetime prediction of polyethylene pressure pipes. *Monatshefte ür Chemie - Chemical Monthly*, 138:347–355. DOI: 10.1007/s00706-007-0618-1.

Plastics Industry Pipe Association (2009). Plastics pipe in water and waste water infrastructure. Technical report.

PlasticsEurope - Association of Plastics Manufacturers (2017). Plastics - The Facts: An analysis of European latest plastics production, demand and waste data. Technical report.

Poduška, J., Hutař, P., Kučera, J., Frank, A., Sadílek, J., Pinter, G., and Náhlík, L. (2016). Residual stress in polyethylene pipes. *Polymer Testing*, 54:288–295. DOI: 10.1016/j.polymertesting.2016.07.017.

Poduška, J., Kučera, J., Hutař, P., Ševčík, M., Křivánek, J., Sadílek, J., and Náhlík, L. (2014). Residual stress distribution in extruded polypropylene pipes. *Polymer Testing*, 40:88–98. DOI: 10.1016/j.polymertesting.2014.08.006.

Rabinovitch, E. B. and Summers, J. W. (1992). The effect of physical ageing on properties of rigid polyvinyl chloride. *Journal of Vinyl and Additive Technology*, 14:126–130. DOI: 10.1002/vnl.730140303.

Rahman, S. and Bird, W. (2006). PVC pipe jointing: The Rieber system in North America. In *Proceedings of the 13th International Conference on Plastics Pipes*, Washington DC, USA.

Randrup, T. (2000). Occurrence of tree roots in Danish municipal sewer systems. *Arboricultural Journal*, 24:283–306. DOI: 10.1080/03071375.2000.9747282.

Read, B. E. and Dean, G. D. (1988). Physical ageing and short-term creep in amorphous and semicrystalline polymers. *Polymer*, 31(7):1204–1215. DOI: 10.1016/0032-3861(90)90209-H.

Read, B. E., Dean, G. D., and Tomlins, P. E. (1988). Effects of physical ageing on creep in polypropylene. *Polymer*, 29(12):2159–2169. DOI: 10.1016/0032-3861(88)90107-3.

Read, B. E., Dean, G. D., Tomlins, P. E., and Lesniarek-Hamid, J. L. (1992). Physical ageing and creep in PVC. *Polymer*, 33 (13):2689–2698. DOI: 10.1016/0032-3861(92)90439-4.

Real, L. P., João, I. M., Pimenta, S. I., and Diogo, H. P. (2018). Evaluating the degree of gelation of PVC-U pipes. Comparison of currently available methods. *Polymer Testing*, 70:481–485. DOI: 10.1016/j.polymertesting.2018.08.001.

Ridgers, D., Rolf, K., and & Stål, Ö. (2006). Management and planning solutions to lack of resistance to root penetration by modern PVC and concrete sewer pipes. *Arboricultural Journal*, 29:269–290. DOI: 10.1080/03071375.2006.9747467.

Robeson, L. M. (2013). Environmental stress cracking: A review. *Polymer Engineering & Science*, 53:453–467. DOI: 10.1002/pen.23284.

Robledo, N., Domínguez, C., and García-Muñoz, R. A. (2017). Alternative accelerated and short-term methods for evaluating slow crack growth in polyethylene resins with high crack resistance. *Polymer Testing*, 62:366–372. DOI: 10.1016/j.polymertesting.2017.07.022.

Rose, J. (2014). *Ultrasonic Guided Waves in Solid Media*. Cambridge University Press, Cambridge. DOI: 10.1017/CBO9781107273610.

Sadler, P. A., Burn, L. S., and Whittle, A. J. (2001). Elastomeric pipe joint performance requirements for use in PVC sewer pipelines. In *Proceedings of the 11th International Conference on Plastics Pipes*, Munich, Germany.

Scharwächter, D. (2001). Long term tightness of sealing joints in non-pressure plastic piping systems. In *Proceedings of the 11th International Conference on Plastics Pipes*, Munich, Germany.

Scholten, F. L., van der Stok, E., Gerets, B., Wenzel, M., and Boege, M. (2016). Residual quality of excavated UPVC gas and water distribution pipelines. In *Proceedings of the 18th International Conference on Plastics Pipes*, Berlin, Germany.

Scussel, O., Brennan, M. J., Almeida, F. C. L., Muggleton, J., Rustighi, E., and Joseph, P. F. (2021). Estimating the spectrum of leak noise in buried plastic water distribution pipes using acoustic or vibration measurements remote from the leak. *Mechanical Systems and Signal Processing*, 147. DOI: 10.1016/j.ymssp.2020.107059.

Scussel, O., Brennan, M. J., Muggleton, J. M., Almeida, F. C. L., and Paschoalini, A. T. (2019). Estimation of the bulk and shear moduli of soil surrounding a plastic water pipe using measurements of the predominantly fluid wave in the pipe. *Journal of Applied Geophysics*, 164:237–246. DOI: 10.1016/j.jappgeo.2019.01.010.

Siegmann, A., Buchman, A., and Kenig, S. (1981). Residual stresses in polymers. II. their effect on mechanical behavior. *Polymer Engineering and Science*, 21:997–1002. DOI: 10.1002/pen.760211503.

Siegmann, A., Buchman, A., and Kenig, S. (1982). Residual stresses in polymers I: The effect of thermal history. *Polymer Engineering and Science*, 22:40–47. DOI: 10.1002/pen.760220107.

Stål, Ö. (1998). The interaction of tree roots and sewers: The Swedish experience. *Arboricultural Journal*, 22:359–367. DOI: 10.1080/03071375.1998.9747221.

Stanic, N. (2016). *Assessment Methods for Structural and Hydraulic Properties of Concrete Sewer Pipes (Doctoral Dissertation)*. Delft University of Technology, Delft, The Netherlands. DOI: 10.4233/uuid:3ea2146b-21cb-49b0-9aca-40ae8338e4d3.

Stein, D. (2001). *Rehabilitation and maintenance of drains and sewers*. Ernst & Sohn, Berlin.

Stephens, J. W. and Gill, B. W. (1982). Service failure experience of uPVC pressure pipes in the water industry. In *Proceedings of the 5th International Conference on Plastics Pipes*, University of York, London, UK.

Stokes, V. K. (1989). Joining methods for plastics and plastic composites: an overview. *Polymer Engineering and Science*, 29:1310–1324. DOI: 10.1002/pen.760291903.

Struik, L. C. E. (1977). *Physical aging in amorphous polymers and other materials (Doctoral Dissertation)*. PhD thesis, Delft University of Technology, The Netherlands. Retrieved from http://resolver.tudelft.nl/uuid:941d2af6-903a-4260-9953-2efb4cb38d2e.

Terselius, B., Jansson, J. F., and Bystedt, J. (1981). Gelation of rigid PVC-pipes. *Journal of Macromolecular Science, Part B: Physics*, 20:403–414. DOI: 10.1080/00222348108219450.

Truss, R. W. (1985). Understanding brittle failure of uPVC (unplasticised polyvinyl chloride) pipe. *Pure and Applied Chemistry*, 57:993–1000. DOI: 10.1351/pac198557070993.

Tscheikner-Gratl, F., Caradot, N., Cherqui, F., Leitão, J. P., Ahmadi, M., Langeveld, J. G., Gat, Y. L., Scholten, L., Roghani, B., Rodríguez, J. P., Lepot, M., Stegeman, B., Heinrichsen, A., Kropp, I., Kerres, K., do Céu Almeida, M., Bach, P. M., de Vitry, M. M., Marques, A. S., Simões, N. E., Rouault, P., Hernandez, N., Torres, A., Werey, C., Rulleau, B., and Clemens, F. (2019). Sewer asset management – state of the art and research needs. *Urban Water Journal*, 16(9):662–675. DOI: 10.1080/1573062X.2020.1713382.

Välimaa, P. (1982). Gravity sewage pipes of uPVC for 10 years in use. In *Proceedings of the 5th International Conference on Plastics Pipes*, University of York, London, UK.

Van der Heuvel, P. (1982). PVC pressure pipe: The importance of gelation to ensure pipe reliability. In *Proceedings of the 5th International Conference on Plastics Pipes*, University of York, London, UK.

Van Riel, W. (2017). *On decision-making for sewer replacement (Doctoral Dissertation)*. Delft University of Technology, Delft, The Netherlands. DOI: 10.4233/uuid:92b10448-795d-43ac-8071-d779af9d374d.

Visser, H. A. (2009). *Residual lifetime assessment of uPVC gas pipes (Doctoral Dissertation)*. University of Twente, Enschede, The Netherlands. DOI: 10.3990/1.9789036529587.

Visser, H. A., Bor, T. C., Wolters, M., Warnet, L. L., and Govaert, L. E. (2011). Influence of physical aging on impact embrittlement of uPVC pipes. *Plastics, Rubber and Composites*, 40:201–212. DOI: 10.1179/1743289810Y.0000000021.

Walton, D. and Elzink, W. J. (1989). The long term behaviour of buried uPVC sewer pipe. *Construction and Building Materials*, 3:58–63. DOI: 10.1016/S0950-0618(89)80001-7.

Wee, J. W. and Choi, B. H. (2016). Modeling of axisymmetric slow crack growth of high-density polyethylene with circular notched bar specimen using crack layer theory. *International Journal of Solids and Structures*, 97-98:189–199. DOI: 10.1016/j.ijsolstr.2016.07.030.

Whittle, A. J. (2003). PVC technical information. Technical report, Australia: PIPA of Australia Limited.

Whittle, A. J. and Tennakoon, J. (2005). Predicting the residual life of PVC sewer pipes. *Plastics, Rubber and Composites*, 34:311–317. DOI: 10.1179/174328905X59773.

Williams, J. G., Hodgkinson, J. M., and Gray, A. (1981). The determination of residual stresses in plastic pipe and their role in fracture. *Polymer Engineering and Science*, 21:822–828. DOI: 10.1002/pen.760211304.

Wypych, G. (2015). *PVC degradation and stabilization*. ChemTec Publishing, Toronto, Canada. DOI: 10.1016/C2014-0-01988-0.

Yu, W., Azhdar, B., Andersson, D., Reitberger, T., Hassinen, J., Hjertberg, T., and Gedde, U. W. (2011). Deterioration of polyethylene pipes exposed to water containing chlorine dioxide. *Polymer Degradation and Stability*, 96:790–797. DOI: 10.1016/j.polymdegradstab.2011.02.009.

Zhao, Y., Choi, B. H., and Chudnovsky, A. (2013). Characterization of the fatigue crack behavior of pipe grade polyethylene using circular notched specimens. *International Journal of Fatigue*, 51:26–35. DOI: 10.1016/j.ijfatigue.2013.01.016.